STUDY
ON THE APPLICATIONS OF ANTENNA ARRAYS
TO SATELLITE TRACKING BY INTERFEROMETRY
AND TO ADAPTIVE REJECTION OF INTERFERENCE

by

Masaharu FUJITA

January 1978

Kashima Branch, Radio Research Laboratories

Ibaraki, Japan

STUDY
ON THE APPLICATIONS OF ANTENNA ARRAYS TO SATELLITE TRACKING BY INTERFEROMETRY AND TO ADAPTIVE REJECTION OF INTERFERENCE

by

Masaharu FUJITA

January 1978

Kashima Branch, Radio Research Laboratories
Ibaraki, Japan

ACKNOWLEDGEMENTS

The author wishes to express his hearty and sincere gratitude to Professor Iwane Kimura for his constant guidance and critical supervision throughout the work.

The author is deeply indebted to Dr. Kazuaki Takao for his continual guidance and encouragement. It would have been impossible to show this thesis without his suggestions and criticisms.

The author also wishes to express his hearty appreciation to emeritus Professor Ken-ichi Maeda for his useful advices and stimulating suggestions and to Professors Susumu Kato and Toru Ogawa for their valuable discussions.

The author is grateful to Drs. Hiroshi Matsumoto, Tsutomu Yabuzaki, Syoichiro Fukao and Takehiko Aso and Messrs. Kozo Hashimoto and Minoru Tsutsui for their many discussions.

The author also wishes to acknowledge many members of Prof. Kimura's group and Ionosphere Research Laboratory of Kyoto University for their discussions.

Thanks are also given to Mr. Kozaburo Ikushima, director of Kashima Branch, Radio Research Laboratories, and to Mr. Risao Hayashi, chief of space communication research section, Radio Research Laboratories for their encouragements.

It should be added that all numerical computations were carried out at the Data Processing Center, Kyoto University.

The works in this thesis were done in the Department of Electronics, Kyoto University, Kyoto, Japan.

PREFACE

This thesis concerns a study on the applications of antenna arrays to satellite tracking by interferometry and to adaptive rejection of interference. The antenna arrays have the feature that their specific characteristics can be specified by appropriately controlling the amplitude and/or phase of the excitation of each element. According to this feature, antenna arrays have been studied by many researchers for various applications. One of the most remarkable features of antenna arrays is, for example, fast scanning capability. Therefore, studies on the phased arrays have been flourished in antenna array engineering.

In addition, antenna arrays have the particular features which cannot be accomplished by a single antenna. They are, for example, (1) accurate direction finding of an incident wave with frequency below VHF (very high frequency) due to the limitation of physical dimension and (2) null steering while maintaining the antenna response toward a certain direction. Two problems discussed in this thesis are mainly related to the features mentioned above.

This thesis consists of two parts, which are as follows.

In PART 1, the interferometer system for satellite tracking is developed for high precision measurement of satellite orbits. Discussions are first made on the new type of receiver for interferometer system. Some experiences on the interferometer measurement of

satellite orbits gave us the idea of modifying the phase-lock-loop which is useful to the interferometer receiver. Next, unequal spacing of the elements of the interferometer itself is also investigated to resolve the ambiguity in angular measurements for satellite tracking. In addition, the star-shaped baseline arrangement for satellite tracking is proposed that gives the optimum compromise between the cost and accuracy. The interferometer system and the receiver are implemented in a small station, which are developed in this thesis and show the sufficient performance for satellite tracking. Error analysis on an interferometer is also carried out, especially with relation to the influence of the secondary wave originating from scattering objects in the environment.

PART 2 deals with the other application of antenna arrays, which is called, in general, the adaptive array for interference rejection. This system cancels out the interferences from the external sources by making use of their coherence at each element. After survey of the previous works on this topic, adaptive array under new constraint condition named "directional constraint" is established. Detailed analyses on this and extended system give the perfect understanding of our systems in transient and steady state. The analysis gives only the mean behavior of the system, and some computer simulation experiments are carried out to investigate the behavior under more realistic environment. The usefulness of the analyses is thus verified with good agreement between the theory and the experiments.

CONTENTS

PART 1.

A RADIO INTERFEROMETER SYSTEM FOR SATELLITE TRACKING

Chapter 1. GENERAL INTRODUCTION

After successful launch of the first artificial satellite "SPUTNIK 1", a large number of satellites have been operating on orbits. These satellites have their own mission objectives, practical, technological or scientific.

For their mission objectives, measurements of a position of the satellite are indispensable for orbit control, accurate pointing of a high-gain antenna of an earth station, reference of the physical parameters in scientific experiments and so on.

The methods to measure satellite orbits are divided into two categories, i.e. the active method such as range and range rate measurement method and the passive method such as Doppler frequency counting method and interferometer method. The active method tends to be larger scaled because it requires a transmitter in the earth station and a transponder on the satellite, which makes this method look more suitable to a large earth station which accedes to geostationary satellites.

On the other hand, passive methods utilize only a received signal so that relatively simple system may suffice for the purpose described above. Among them, Doppler frequency counting method[1] is not self-supporting and requires some complementary measurements. On the contrary, the interferometer measurements give the angular data versus time in self-contained manner, so it may be especially suitable to small independent stations.

The well known system for satellite tracking by interferometry is the minitrack system by NASA[2]. In Japan, an experimental interferometer system with simplified configuration for satellite tracking was constructed and tested at Kyoto University[3]. Based on the experience of the latter, this PART 1 of the present thesis describes the advanced interferometer system for satellite tracking. In the following chapters, the efforts to accomplish the system are described.

Chapter 2 deals with the receiver system which possesses an improved phase-lock-loop designed for the use in interferometer measurements. The signal from a satellite suffers from Doppler frequency shifts so that the frequency tracking by a phase-lock-loop is necessary for signal reception with high signal-to-noise ratio. In addition, the signal level from an interferometer varies according to the travel and attitude of a satellite and Faraday rotation effect, and sometimes falls below the noise level of a receiver. Therefore, the improved phase-lock-loop needs to be modified to ensure the stationary reception of the signal described above.

In Chapter 3, an optimal baseline arrangement of an interferometer system for satellite tracking is described. First, a comparison between several baseline arrangements is carried out through evaluation of the tracking sensitivity. For rating these baseline arrangements, the other approach is also carried out through comparison of the ranges of orbital inclination and right ascension of ascending node for which a satellite passes across two or more array normal planes of interfer-

ometers. In addition, an interferometer composed of four unequally spaced antennas is proposed which is effective for ambiguity resolution. The experimental results using the interferometer receiver and the interferometer system developed in this chapter are discussed briefly.

Error analysis of an interferometer is written in Chapter 4. Our discussion is concerned mainly to the problem of secondary waves retransmitted from surrounding objects of the interferometer. To generalize the treatment of this problem, statistical approach is proposed. Numerical analysis is described for the case of two-element interferometer.

Summary and conclusion are described in the final chapter to drop a curtain for PART 1.

Chapter 2. AN INTERFEROMETER RECEIVER FOR SATELLITE TRACKING[4],[5]

2.1 Introduction

As widely known, an interferometer system makes use of the interference phenomenon to measure the incident direction of a wave. Among them, simple additive interferometer utilizes the feature the amplitude of combined signal varies in accordance with the angle of incidence of a wave. For easy understanding of the following explanations, the principle of a radio interferometer is given here.

For simplicity, we treat the case of an interferometer consisting of two element-antennas. As shown in Fig.I.2.1, assume that the radio wave with a wavelength of λ, is incoming from the direction of angle θ to the antenna system, then we have the amplitude, V_s, as the sum of the outputs of both antennas produced by the hybrid circuit, which is given as follows.

$$V_s \propto \left|\cos \frac{\psi}{2}\right| \qquad \text{(I.2.1)}$$

$$\psi = \frac{2\pi d}{\lambda} \cos \theta \qquad \text{(I.2.2)}$$

where ψ is the phase difference caused by the path-length difference, d cos θ, and d is a separation between two antennas. The amplitude V_s is shown in Fig.I.2.2 in terms of ψ. Thus, if the incident angle of a wave varies with time, amplitude detected signal may give a relationship between the incident angle of a wave and the time. According to

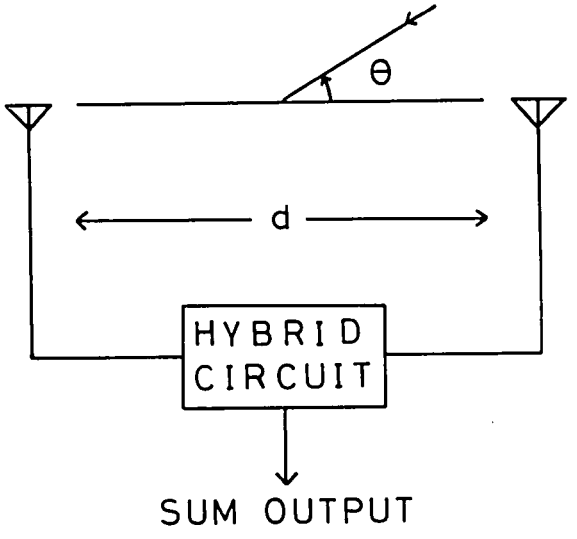

Fig.I.2.1 Two-element interferometer

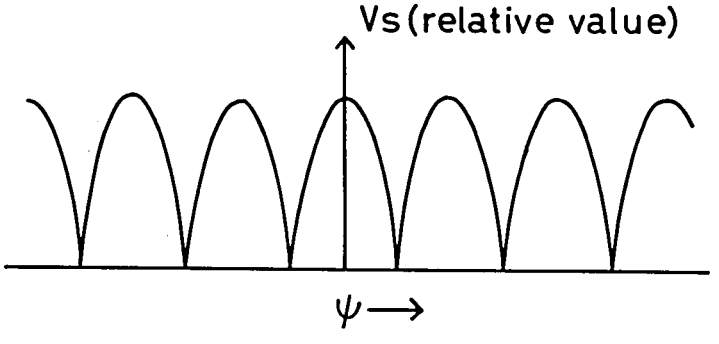

Fig.I.2.2 Interferogram of a two-element interferometer

this principle, the path of a satellite on the celestial sphere can be measured by means of an interferometer system.

Then, it is to be noted that the frequency of a wave transmitted from a satellite generally suffers from Doppler frequency shifts and turns to be higher when a satellite is approaching to the observer and lower when going away (up to the part of $\pm 3 \times 10^{-5}$ of the primary frequency). Therefore, it is necessary to set a phase-lock-loop (PLL) in the receiver to compensate the Doppler frequency shifts. By doing this, we can design a narrow bandwidth of a receiver because of the function of a PLL, which results in better signal-to-noise ratio reception. When we employ this technique in an interferometer system, however, we get a great disadvantage. As described in this section, because of the existence of null points in the interferograms, conventional PLL may run out of locking at these points, and the frequency of voltage-controlled oscillator (VCO) may change freely from the frequency of incident signal. We had to develop a new technique to prevent this malfunction of VCO by inserting a switching circuit into the PLL and manufactured an improved receiving system.

In the following sections, the outline of a new PLL is described.

2.2 Conventional Phase-Lock-Loop

Phase-lock system is an application of feedback control concept. In Fig.I.2.3, the block diagram of a basic phase-lock-loop

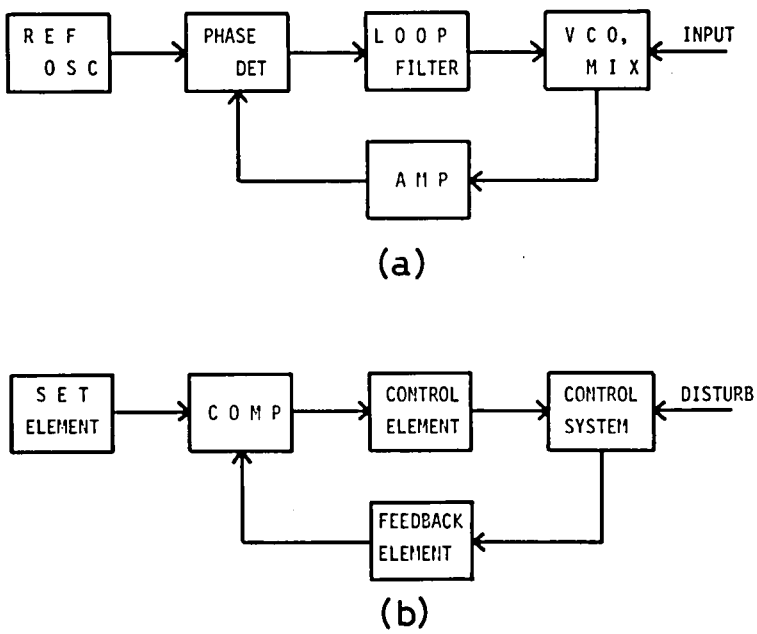

Fig.I.2.3 Comparison between a basic phase-lock-loop and an automatic control system
(a) Block diagram of a basic phase-lock-loop
(b) Block diagram of an automatic control system

and an automatic control system are shown for comparison. The operation of a PLL is explained according to these figures.

The received signal is translated into the intermediate frequency (IF) by a mixing circuit. The output of VCO is used as a local oscillator signal. The IF signal obtained by a mixer is compared with a reference signal on frequency and phase. This comparison is made by means of a phase detector whose output is proportional to phase difference between the IF signal and the reference signal. The phase detector corresponds to the comparator in the automatic control system shown in Fig.I.2.3. The frequency and phase of VCO signal are controlled by the DC component of the output of the phase detector which is proportional to the phase difference between those two signals (error signal) to minimize it. By this operation, the frequency and the phase of IF signal are made equal to those of the reference signal. Loop filter shown in Fig.I.2.3 eliminates the remaining IF signal component from the phase detector output and extracts the DC component to drive the VCO. It is to be noted, however, to maintain the control voltage needed for locking, it is generally necessary to have nonzero output from the phase detector[6]. Thus, the loop operates with some phase error presents. As a practical matter, however, this error tends to be small if the loop gain is sufficiently high.

In the above discussion, we assumed that the DC component of the output of the phase detector is proportional to the phase difference between two input signals. The amplitude of the reference signal

may be constant, but, if the field strength of a received signal is small, the DC component may not be proportional to the phase difference because of nonlinear characteristics of a phase detector. When the control voltage drops, the frequency of the VCO shifts to run out of locking and we miss the signal. Thus, it is not always suitable to adopt the phase-lock technique into an interferometer system for satellite tracking.

Say, the output of an interferometer, as shown in Fig.I.2.2, has many null points (at these points the input signal disappears), and it is easy to lose locking as mentioned above. And it is impossible to determine the path of a satellite on the celestial sphere when the loop is out of locking. To avoid this fault, master-slave method is effective in which the receiver connected to the broad directivity antenna supplies the stable VCO signal to the interferometer receiver as shown in Fig.I.2.4[7]. However, in this method, an additional antenna and receiver are necessary, and the system will be more complicated and it is a disadvantage from the economical point of view. So, we must develop a new phase-lock technique which is suitable to the interferometer receiver.

2.3 Improved Phase-Lock-Loop[4],[5]

2.3.1 Principle

As described previously, an output from an interferometer suffers from a large amount of variation in its amplitude when receiving

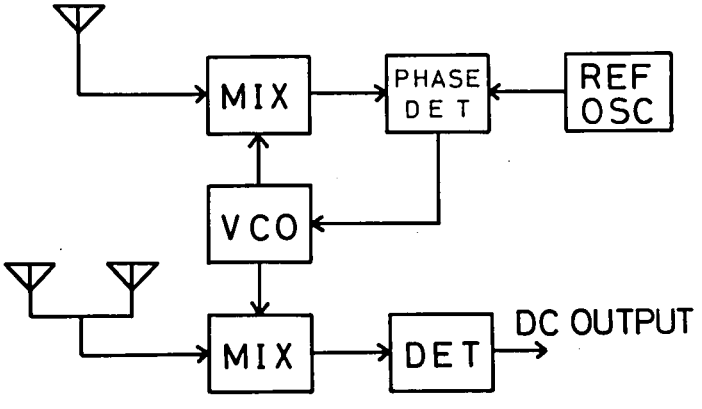

Fig.I.2.4 Example of a phase-lock system for an interferometer receiver

a signal from a satellite. But, we notice that the time interval during which the input signal level is lower than the threshold level of the loop is very short in the neighborhood of these null points of the interferogram. It is, therefore, to be considered that the difference between the received signal frequency before and after the interval described above is negligibly small due to the short period of time. But, closed loop may run out of locking even if the time interval when the signal level undergoes below the threshold level is short. Thus, the loop must be interrupted when the input signal drops below the predetermined level. When the input signal again arises to exceed the predetermined level, its frequency varies only slightly to the value before the time when the loop is interrupted. The control voltage holds the previous value because its time constant of discharge is very large, so that both frequencies of VCO and the received signal are almost identical to each other and the loop is easily relocked.

In Fig.I.2.5, a block diagram of the interferometer receiver with improved phase-lock-loop is shown. This system is composed of the ready made double conversion type receiver and the frequency conversion section from UHF to HF band consisting of the PLL mentioned above. For the recording, the AGC voltage and the phase sensitive detector output are provided. Reference oscillator (REF OSC) supplies the 455 KHz signal which is generated by frequency dividing the output of the crystal oscillator. And to stabilize the frequency, we use a voltage-controlled-crystal-oscillator (VCXO) as a local oscillator.

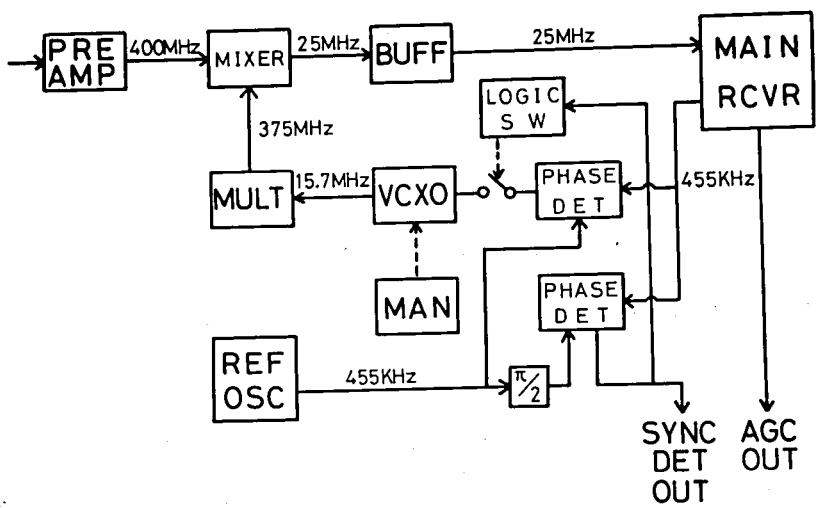

Fig.I.2.5 Block diagram of the interferometer receiver

The external view of the receiver is shown in Fig.I.2.6 and the performance of this receiver is summarized in Table I.2.1.

2.3.2 Operation

The block diagram of the PLL for interferometer receiver is shown in Fig.I.2.7 and the operation is explained in accordance with this figure. At first, the "FORCED LOCK" switch is closed. So the flip-flop circuit (FF) is driven to close the relay-2 and to open the "OR" gate by this pulse signal, and the relay-1 is closed by the operation of the Drive-circuit. Thus, the loop is closed by these operations. Next, the biased voltage of the VCXO is controlled to tune in the incident signal by adjusting the "MANUAL SLEW" knob. At this time, the output voltage of the phase sensitive detector (PD 2) appears and the Schmidt-circuits are driven. The relay-2 is also driven by the output of the Schmidt-circuit. When the field strength of the input signal decreases because of the interference, the intermediate frequency (IF) signal also decreases and as described in 2.3.1, the output voltage of the PD 2 becomes smaller. As soon as this voltage becomes smaller than the predetermined voltage, the "OR" gate is closed and the relay-2 is opened, as the output voltage of the Schmidt-circuit decreases to zero. Thus, the loop remains cut off. In these intervals, the VCXO is controlled by the voltage held by the "CHARGE" circuit. This voltage is discharged with sufficiently large time constant. If the satellite's signal recovers very soon, the frequency variations of the VCXO and

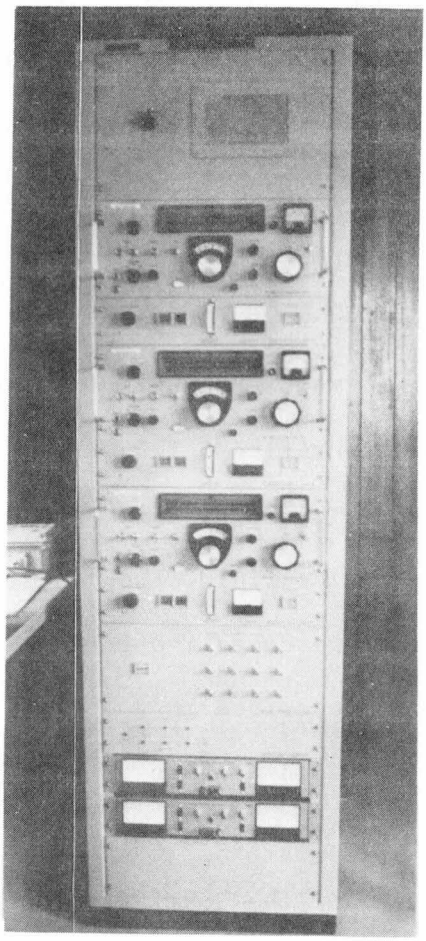

Fig.I.2.6 External view of the interferometer receiver

FREQUENCY RANGE OF RECEPTION	399-403 MHz
TYPE OF RECEIVER	THREE CONVERSION TYPE PHASE SYNCHRONOUS DETECTION
SENSITIVITY	-140 dBm (S/N 10 dB)
NOISE FIGURE	LESS THAN 3 dB
INPUT IMPEDANCE	50 ohms
FREQUENCY STABILITY	LESS THAN 10^{-8}/10 min.
FREQUENCY RANGE OF TRACKING	15 KHz
EQUIVALENT NOISE BANDWIDTH	50 Hz, 200 Hz
NUMBER OF CHANNELS	3*
OUTPUT VOLTAGES OF PHASE SYNCHRONOUS DETECTOR	2 volts (input power -140 dBm)
HF SECTION	NRD-1EL

*Three interferometers are provided.

Table I.2.1 Performance of the interferometer receiver

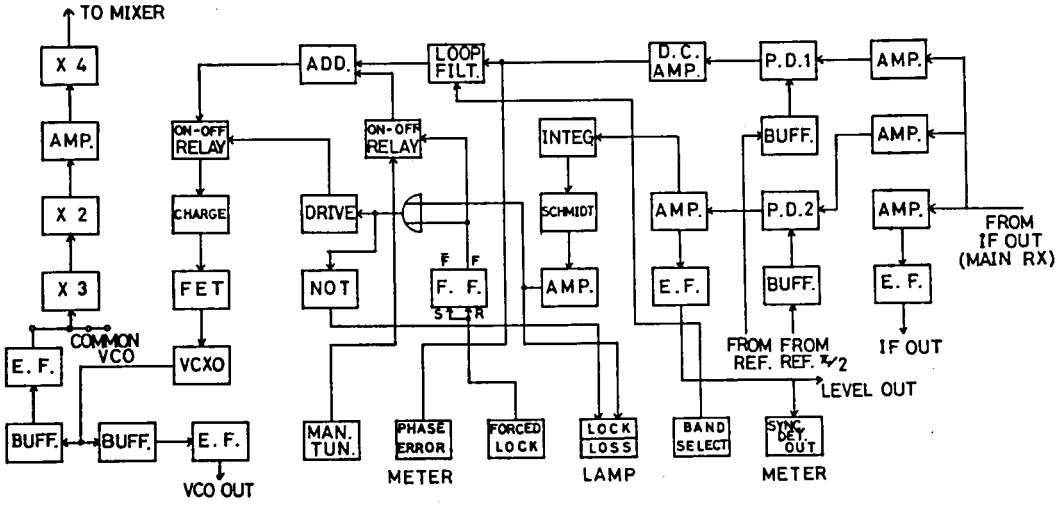

Fig.I.2.7 Block diagram of the improved phase-lock-loop

the satellite's signal are so slight that it is sufficient for relocking. Then, the voltage appears at the output terminal of the Schmidt-circuit. By this output voltage, the OR-gate is driven to open and the relay-2 is closed. And the loop is reconnected. As previously discussed, the frequency of IF signal may be within the capture range of PLL, relocking will be performed when loop is reconnected. When the PLL is in locking, the indicator "LOCK" is lighted up by the output voltage of the Schmidt-circuit and when out of locking, "LOSS" is lighted up by the NOT output voltage of the OR-gate.

If the PLL is still out of locking by some reasons, retuning will be performed as done in initial acquisition described in the previous part of this section.

2.4 Performance of the System

To verify the performance of this new developed PLL system, some experimental observations were carried out by receiving the signal from the satellite OGO-6 (1967-51A). The antenna system used in this experiment consists of two half-wavelength dipole antennas whose spacing is about 15 meters oriented almost in the north-south direction. As the satellite OGO-6 is a polar orbitting satellite so that there are many occasions when its path on the celestial sphere lies almost in the north-south direction.

The record of the interferogram obtained by the experimental observation of the signal from the satellite OGO-6 is shown in Fig.I.2.8.

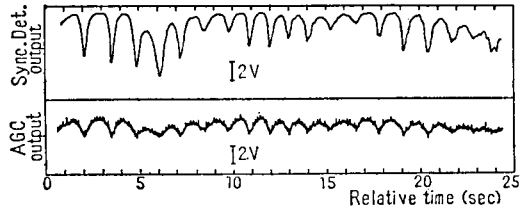

Fig.I.2.8 Observed interferogram using the signal from OGO-6.

Any efforts are not given to the phase adjustment and impedance matching procedures, however, the effect of interference is indicated clearly in this figure. Nonuniformity of null depths in the interferogram is caused by the phase characteristics of the antennas and the effect of standing wave.

In this experiment, we did not see the time lag of the rising of recording voltage just after the null points of the interferogram which might have affected our purpose. It is to be considered that the reconnection of the loop is well performed to relock in to the satellite signal. Thus, this proved the usefulness of this technique described above to the interferometer receiver.

2.5 Concluding Remarks

The principle and operation of the improved phase-lock-loop are described for the interferometer receiver for satellite tracking. In accordance with the motion of satellites, the output of an interferometer system varies periodically so that it is difficult to operate a phase-lock-loop stably. However, it is necessary for compensating the frequency shift of satellite signal due to Doppler effect. By making use of a very short period during which the signal level is lower than the threshold for holding PLL in locking, improved phase-lock-loop is developed in which loop is connected or cutted off by the logic switch in accordance with the level of received signal.

A receiver system is designed and manufactured including this

concept of PLL, and this exhibits the sufficient performance as an interferometer receiver for satellite tracking through some experimental observations.

Chapter 3. BASELINE ARRANGEMENT OF A RADIO INTERFEROMETER SYSTEM FOR SATELLITE TRACKING

3.1 Introduction

To determine the path of a satellite on the celestial sphere, two angular parameters (the elevation angle and the azimuth angle, for example) are usually necessary. The quantity measured with an interferometer is the phase difference caused by the path length difference of propagation to each antenna. This phase difference is proportional to the direction cosine of the angle between the ray direction of incident wave and the baseline of an interferometer. As shown in Fig.I.3.1, measured phase difference for A-B baseline interferometer and C-D baseline interferometer are given by the followings, respectively.

$$\psi_{AB} = \frac{2\pi d}{\lambda} \cos\theta \cos\phi \qquad \text{(I.3.1)}$$

$$\psi_{CD} = \frac{2\pi d}{\lambda} \cos\theta \sin\phi \qquad \text{(I.3.2)}$$

where d is a spacing between two element-antennas, λ is the wavelength of the incident signal, θ is the elevation angle and ϕ is the azimuth angle of a satellite. As the spacing d and the wavelength λ are the known parameters, by measuring the phase differences we can calculate the two direction cosines. But, direction cosine generally consists of two angular parameters. Therefore, by arranging two base-

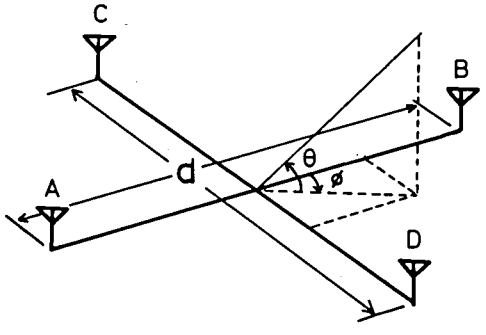

Fig.I.3.1 Baselines of an interferometer system and an incident wave

lines of an interferometer system at right angle as above, we can calculate the direction cosines with respect to both baselines and obtain the elevation angle θ and the azimuth angle ϕ of a satellite as follows.

$$\phi = \tan^{-1} \frac{\psi_{CD}}{\psi_{AB}} \tag{I.3.3}$$

$$\theta = \cos^{-1} \left\{ \frac{\lambda \psi_{AB}}{2\pi d \cos(\tan^{-1} \frac{\psi_{CD}}{\psi_{AB}})} \right\} \tag{I.3.4}$$

The measurements of the phase differences ψ_{AB} and ψ_{CD} can be performed through evaluations of the interferograms which are generated by the motion of a satellite crossing the lobes of interferometers.

However, if the path of a satellite is assumed to be almost perpendicular to the baseline, i.e. almost parallel to the lobes of an interferometer, it is impossible to measure the changes of direction cosine accurately. Say, the system's sensitivity to the changes of satellite position decreases in such case. "Tracking sensitivity" was defined by Takao and Abe[8] to evaluate the performance of satellite tracking system to the changes of orbit parameters of a satellite. According to their paper, tracking sensitivity for an interferometer decreases as the angle between the path of a satellite and the baseline of an interferometer increases from 0 degrees and finally falls to zero at 90 degrees. In the case of conventional cross type baseline arrangement, we have such chance certainly when the angle between the

path of a satellite and the baseline of an interferometer is almost perpendicular. Especially if the orbital inclination of a satellite is near 90 degrees or almost equal to the observer's latitude, very often occurs this phenomenon.

Therefore, we must develop a new interferometer system which can measure the path of a satellite with any orbital elements.

3.2 Spacing Design of a Linear Four-Element Interferometer[9]

Prior to the discussions of the baseline orientation, composition of an interferometer is described briefly. The total directivity of an additive type interferometer consisting of two antennas is given by the followings.

$$f(\psi) = E_0 \left|\cos \frac{\psi}{2}\right| \qquad \text{(I.3.5)}$$

where $f(\ )$ is the directivity of an interferometer system, E_0 is the element factor and ψ is the phase difference described as (I.3.1) or (I.3.2), $\left|\cos \frac{\psi}{2}\right|$ is the array factor produced by two antennas.

A spacing between two antennas is generally chosen large enough compared with the wavelength of operating frequency so that the beamwidth of the element-antenna is wide enough compared with the beamwidth of grating lobes. Thus, as shown in Fig.I.3.2, the grating lobes with almost equal amplitude appear, which results in the ambiguity to determine the angular parameters of a satellite.

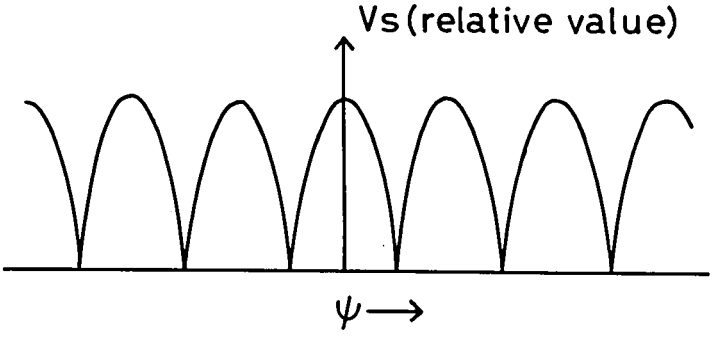

Fig.I.3.2 Interferogram of a two-element interferometer

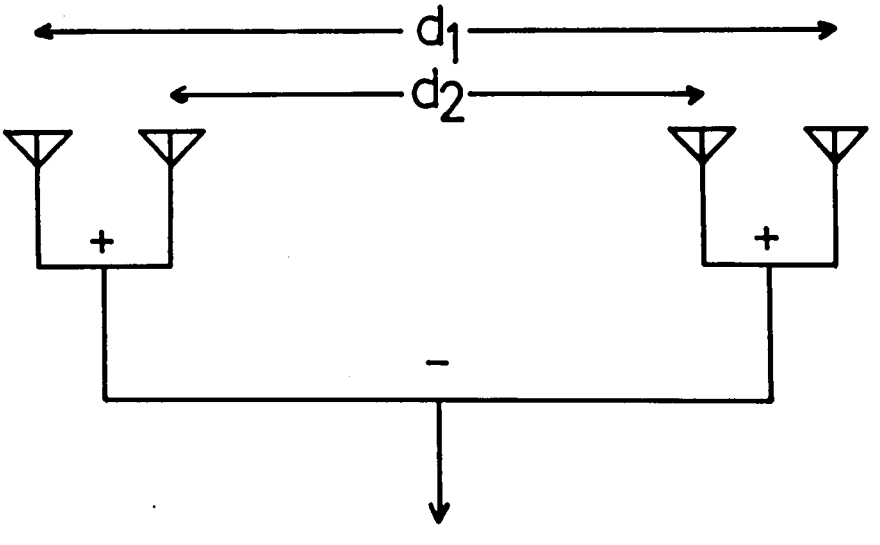

Fig.I.3.3 Four-element interferometer

To resolve this ambiguity, it is sufficient to add one more element-antenna to an interferometer composed of two element-antennas[10]. For the ease of a design of feed network, however, it is considered to develop an interferometer composed of four element-antennas by adding a pair of element-antennas. The interferometer is designed to be symmetric with respect to the midpoint of two sub-arrays. The arrangement is shown in Fig.I.3.3. It is desirable to detect the time when a satellite crosses the array normal because the measurement in this direction can be performed accurately than the others[9]. Thus, the directive pattern with null toward the array normal direction is suitable for this purpose. This feature can be realized by subtracting the outputs of two sub-arrays to each other. Thus, the far field pattern of an interferometer composed of four antennas with subtractive beam can be described referring to Fig.I.3.3, as follows.

$$f(\theta) = E_0 \left| \cos\left(\pi \frac{d_1-d_2}{2\lambda} \cos\theta\right) \times \sin\left(\pi \frac{d_1+d_2}{2\lambda} \cos\theta\right) \right| \quad \text{(I.3.6)}$$

where E_0 is the element factor and is assumed to be identical at each element-antenna. d_1 and d_2 are the separations of outer and inner pair of antennas. λ is a wavelength of incident signal and θ is an incident angle of a signal measured from the baseline of an interferometer.

To determine the optimal ratio d_1/d_2, we define the additional two variables as follows.

$$r = d_1/d_2 \quad , \quad d_1 > d_2 \tag{I.3.7}$$

$$\phi_T = (2\pi d_2/\lambda)\ \cos\theta \tag{I.3.8}$$

Thus, the array factor of (I.3.6) can be rewritten by the following equation.

$$F_a = \left|\cos \frac{\phi_T}{4}(r-1) \times \sin \frac{\phi_T}{4}(r+1)\right| \tag{I.3.9}$$

In Fig.I.3.4, the array factors are shown as a function of ϕ_T with changing the parameter r. Referring to these figures, depicted patterns consist of two spatial frequency components, i.e. a component with short period repetition which corresponds to the term containing $(d_1+d_2)/2$ and a component with long period repetition which corresponds to the term containing $(d_1-d_2)/2$. In addition to them, much lower spatial frequency component introduced by the element factor is, in practice, multiplied to these figures[11]. In the case with larger r, it is easy to distinguish the higher spatial frequency component, however, on the contrary, it is difficult to identify the lower spatial frequency component because of the approach of these components to each other. On the other hand, with small r, the contrary effect to the above statement occurs. The strength of the signal from a satellite varies largely due to the effect of spin fading and/or Faraday rotation of polarization

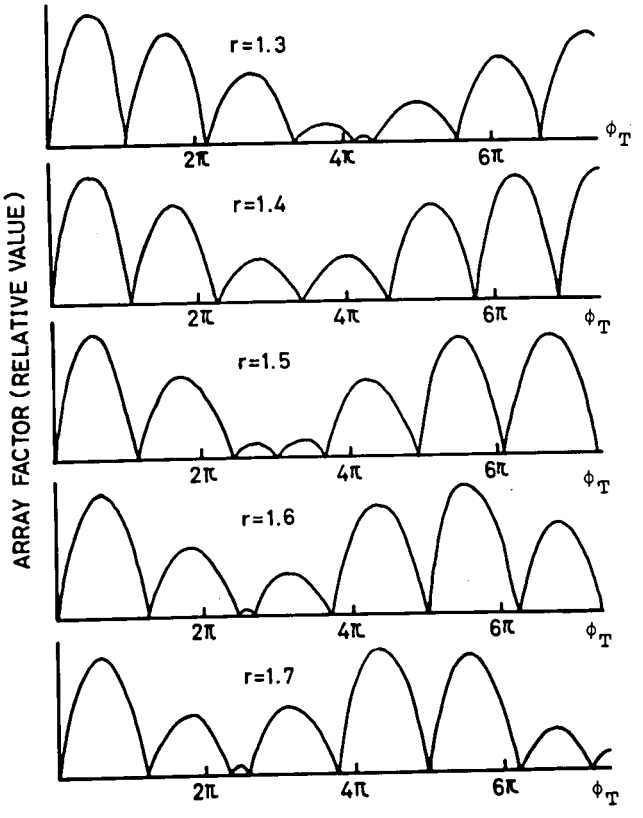

Fig.I.3.4 Variation of an array factor of a four-element interferometer as a function of a ratio of spacings between the inner and the outer pair of element-antennas

angle. Thus for the accurate identification of an incident angle and a null direction in an interferogram, it is necessary to have sufficient difference between the peak and the null in an interferogram. With consideration to these points, spacing ratio r is chosen to be equal to 1.5. Thus, (I.3.9) is rewritten as follows.

$$F_a = |\cos\psi_r \times \sin 5\psi_r| \qquad \text{(I.3.10)}$$

$$\psi_r = \frac{\pi d_2}{4\lambda} \cos\theta \qquad \text{(I.3.11)}$$

The array factor of (I.3.10) is again depicted in Fig.I.3.5 as a function of ψ_r. In Fig.I.3.5, solid line denotes the array factor F_a, broken line denotes the term $\sin 5\psi_r$ and chain line denotes the term $\cos\psi_r$ in (I.3.10), respectively. The term $\cos\psi_r$ is an array factor of sub-arrays which are composed of two antennas located on one side with respect to the midpoint of the four-element interferometer. And the term $\sin 5\psi_r$ is an array factor of an array with two imaginary antennas which are located at the midpoints of each sub-array. In practice,the array factor shown in Fig.I.3.5 is multiplied by an element factor so that it is easy to resolve the ambiguity of this interferometer system. Thus, it is easy to identify the nulls of interferogram with incident angles of a signal from a satellite.

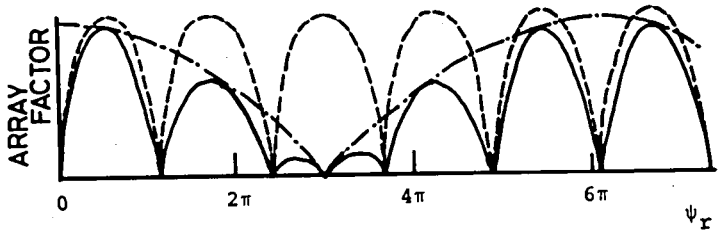

Fig.I.3.5 Array factor and spatial frequency components

3.3 Insensibility of an Interferometer against a Certain Satellite Path

Measurements of satellite path on the celestial sphere by means of a radio interferometer system are made by observing a signal from a satellite which is amplitude modulated due to the motion of a satellite passing through the interferometer pattern. The interferometer pattern is fan-shaped with multiple null points along the baseline like a comb. And the interferometric observation is carried out by reading the time when a satellite passes across a certain null direction. The steepness of the interferometer pattern near null points is almost proportional to the cosine of the angle between the baseline and a satellite path projected onto the ground. Thus, it is desirable that the baseline orientation is parallel to a satellite path because of the steepness of the null pattern.

To evaluate the accuracy of the measured quantity by means of an interferometer, the concept of "tracking sensitivity" was introduced by Takao and Abe. In their paper, tracking sensitivity for Doppler measurement was also treated, however, only for interferometer measurement is discussed here. Tracking sensitivity was defined as a partial derivative of the measured quantity with respect to the orbital element. Namely, tracking sensitivity is a measure how the measured quantity is modified when the orbital elements vary slightly from their nominal values. Among them, tracking sensitivity for time is suitable to discuss the baseline orientation of an interferometer.

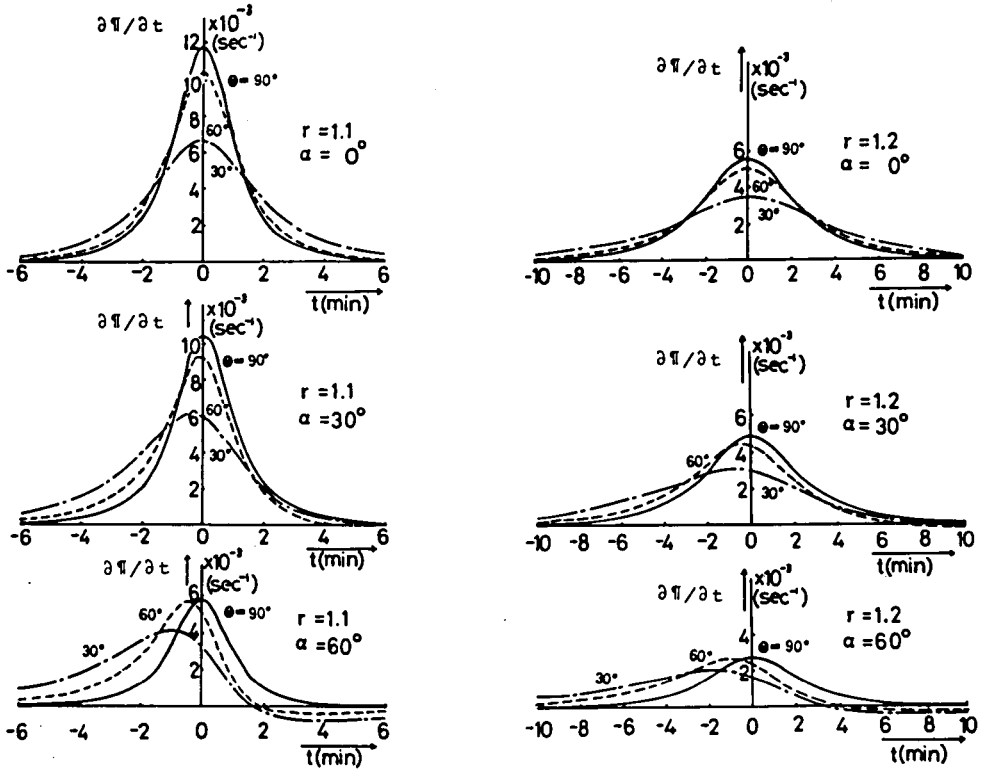

Fig.I.3.6 Tracking sensitivity of an interferometer for time (after Takao and Abe[8])

Calculated results of tracking sensitivity for time is shown in Fig.I.3.6[8]. Calculations were made under the assumptions that the satellite orbit is circular and the earth is a spherical body. In these figures, ¶ is a cosine of the angle between the baseline and the direction of a satellite, Θ is a maximum elevation angle of a satellite seen from the observer, r is an orbital radius normalized by the earth's radius and α is the angle between the baseline and a satellite path projected onto the topoplane. Apparently, in the case with $\alpha=0°$, in which satellite path is parallel to the baseline, tracking sensitivity is maximized. And as increasing α, tracking sensitivity decreases for all cases. Comparing with these figures, it can be seen that tracking sensitivity in the neighborhood of the peak is almost governed with $\cos\alpha$. Therefore, in the following discussions, we will be mainly concerned with α.

3.4 Three-Baseline Arrangement of a Radio Interferometer System[9]

To determine the path of a satellite on the celestial sphere, two angular parameters, for example azimuth and elevation angle, are needed. According to this reason, an interferometer system is generally composed of two baselines which are arranged orthogonally to each other[2),(3)]. These baselines are usually oriented in the north-south and the east-west direction. In this configuration, if a satellite path lies parallel to one of the baselines, tracking sensitivity is maximized, on the contrary, when a satellite path is orthogonal to the other baseline,

the tracking sensitivity is minimized, so that it is difficult to determine the satellite path on the celestial sphere. To avoid this fault, it is sufficient to prepare a large number of interferometers whose baselines are oriented in several directions. But it is inappropriate because of the complexity of data processing and the economical point of view.

Now, let us consider the interferometer system with n baselines which cross at equal angle with each other. In this case, the angle between the adjacent baselines is π/n (n=2 for example, corresponds to the conventional cross type baseline arrangement). We can set the angle ζ between the path of a satellite and a baseline as,

$$\pi/n \geqq \zeta \geqq 0 \qquad \text{(I.3.12)}$$

By choosing the proper two baselines out of n, (I.3.12) is valid. The geometry of this relationship is shown in Fig.I.3.7. As described previously, the tracking sensitivity is about one half of the maximum value at the angle ζ equaled to $\pi/3$. Therefore, for restraining the decrease of tracking sensitivity within a half of its maximum value, it is desirable that the number of baselines n should be equal to or greater than 3. A larger number of baselines n will make the condition of observation better according to (I.3.12). However, the system will be more complicated and its expense will be larger.

In n baseline interferometer system, the elevation angle θ

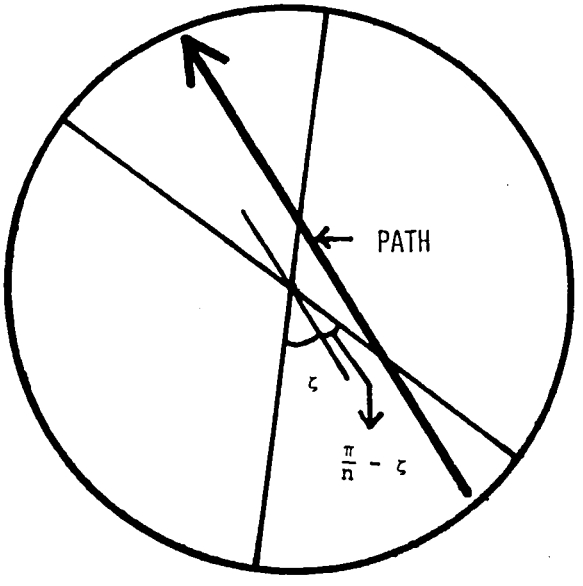

Fig.I.3.7 Geometrical relationship between interferometer's baselines and a path of a satellite

and the azimuth angle ϕ of a satellite can be calculated easily as a following manner from the direction cosines a and b obtained by two baselines out of n.

$$a = \cos\theta \cos(\phi - \frac{m}{n}\pi) \tag{I.3.13}$$

$$b = \cos\theta \cos(\phi - \frac{m+1}{n}\pi) \tag{I.3.14}$$

From (I.3.13) and (I.3.14), the following equation is obtained.

$$\frac{a}{b} = \frac{\cos(\phi - \frac{m}{n}\pi)}{\cos(\phi - \frac{m+1}{n}\pi)} \tag{I.3.15}$$

Then, expanding (I.3.15) and solving with respect to ϕ, the azimuth angle ϕ can be derived as follows.

$$\phi = \tan^{-1} \frac{-a \cos\frac{m+1}{n}\pi + b \cos\frac{m}{n}\pi}{a \sin\frac{m+1}{n}\pi - b \sin\frac{m}{n}\pi} \tag{I.3.16}$$

As the azimuth angle is obtained, the elevation angle θ can be obtained by substituting this into (I.3.13) or (I.3.14) as follows.

$$\theta = \cos^{-1} \frac{a}{\cos(\phi - \frac{m}{n}\pi)} = \cos^{-1} \frac{b}{\cos(\phi - \frac{m+1}{n}\pi)}$$

By summing up these results, we choose n = 3, which means that the baselines are crossed on each other with the angle of $\pi/3$ in the shape of

asterisk. This selection is based upon the study on the tracking sensitivity in terms of time.

Here, let us change our standpoint and pay our attention to the number of times when a satellite crosses the direction of the array normal plane of the interferometer system. The reason of this is as;

(1) For the linear four-element interferometer discussed in 3.2, in the array normal direction, interferometer pattern has null which is independent of the error of the spacing between element-antennas.

(2) By assuming that the structure of the troposphere and the ionosphere is concentric spherical, the influence of the refraction in the troposphere and the ionosphere appears only in the elevation angle and we have no errors in the measurements of the azimuth angle.

The comparison is made for the case of n=2 (+), n=3(✳) and n=4(✳) with a criterion whether a satellite may or may not cross the array normal planes at least twice, because of the angular position of a satellite can be expressed by the two angular parameters so that more than two error free measurements are required for accurate observation.

For n=3, the characteristics are different when one of the baselines is oriented in the north-south direction or in the east-west direction. Therefore, in the case of n=3, we will consider these two conditions. In Fig.I.3.8, baseline arrangements of an interferometer system under consideration are shown.

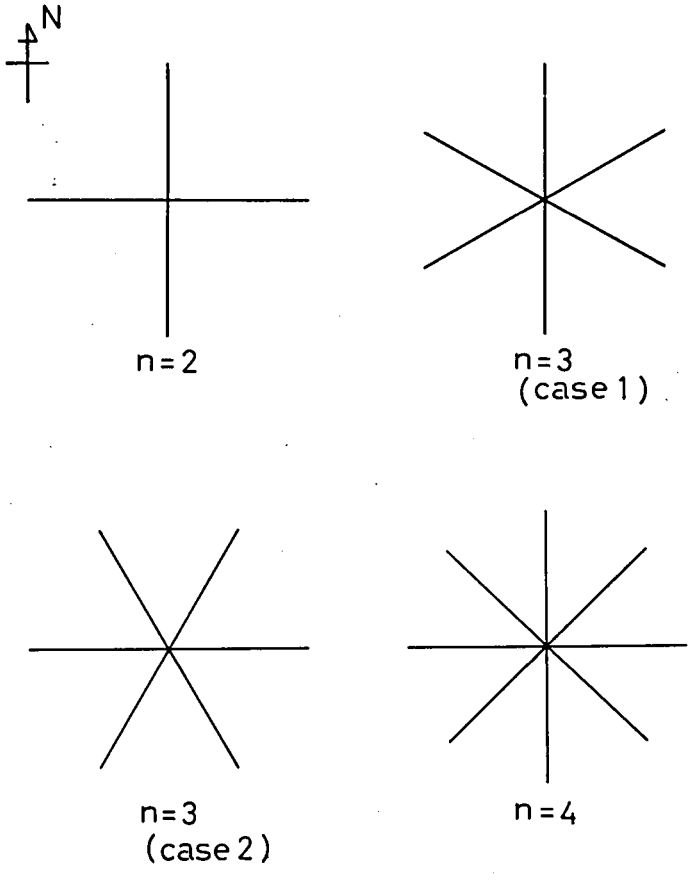

Fig.I.3.8 Some baseline arrangements of an interferometer system under consideration

For evaluation, we choose the coordinate systems shown in Fig.I.3.9. Satellite orbit is assumed to be circular for simplicity of the analysis. Then, a position of a satellite with circular orbit seen from an arbitrary point on the earth can be derived in the topocentric coordinate system as follows[12]. (see Appendix)

$$X_h = R_o\{\cos\omega_s t \sin\Theta \cos(\Phi+\omega_e t) + \sin\omega_s t \cos i \sin\Theta \times \sin(\Phi+\omega_e t) - \sin\omega_s t \sin i \cos\Theta\} \quad (I.3.17)$$

$$Y_h = R_o\{\sin\omega_s t \cos i \cos(\Phi+\omega_e t) - \cos\omega_s t \times \sin(\Phi+\omega_e t)\} \quad (I.3.18)$$

$$Z_h = R_o\{\sin\omega_s t \cos\Theta \cos(\Phi+\omega_e t) + \sin\omega_s t \cos i \cos\Theta \times \sin(\Phi+\omega_e t) + \sin\omega_s t \sin i \sin\Theta\} - R_E \quad (I.3.19)$$

where R_o is the orbital radius, R_E is the earth's radius, Θ is the observer's latitude, Φ is the difference between the observer's longitude and the longitude of the ascending node (for convenience of the analysis, reference point for longitude is chosen to the ascending node), i is the orbital inclination, ω_s is the angular velocity of satellite motion, ω_e is the angular velocity of earth rotation and t is the current time with reference to the time when a satellite passes across the equatorial plane northward. Azimuth and elevation angle can be derived using (I.3.17), (I.3.18) and (I.3.19) as follows.

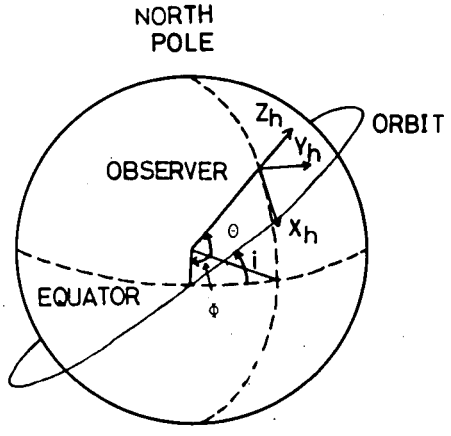

Fig.I.3.9 Longitude-latitude coordinate system and topocentric coordinate system

$$\phi = \tan^{-1}\left(-\frac{Y_h}{X_h}\right) \tag{I.3.20}$$

$$\theta = \cos^{-1}\frac{X_h^2 + Y_h^2}{X_h^2 + Y_h^2 + Z_h^2} \tag{I.3.21}$$

The azimuth and the elevation angle coordinate system is translated into the characteristic coordinate system for antenna arrays (ξ, η) as follows.

$$\xi = \cos\theta \sin\phi \tag{I.3.22}$$

$$\eta = \cos\theta \cos\phi \tag{I.3.23}$$

where ξ and η are the direction cosines at the observation point for east-west direction and the north-shouth direction, respectively. In Fig.I.3.10, characteristic coordinate system for antenna arrays is shown.

Using (I.3.17), (I.3.18), (I.3.19), (I.3.20) and (I.3.21), computations are carried out to find a range of a difference angle between the longitude of observer and the longitude of ascending node in which a satellite passes across the array normal planes at least twice in terms of orbital inclination. The regions in which the necessary condition is satisfied are shown in Fig.I.3.11 for four cases discussed previously. In computations, observer's latitude is chosen to be equal to 34.9064°N which is the latitude of our tracking station in Uji city, Kyoto.

As a result of computations, the shape of a region in which the necessary condition is satisfied is slightly changed with the alti-

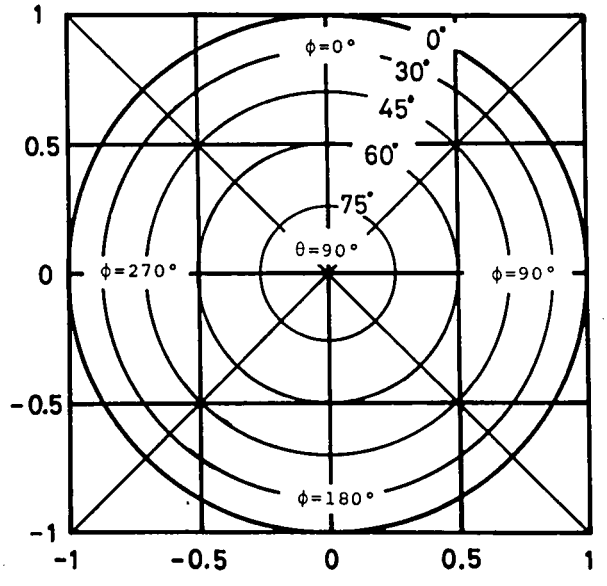

Fig.I.3.10 Characteristic coordinate system for antenna arrays[13]

tude of a satellite. Only its area increases when the altitude becomes higher and decreases when lower. On the other hand, with respect to the observer's latitude Θ, the amplitude of these figures in the orbital inclination domain increases when Θ approaches to 0 degree and decreases when approaches to 90°N or S. Therefore, better observations may be expected for a satellite with small orbital inclination as the observer's latitude approaches toward the equator.

Now, referring to Fig.I.3.11, the area in which the necessary condition is satisfied is wider for an interferometer system with large number of baselines. The calculated areas in angular domains are 11000 (deg^2) for n=2, 20200 (deg^2) for n=3, case 1, 20200 (deg^2) for n=3, case 2, and 23200 (deg^2) for n=4, respectively. Then it is to be noted that the improvement of the performance is remarkable when n is increased from 2 to 3 than when 3 to 4. Special attention is paid to the arrangement n=3, case 1 because of the wider coverage of the acceptable range of orbital inclination than the arrangement n=4.

Summarizing the above discussions, it is concluded that the number of baselines must be chosen to be equal to 3 and one of the baselines must be oriented in the north-south direction. This conclusion is supported by the investigations on the tracking sensitivity discussed previously.

3.5 Results of Observations

Based upon the discussions in the previous section, the inter-

(a)

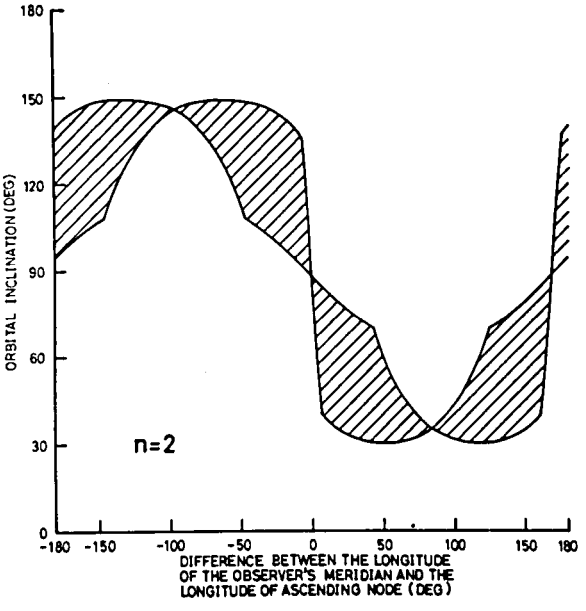

(b)

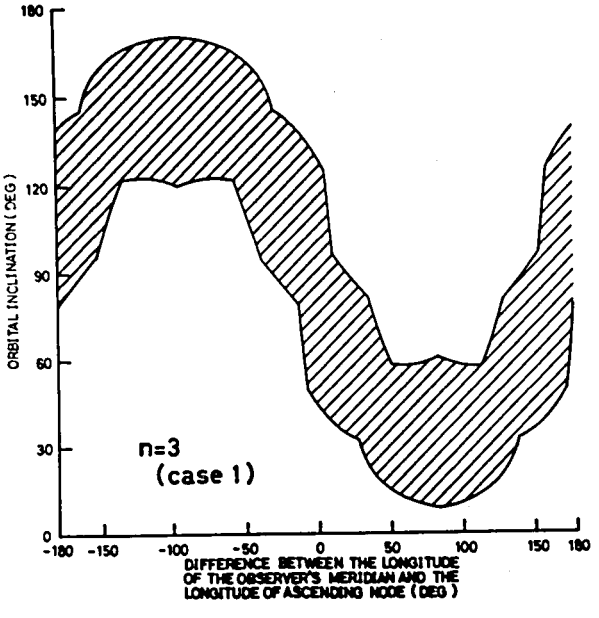

Fig.I.3.11 Comparison of the performance of several baseline arrangements
(a) Two baselines
(b) Three baselines (case 1)

(c)

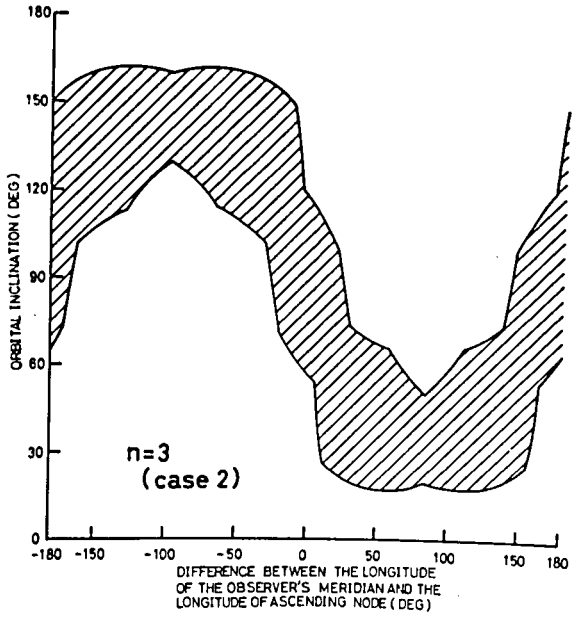

(d)

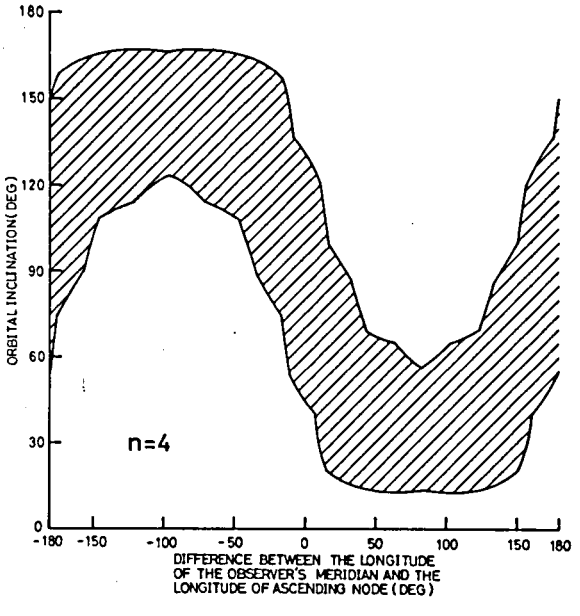

Fig.I.3.11 Comparison of the performance of several baseline arrangements
(c) Three baselines (case 2)
(d) Four baselines

ferometer system for satellite tracking is designed and constructed for the frequency band of 400 MHz. The arrangement of element-antennas and the view of the interferometer system are shown in Figs.I.3.12 and I.3.13, respectively. Spacings between element-antennas d_1 and d_2 (see 3.2) are chosen as 40 meters and 26.7 meters, respectively. Each element-antenna is a circularly polarized one, i.e. five-element crossed Yagi-Uda type with three directors and one planar reflector as shown in Fig.I.3.14, to prevent the fading due to the Faraday rotation of polarization angle of a satellite signal through the ionosphere. Signal subtraction between two sub-arrays is performed by using the feature of a circularly polarized antenna that the phase of the output signal shifts with the rotation of an antenna around its axis. This can be performed independently of the frequency in the bandwidth.

Using the interferometer system described above and the interferometer receiver discussed in Chapter 2, some observations of satellite paths are carried out. In Fig.I.3.15, an example of the interferogram obtained through observation of the satellite OGO-6 (1967-51A) is shown. By comparing Figs.I.3.5 and I.3.15, correspondence between large lobes, medium lobes and small lobes may be clearly indicated which is sufficient to resolve the ambiguity. The satellite path can be calculated from these three interferograms as discussed in 3.4. Figs.I.3.16 and I.3.17 show the observed paths and the predicted paths of the satellite OGO-6 by NASA (National Aeronautics and Space Administration, U.S.A.) in solid lines and broken lines, respectively. The numbers

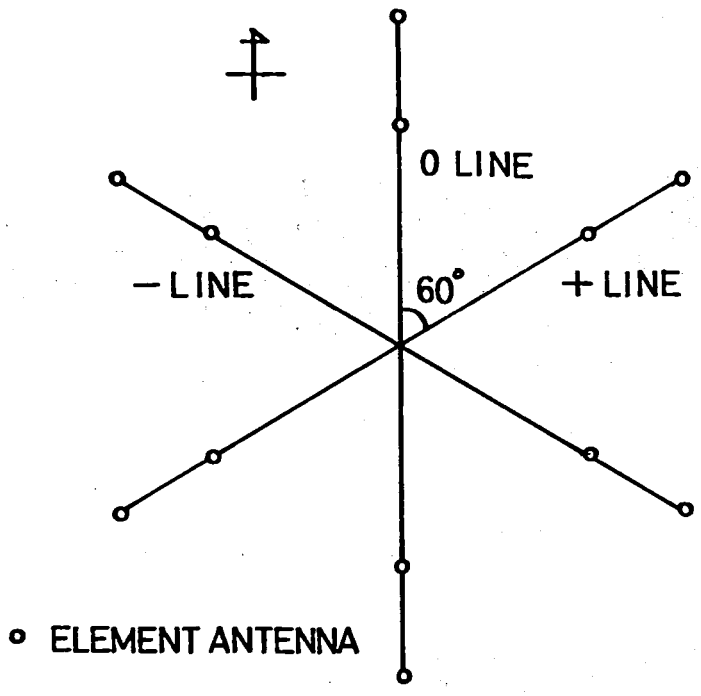

Fig.I.3.12 Arrangement of element-antennas of three-baseline prototype interferometer system

Fig.I.3.13 View of the three-baseline prototype interferometer system

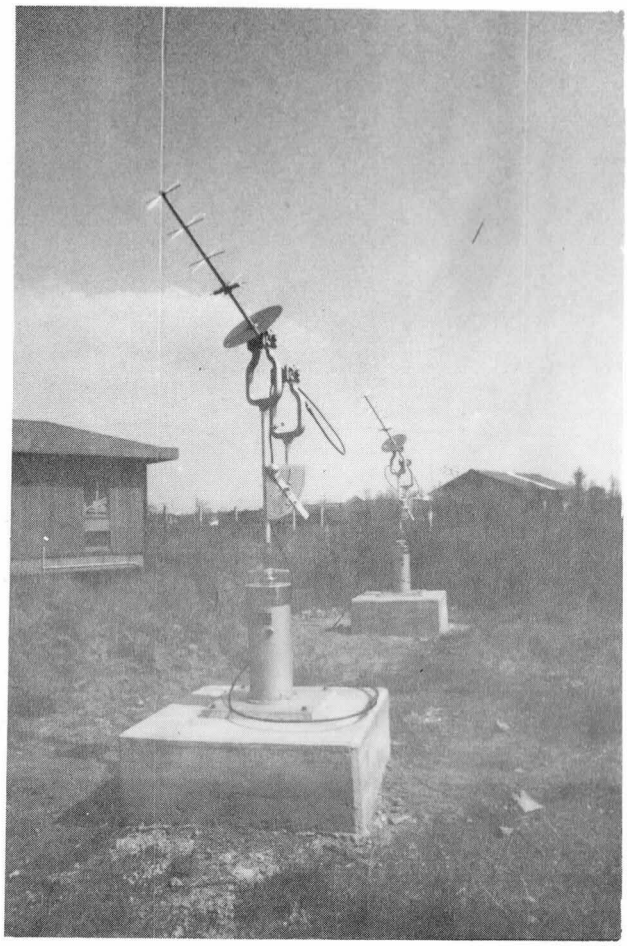

Fig.I.3.14 Element-antenna of the three-baseline prototype interferometer system

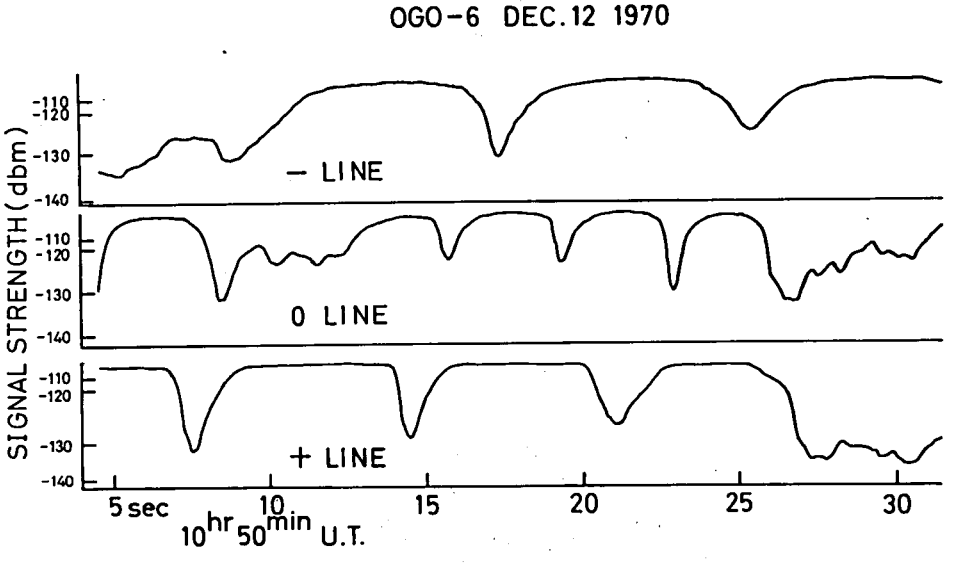

Fig.I.3.15 Example of observed interferogram on December 12, 1970. The satellite is OGO-6 (1967-51A).

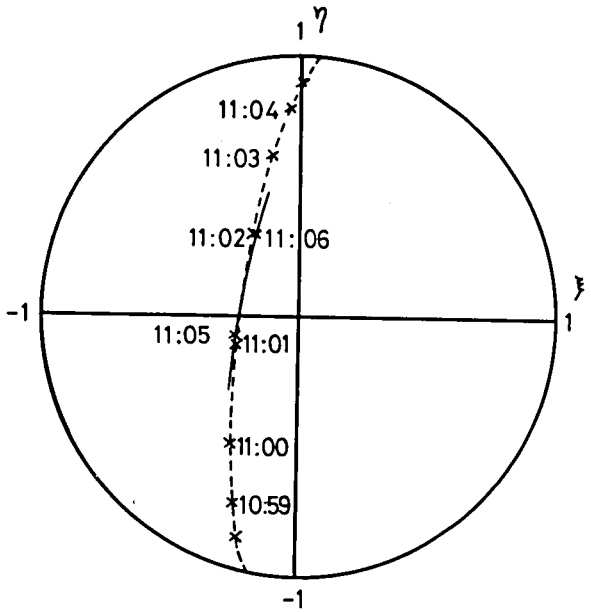

OGO-6 DEC. 10 1970
(10:54 UT - 11:10 UT)

Fig.I.3.16 Experimental result of angle tracking of the satellite OGO-6
——— : observed
----- : predicted (by NASA)

Fig.I.3.17 Experimental result of angle tracking of the satellite OGO-6
——— : observed
----- : predicted (by NASA)

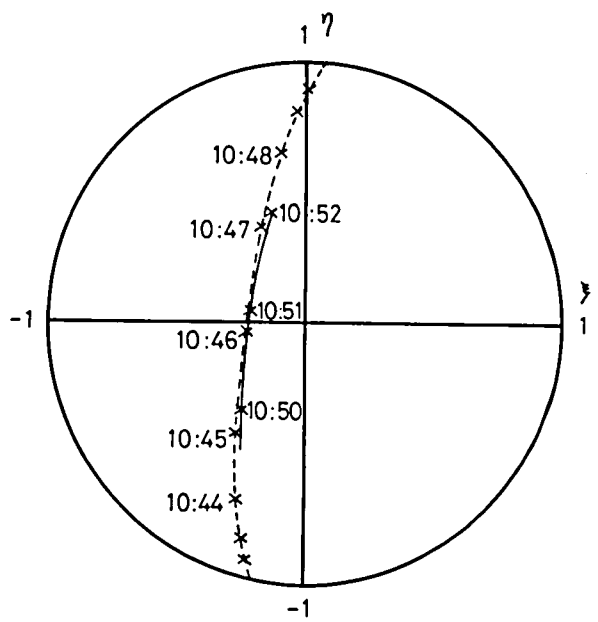

OGO-6 DEC.12 1970
(10:39 UT - 10:55 UT)

seen in Figs.I.3.16 and I.3.17 show the times in U.T. when the satellite passed across those directions. Predicted and observed path shown in Fig.I.3.16 and I.3.17 agree well except for the shift in time domain. This may be interpreted as the variation of the period of satellite motion is so large compared with the remaining orbital elements. This is due to the fact the period of revolution may be easily disturbed by the effects of earth's upper atmosphere, irregularities of earth's gravitational constant and other external forces. Therefore, prediction of satellite orbits may be considered to have some errors in time domain.

The satellite OGO-6 is one of the polar orbitting satellites whose path laid almost in the north-south direction. For such satellite, it was difficult to determine the satellite path by means of a conventional cross type interferometer system. However, through the experimental observations, sufficient performance of the three-baseline interferometer system is proved even for such polar orbitting satellites.

3.6 Concluding Remarks

In this chapter, discussions have been first made on the problem to resolve the ambiguity in an interferometer. The optimum spacing ratio is determined for four-element interferometer, and the experiments show the effectiveness of its performance of ambiguity resolution in spite of its simpleness.

In addition to them, systematic study for optimum design of

an interferometer system for satellite tracking has been carried out. Considerations are made based on the concept of tracking sensitivity. Optimum number of baselines is determined through compromise between the tracking sensitivity and the expense. The same considerations are carried out from the other point of view, say the number of array normal crossing of a satellite may or may not exceed twice for some baseline arrangements because of the peculiarity of its dierction. This result also shows the predominance of three-baseline interferometer system. In addition, it is indicated clearly that one of three baselines must be oriented in the north-south direction.

According to the results obtained in this chapter, the three-baseline interferometer system is designed and constructed for 400 MHz band. Some observations are carried out and its superior performance is proved even for a polar orbitting satellite. This arrangement of baselines can avoid the fault of the conventional cross type interferometer system whose tracking sensitivity is very low for a satellite with polar orbit or small orbital inclination.

Chapter 4. PHASE ERROR OF A RADIO INTERFEROMETER DUE TO A SECONDARY WAVE

4.1 Introduction

As it is widely known, a radio interferometer is a powerful tool for measuring the incident angle of a propagating wave. We have carried out the interferometer measurements of satellite paths as described in the previous chapters and proved the performance for angular measurement. For designing a radio interferometer, evaluations on the measurement error are significant whose sources may be considered as the inaccuracy of hardwares and the ray refraction in the ionosphere and the troposphere. Among the errors caused by inaccurate hardwares, difference of phase characteristics in antennas and in feed cables may cause the phase error in measured value as a constant bias. Thermal noise in receiver may contaminate nulls in the interferogram which results in the erroneous measurement of incident angle. These effects were discussed, for example, by Takao[14]. The effects of the ionosphere and the troposphere were discussed in terms of seasonal variations and solar activities, for example, by Tao[15] and shibata[16] Some studies were published on the effect of refraction of a wave to a radio interferometer[17],[18].

In addition, it is to be considered the existence of secondary waves reflected or scattered from surrounding objects of a radio interferometer also results in the erroneous angular measurements. On this

problem, Duncan[19] studied the effect of ground reflected waves on a radio interferometer. He pointed out that for an interferometer with horizontal baseline located on an idealized ground, the secondary wave reflected from this specular ground does not cause any phase error. But, diffusely scattered secondary waves may cause error because, they may be incoherent to each other. The discussions were also made on a vertical interferometer in which not only the diffusely scattered but also the specularly reflected secondary waves may cause error in radio interferometer measurements.

In this chapter, we will present the effect of reflected wave from inclined ground on a horizontal interferometer. Next, the discussion will be extended toward the statistical treatment of phase error due to the secondary wave for general understanding of the problem.

4.2 Effect of a Secondary Wave from Earth's Surface on a Radio Interferometer[20]

For accurate measurements of incident angle of a wave by means of a radio interferometer, spacing between antennas may be chosen large enough compared with wavelength of operating frequency. In 136 MHz or 400 MHz band, wavelength is of the order of a meter, so that physical separation between antennas generally becomes of the order of 10 or 10^2 meters. It may be, therefore, considered that the effect of inclined ground above which a radio interferometer is located exists, which results in the erroneous measurements.

To simplify the problems, a radio interferometer is assumed to consist of two antennas. The model of a situation is shown in Fig.I.4.1. As depicted in Fig.I.4.1, a separation between two antennas is expressed by d, h_1 and h_2 are height of antennas 1 and 2 measured from ground, respectively. The inclination of the earth's surface is denoted by β and the incident angle of a wave is denoted by θ. The relation between h_1 and h_2 can be obtained through consideration of a geometrical configuration as follows.

$$h_2 = h_1 + d \tan\beta \tag{I.4.1}$$

Additional assumption is made that ray direction is along a baseline, say the problem is in two dimensions. To determine the incident angle of reflected ray to both antennas and reflection points x_1 and x_2, we will utilize the following geometrical relationship.

$$D_r = D_i - 2(D_i \cdot N_a)\, N_a \tag{I.4.2}$$

where D_i and D_r are the unit vector of incident ray and that of reflected ray, respectively, and N_a is a unit normal vector to a reflection surface. Referring to Fig.I.4.1, D_i and N_a are given as follows, respectively.

$$D_i = -I \cos\theta - J \sin\theta \tag{I.4.3}$$

$$N_a = -I \sin\beta - J \cos\beta \tag{I.4.4}$$

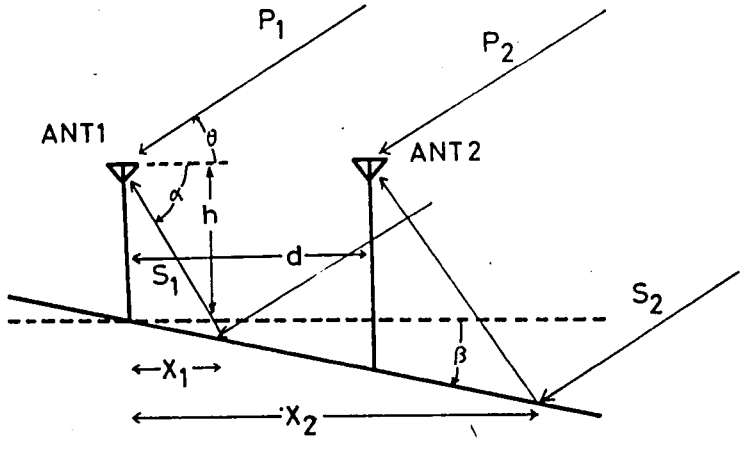

Fig.I.4.1 Effects of reflected wave from an inclined ground on an interferometer

where I and J are unit vectors in x and y direction, respectively. Substituting (I.4.3) and (I.4.4) into (I.4.2), D_r can be calculated as,

$$D_r = -I \cos(\theta-2\beta) + J \sin(\theta-2\beta) \qquad (I.4.5)$$

Therefore, referring to Fig.I.4.1, following equation is obtained.

$$\tan\alpha = -\tan(\theta-2\beta) = -\frac{h_1-x_1\tan\beta}{x_1} = -\frac{h_2-(x_2-d)\tan\beta}{x_2-d} \qquad (I.4.6)$$

The additional path lengths introduced by the reflection for two antennas are, thus, obtained through geometrical consideration as follows, respectively.

$$l_1 = \{x_1^2 + (h_1-x_1\tan\beta)^2\}^{1/2} [1-\cos2(\theta-\beta)] \qquad (I.4.7)$$

$$l_2 = [(x_2-d)^2 + \{h_2-(x_2-d)\tan\beta\}^2]^{1/2} [1-\cos2(\theta-\beta)] \qquad (I.4.8)$$

The phases of reflected ray at two antennas are lagged compared with direct ray because of the additional path lengths. In addition, phase shift due to reflection is also introduced. Reflection coefficient for vertical and that for horizontal polarization are given as follows[21),(22)].

$$R_h = (e^{-d_\psi^2})^{1/2} \frac{\sin\psi - [(\varepsilon_r-jx)-\cos^2\psi]^{1/2}}{\sin\psi + [(\varepsilon_r-jx)-\cos^2\psi]^{1/2}} \qquad (I.4.9)$$

$$R_v = (e^{-d_\psi^2})^{1/2} \frac{(\varepsilon_r-jx)\sin\psi - [(\varepsilon_r-jx)-\cos^2\psi]^{1/2}}{(\varepsilon_r-jx)\sin\psi + [(\varepsilon_r-jx)-\cos^2\psi]^{1/2}} \qquad (I.4.10)$$

$$d_{\psi} = \frac{4\pi}{\lambda} \Delta h \sin\psi \qquad \text{(I.4.11)}$$

where ψ is an incident angle measured from grazing, ε_r is an equivalent specific inductive capacity and x is a function of the conductivity of earth, which is expressed by $1.8\times10^{4}\sigma/f$(in MHz). Δh is the standard deviation of earth's surface. λ is an wavelength of operating frequency.

Using these coefficients, received signals at two antennas are written as follows.

$$V_1 = F(0)\ e^{j\frac{\pi d}{\lambda}\cos\theta} + F(\theta-\alpha)\ R_h(\text{or } R_v)\ e^{-j\frac{2\pi}{\lambda}l_1} \qquad \text{(I.4.12)}$$

$$V_2 = F(0)\ e^{-j\frac{\pi d}{\lambda}\cos\theta} + F(\theta-\alpha)\ R_h(\text{or } R_v)\ e^{-j\frac{2\pi}{\lambda}l_2} \qquad \text{(I.4.13)}$$

where F( ) is the directive pattern of antennas whose main beams are assumed to direct toward the direct ray direction. Two antennas are assumed to be identical to each other and phase characteristics are neglected here. Phase diagram showing the effect of reflected ray to the phase difference measurement is shown in Fig.I.4.2.

For convenience, absolute value and phase angle notation of reflection coefficient $\rho e^{-j\phi}$ is introduced to derive the phase error formula. Substituting this notation into (I.4.12) and (I.4.13), the following formula to give a phase error due to the reflected wave can be derived.

$$\Phi_{error} = \tan^{-1} \frac{\rho F(\theta-\alpha)\sin(\phi+\frac{2\pi}{\lambda}l_1)}{F(0)+\rho F(\theta-\alpha)\cos(\phi+\frac{2\pi}{\lambda}l_1)}$$

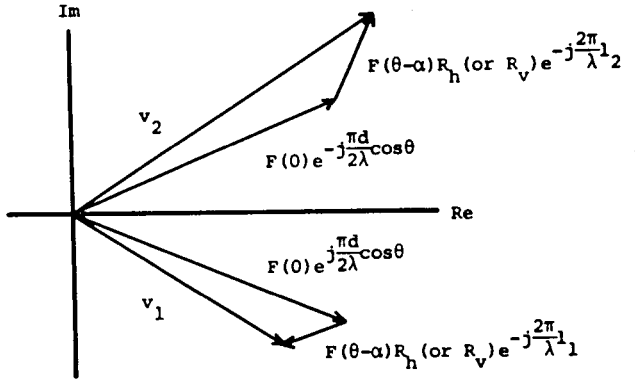

Fig.I.4.2 Phase diagram showing the effect of reflected wave on the phase difference measurements by means of an interferometer

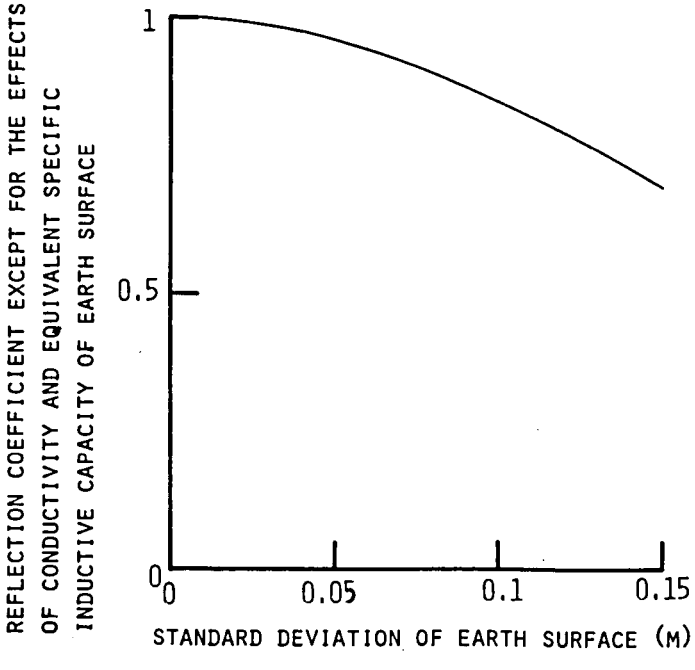

Fig.I.4.3 Asbolute value of the reflection coefficient versus standard deviation of a surface (θ=90°, λ=2.2m)

$$- \tan^{-1} \frac{\rho F(\theta-\alpha)\sin(\phi+\frac{2\pi}{\lambda} l_2)}{F(0)+\rho F(\theta-\alpha)\cos(\phi+\frac{2\pi}{\lambda} l_2)} \qquad \text{(I.4.14)}$$

By using (I.4.14), phase error can be calculated under the given conditions.

First of all, the relation between the absolute value of reflection coefficient and the standard deviation of surface except for the effects of conductivity and equivalent specific inductive capacity of ground is shown in Fig.I.4.3. Calculations are made under the condition $\theta=90°$ and $\lambda=2.2$m. Apparently, absolute value of reflection coefficient decreases monotonically as the standard deviation increases.

To verify the effect of ground reflection, some examples are shown in the followings. In Figs.I.4.4, I.4.5 and I.4.6, calculated incident angles which consist of the errors due to the secondary wave are shown in terms of the inclination angle of earth's surface. True incident angles are chosen to be equal to 30°, 60° and 90°, respectively. Directive patterns of both antennas are assumed to be a cosine shape with front-to-back ratio of 20 dB. Operating frequency, spacing between two antennas, standard deviation of the earth's surface, equivalent specific inductive capacity and conductivity of the earth are assumed to be 136 MHz, 10λ, 0.05m, 30 and 1.2×10^{-2}mho/m[23], respectively. This condition of earth's surface corresponds to a damp ground. Apparently, as varying an inclination of the earth, calculated incident angle varies

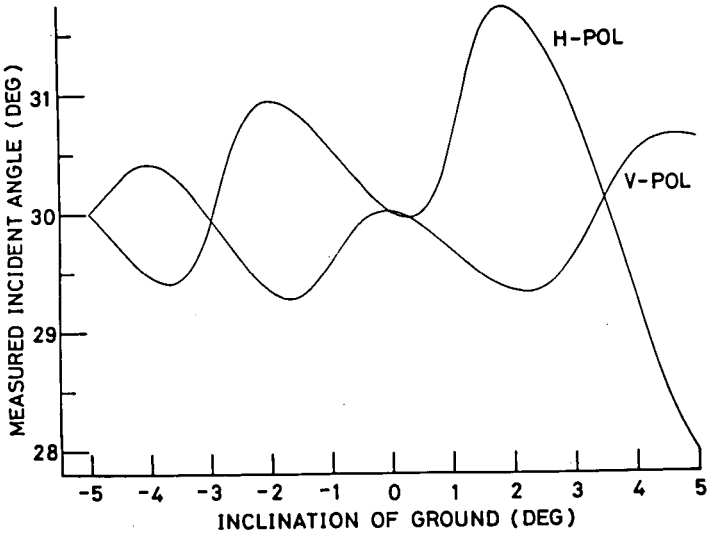

Fig.I.4.4 Variation of measured incident angle as a function of the inclination of the ground above which an interferometer is located. (actual angle:30°)

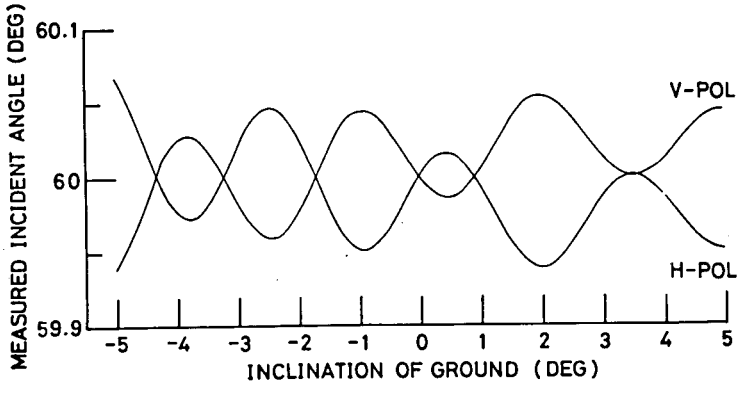

Fig.I.4.5 Variation of measured incident angle as a function of the inclination of the ground above which an interferometer is located. (actual angle:60°)

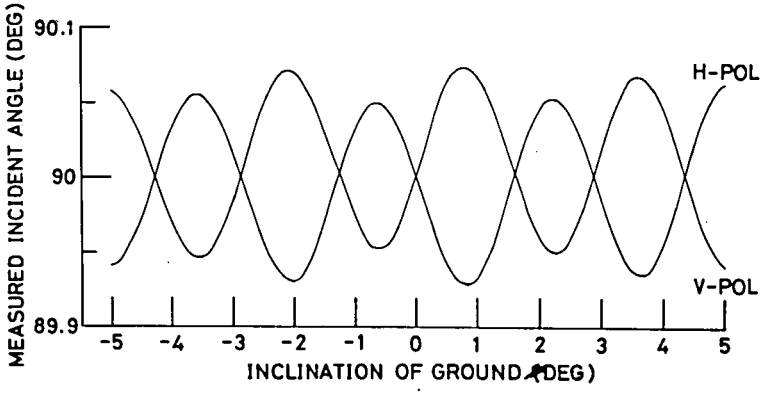

Fig.I.4.6 Variation of measured incident angle as a function of the inclination of the ground above which an interferometer is located. (actual angle:90°)

almost sinusoidally. The variation for horizontal polarization seems to be out of phase with that for vertical polarization, because the reflection coefficients R_h and R_v have almost the same absolute values with opposite sign when incident angle is high from grazing. Thus, phase relationships are seemed to be out of phase with each other. This feature is not maintained for incident angle of 30°. The strengths of the secondary waves are -6 dB, -26 dB and -20 dB compared with those of the direct waves for 30°, 60° and 90° of incident angle, respectively. With small secondary wave suppressions, phase error is large so that readings of incident angle contain relatively large amount of errors.

In Figs.I.4.7, I.4.8 and I.4.9, the effects of antenna separation on the phase error are shown for 30°, 60° and 90° of incident angle, respectively. As shown in these figures, larger the antenna separation becomes, smaller the measurement error decreases. This is due to the fact that constant phase error may result in the smaller measurement error for larger separation of two antennas because whose phase difference is larger. In these figures, measurement accuracies bounded by the imperfect hardwares[24] are depicted by broken lines. Again, the strengths of secondary waves are about -6 dB, -26 dB and -20 dB for the incident angle of 30°, 60° and 90°, respectively. Thus, it is to be said that with secondary wave whose strength is -20 dB compared with the direct wave for the case under consideration, phase error caused by the secondary wave is almost the same with those due to imperfect hardwares and can be neglected in practice.

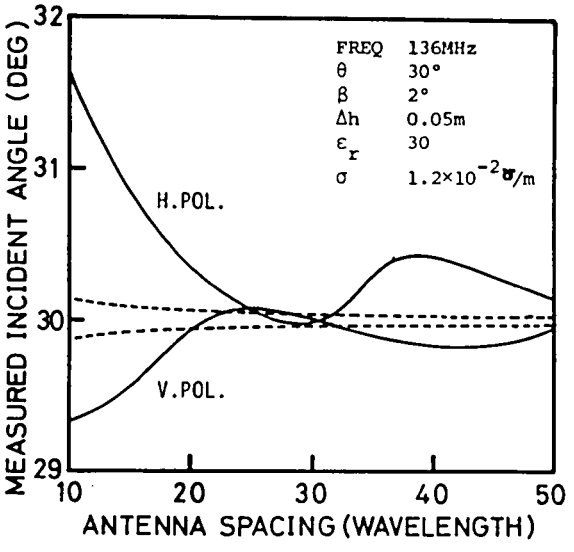

Fig.I.4.7 Variation of measured incident angle as a function of an antenna spacing. (actual angle:30°)

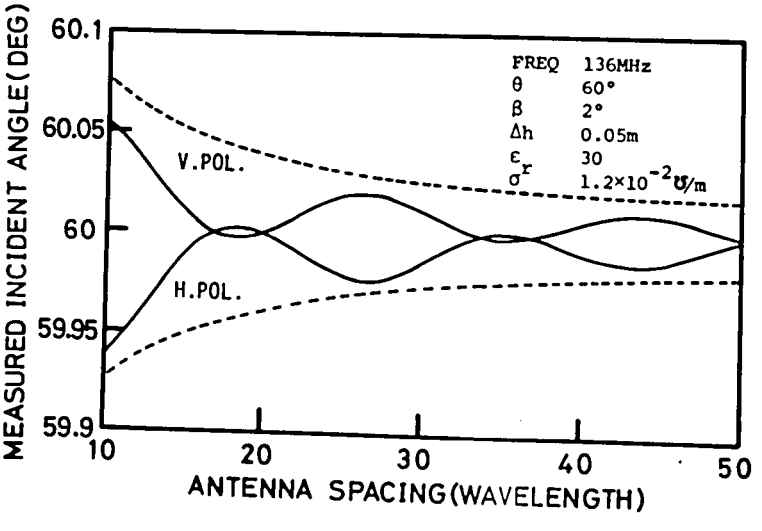

Fig.I.4.8 Variation of measured incident angle as a function of an antenna spacing. (actual angle:60°)

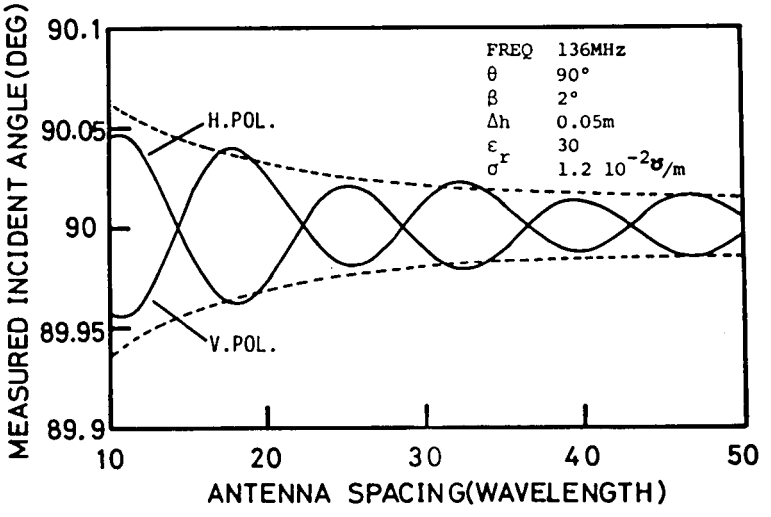

Fig.I.4.8 Variation of measured incident angle as a function of an antenna spacing. (actual angle:90°)

4.3 Statistical Description of a Phase Error due to a Secondary Wave[25]

As discussed in the previous section, signals which are reflected from earth's surface may bring on the erroneous measurements of the incident angle. These quantities can not always be neglected. However, the results discussed previously include the parameters which denote the arrangement of element-antennas such as the antenna height from the ground and the spacing between antennas, and the incident angle of a signal so that an interferometer system must be designed in case by case. Thus, for the benefit of an easy design of an interferometer system, we will present the statistical approach to this problem.

4.3.1 Case of Near Field Reflection

For ease of treatment, again we consider the case of a radio interferometer composed of two antennas. A sketch of the case under consideration is shown in Fig.I.4.10. In the definite case as in the previous section, phase of a secondary wave with respect to that of a direct wave can be estimated under some assumptions such as the condition of the earth. In general case, however, this quantity may distribute statistically according to its environment in which a radio interferometer system locates and the incident angle of a wave. Therefore, we will treat the phases of a secondary wave with respect to that of the direct wave at two antennas as random variables which are distributed uniformly over the range $[0, 2\pi]$ and are independent with each other. The assumptions are made that one secondary wave is predominant and the

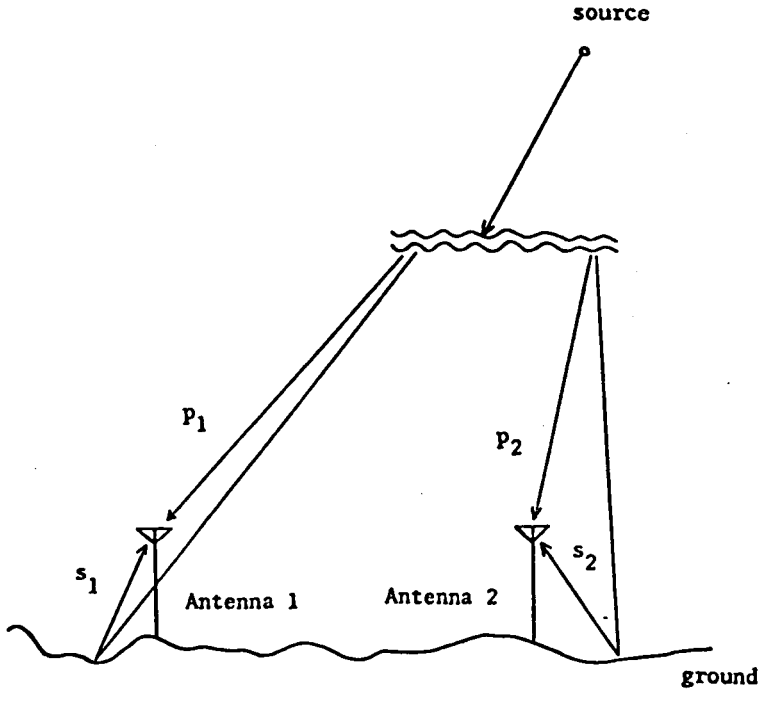

Fig.I.4.10 Sketch showing the effects of secondary waves which bring on the phase error in angle measurements.

others can be neglected.

Phase error is then defined as the difference between the phase differences between two antennas in the case with and without secondary waves. Now, we denote the amplitude of direct waves as P_1 and P_2 and the amplitude of secondary waves as S_1 and S_2 at each antenna, respectively. ψ_{p1} and ψ_{p2} are the phases of direct waves and ψ_{s1} and ψ_{s2} are those of secondary waves with respect to a certain reference, at each antenna respectively. Sufficies 1 and 2 refer to the antenna 1 and 2, respectively.

The phase diagram of this situation is shown in Fig.I.4.11. v_1 and v_2 in this figure show the sum vectors of direct and secondary wave at two antennas, respectively. The amplitude ratios r_1 and r_2 are now introduced as follows. (They should be called "secondary wave suppression ratio" hereafter.)

$$r_1 = \frac{S_1}{P_1} \tag{I.4.15}$$

$$r_2 = \frac{S_2}{P_2} \tag{I.4.16}$$

It is obvious the phase error does not exist when the secondary wave does not exist. In addition, under the condition of $r_1 = r_2$ and $\psi_{s1} = \psi_{s2}$, the phase error does not also exist. This corresponds to the case in which the secondary wave is reflected from an idealized horizontal ground above which horizontal interferometer is located.

Now, two direct wave vectors denoted as P_1 and P_2 in Fig.

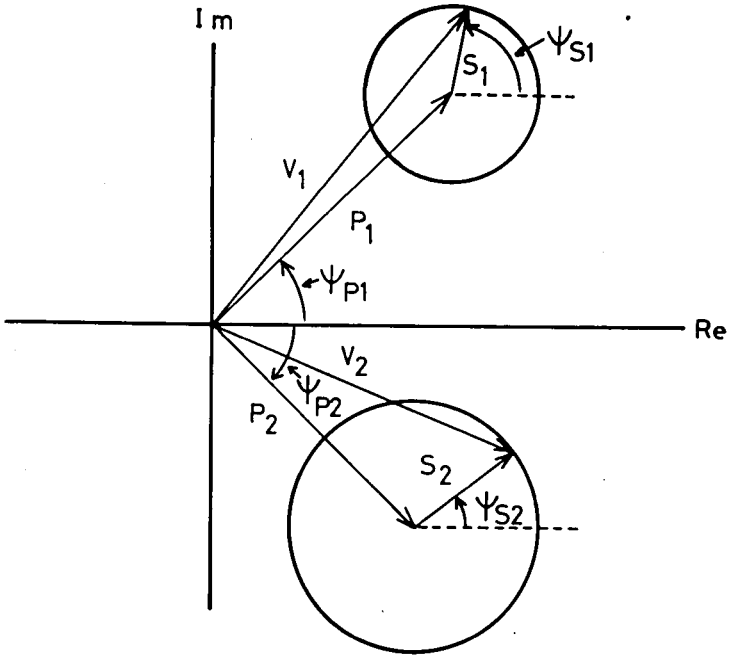

Fig.I.4.11 Phase diagram of the primary and the secondary waves at antenna 1 and 2.

I.4.11 are turned around the origin till which coincide with the positive real axis with fixed relationship between the direct wave vector and the secondary wave vector. As a result, we obtain the phase diagram as shown in Fig.I.4.12. Referring to this figure, the angle δ between the vectors v_1 and v_2 is the phase error itself to which we are paying our attentions. The angles between the secondary waves and the positive real axis are denoted as ϕ_1 and ϕ_2 which refer to antenna 1 and 2, respectively. ϕ_1 and ϕ_2 are given by the following equations.

$$\phi_1 = \psi_{s1} - \psi_{p1} \tag{I.4.17}$$

$$\phi_2 = \psi_{s2} - \psi_{p2} \tag{I.4.18}$$

ϕ_1 and ϕ_2 are the functions of the shape and electromagnetic properties of reflector or scatterer and the distance between the interferometer system and the sources of direct wave and secondary wave. The variations of the order of wavelength in the distance between the interferometer system and the source may bring out the large displacement in ϕ_1 and ϕ_2. It can be therefore, considered that ϕ_1 and ϕ_2 are random variables whose probability density functions are uniform over the range between 0 and 2π.

Following discussions are performed by referring to Fig.I.4.12. The phase error δ is given by the following equation.

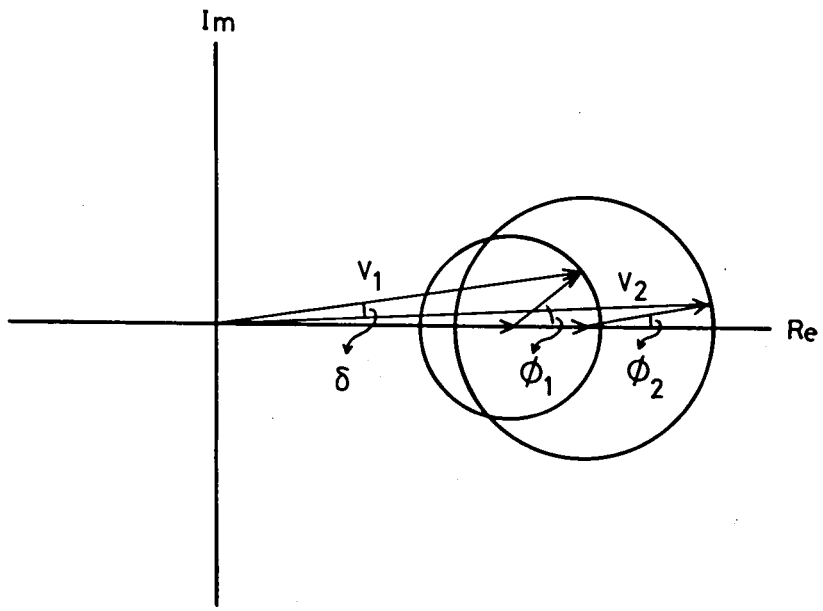

Fig.I.4.12 Phase diagram showing the error component of the observed phase difference due to a secondary wave

$$\delta = \tan^{-1} \frac{r_1 \sin\phi_1}{1 + r_1 \cos\phi_1} - \tan^{-1} \frac{r_2 \sin\phi_2}{1 + r_2 \cos\phi_2} \quad \text{(I.4.19)}$$

under the conditions of $r_1 \ll 1$ and $r_2 \ll 1$, (I.4.19) can be well approximated as follows.

$$\delta \cong r_1 \sin\phi_1 - r_2 \sin\phi_2 \quad \text{(I.4.20)}$$

Now, let us consider the maximum phase error δ_{max}, i.e. the worst case under the given conditions. As pointed out by Duncan[19], the worst case is realized when the secondary wave vectors have phases as shown in Fig.I.4.13. δ_{max} can be written as follows.

$$\delta_{max} = \sin^{-1} r_1 + \sin^{-1} r_2 \quad \text{(I.4.21)}$$

In Fig.I.4.14, contours of maximum phase error with various secondary wave suppression ratios are shown. Again, under the conditions of $r_1 \ll 1$ and $r_2 \ll 1$, δ_{max} can be also well approximated as follows.

$$\delta_{max} \cong r_1 + r_2 \quad \text{(I.4.22)}$$

As discussed previously, ϕ_1 and ϕ_2 may have values with random nature so that statistical considerations will be important to evaluate the performance. Therefore, first of all, considerations on the prob-

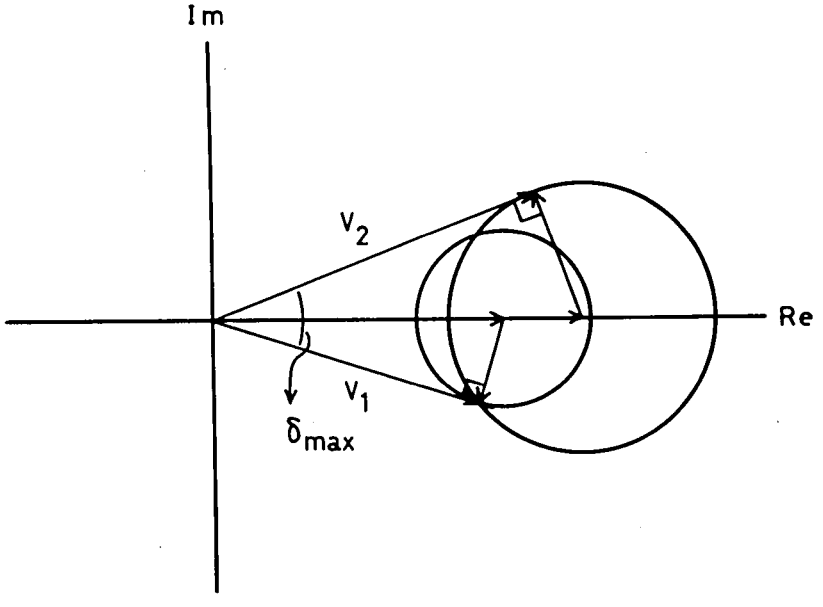

Fig.I.4.13 Diagram showing the phases of the secondary waves relative to that of the primary waves at two antennas that produce the maximum phase error.

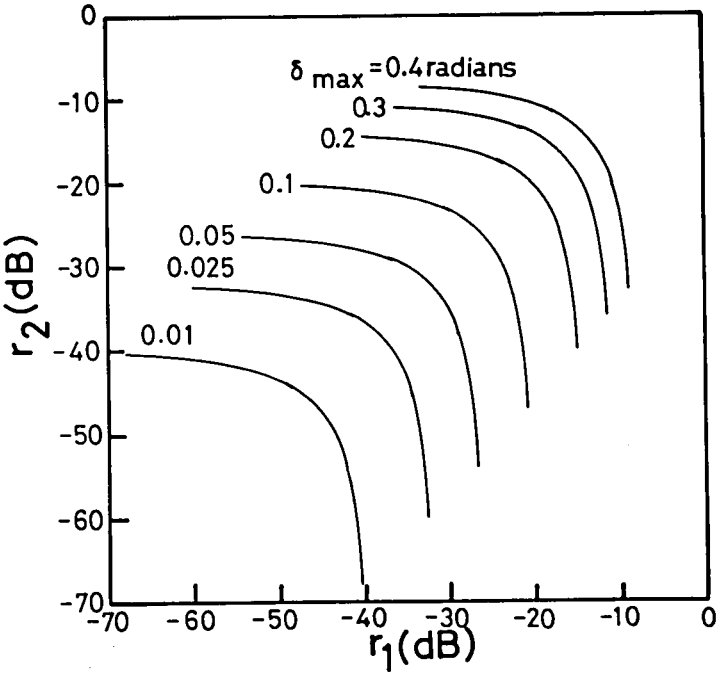

Fig.I.4.14 Calculated maximum phase error versus the secondary wave suppression ratios at two antennas.

ability density of a phase error are made in the followings.

In our case, however, it is impossible to derive the probability density function for a phase error analytically. Numerical technique is, therefore, adopted for understandings of the problem. Calculations are made under the assumptions that ϕ_1 and ϕ_2 are random variables with uniform probability of occurrence within the range $[0, 2\pi]$ and independent with each other. The results for two cases are shown in Fig.I.4.15. In the case with equal secondary wave suppression ratio at two antennas, only a peak of probability density exists at zero phase error. On the other hand, with different secondary wave suppression ratios, double peaks appear which are symmetric with respect to zero phase error. This can be interpreted qualitatively as follows.

As ϕ_1 and ϕ_2 have uniform probability over the range $[0, 2\pi]$, the probability that ϕ_1 and ϕ_2 have the values near the tangents to the trajectories of secondary wave vectors may be relatively high. If, with the same secondary wave suppression ratios, the regions with high probability of occurrence are coincident with each other so that probability of no error increases than the others. With different secondary wave suppression ratios, the regions of high probability of occurrence differ to each other with angle determined by the relationship between r_1 and r_2. From this reason, double peaks appear in the probability density as shown in Fig.I.4.15. The importance of equalizing the secondary wave suppression ratios at two antennas is,

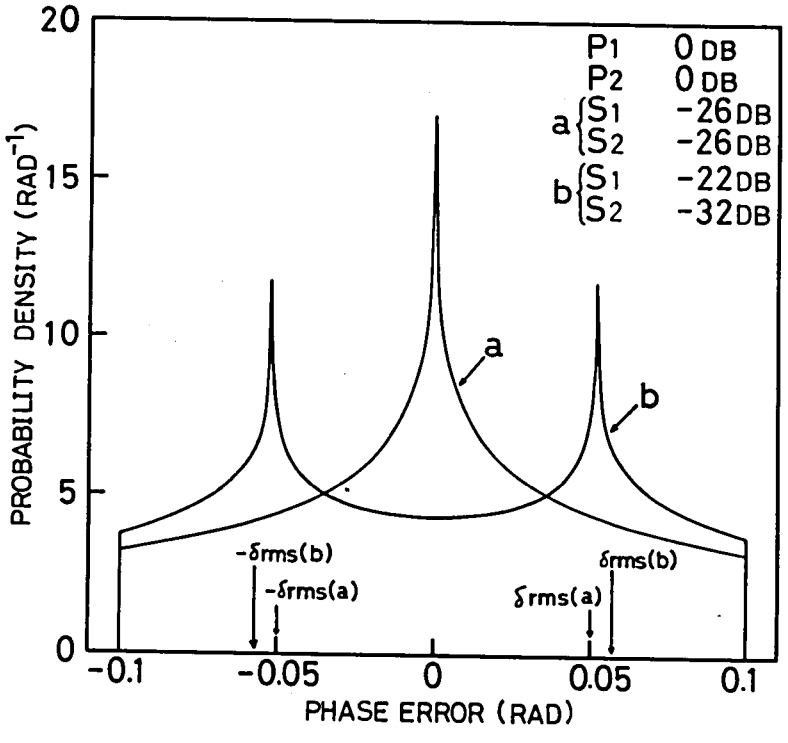

Fig.I.4.15 Probability density of a phase error δ when phase differences ϕ_1 and ϕ_2 are random variables and independent to each other.

therefore, clearly indicated for increasing the probability of small errors.

For evaluating the statistical nature of the phase error, let us consider the RMS (root-mean-square) value of it. The RMS value of the phase error, δ_{RMS} is given by the following equation.

$$\delta_{RMS} = \frac{1}{2\pi} \{ \int_0^{2\pi} \int_0^{2\pi} (\tan^{-1} \frac{r_1 \sin\phi_1}{1 + r_1 \cos\phi_1} - \tan^{-1} \frac{r_2 \sin\phi_2}{1 + r_2 \cos\phi_2})^2 \, d\phi_1 d\phi_2 \}^{1/2} \qquad \text{(I.4.23)}$$

Again under the conditions of $r_1 \ll 1$ and $r_2 \ll 1$, (I.4.23) can be well approximated as,

$$\delta_{RMS} \cong \frac{1}{2\pi} \{ \int_0^{2\pi} \int_0^{2\pi} (r_1 \sin\phi_1 - r_2 \sin\phi_2)^2 \, d\phi_1 d\phi_2 \}^{1/2} \qquad \text{(I.4.24)}$$

Analytical calculation of (I.4.24) gives the following expression.

$$\delta_{RMS} \cong (\frac{r_1^2 + r_2^2}{2})^{1/2} \qquad \text{(I.4.25)}$$

It is thus proved that approximated RMS value of the phase error is a half of the maximum value of it when the secondary wave suppression ratios at two antennas are set to be equal. If, r_1 or r_2 or both

exceed -10 dB, the approximations above lead to the erroneous results so that evaluations must be performed by using (I.4.23). Numerical integrations are carried out and the results are shown in Fig.I.4.16 with some contours as a function of r_1 and r_2. Then, let us pay our attention to the relationship between the maximum and the RMS value of the phase error, i.e. δ_{max} and δ_{RMS}. The parameter is chosen as r which is defined as (I.4.26).

$$r = \frac{r_1}{r_2} \tag{I.4.26}$$

The assumption is made that $r_1 \geq r_2$, however, generality is not lost because r_1 and r_2 can be exchangeable to each other as shown in (I.4.23). Fig.I.4.17 shows the $\delta_{RMS}/\delta_{max}$ in terms of r. The upper of the area with hatching shows the case with larger r_1 and r_2 than the lower with equal value of r. When r=0 dB ($r_1=r_2$), δ_{RMS} is about a half of δ_{max} and is minimized. This result also indicates the importance of equalizing the secondary wave suppression ratios at two antennas.

For evaluating the admissible level of secondary wave suppression ratios, comparison of phase error is made with the 136 MHz interferometer for satellite tracking[24]. The phase error due to imperfect hardwares, i.e. error of antenna impedance was 5 degrees and of feeder cable was 2 mm in electrical length, was 0.1 radians so that r_1 and r_2 must be reduced smaller than -20 dB for decreasing δ_{RMS} smaller than the phase error due to imperfect hardwares.

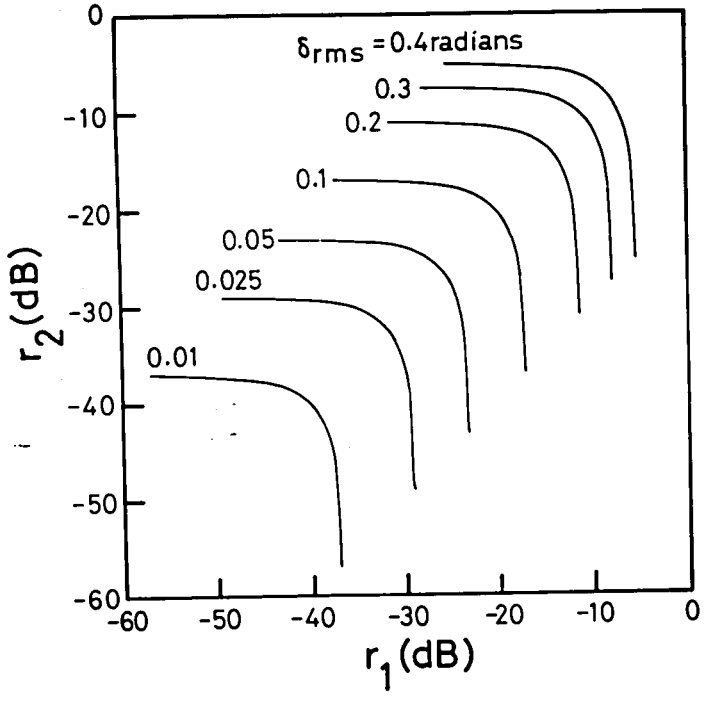

Fig.I.4.16 Calculated RMS value of a phase error versus the secondary wave suppression ratios at two antennas.

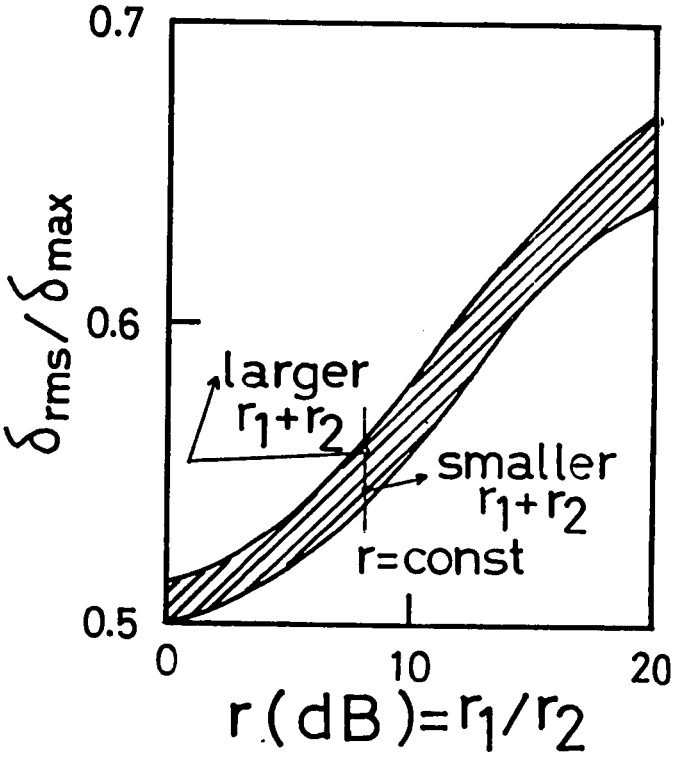

Fig.I.4.17 Plot of $\delta_{RMS}/\delta_{max}$ (ratio of RMS value and maximum value of phase error) as a function of r (ratio of secondary wave suppression ratios at two antennas)

4.3.2 Case of Far Field Reflection

In the case, however, the source of secondary wave is located far away from the interferometer system, the secondary wave is also regarded as a plane wave. The incident direction of the secondary wave is generally different from that of the direct wave. The model considered here is shown in Fig.I.4.18. Under such situation, phases of the direct and the secondary wave at two antennas can be written by the following equations, respectively.

$$\psi_{p1} = \psi_d - \frac{\pi d}{\lambda} \cos\theta_p \qquad \text{(I.4.27)}$$

$$\psi_{p2} = \psi_d + \frac{\pi d}{\lambda} \cos\theta_p \qquad \text{(I.4.28)}$$

$$\psi_{s1} = \psi_s - \frac{\pi d}{\lambda} \cos\theta_s \qquad \text{(I.4.29)}$$

$$\psi_{s2} = \psi_s + \frac{\pi d}{\lambda} \cos\theta_s \qquad \text{(I.4.30)}$$

where λ is the wavelength of incident wave, d is the separation between two antennas, and ψ_d and ψ_s are phases of the direct and the secondary wave at midpoint of two antennas, respectively. θ_p and θ_s are the incident angles of the direct and the secondary wave measured from a baseline.

Therefore, independence between ϕ_1 and ϕ_2 is lost which results in the following relationship.

$$\phi_2 = \phi_1 + \alpha \qquad \text{(I.4.31)}$$

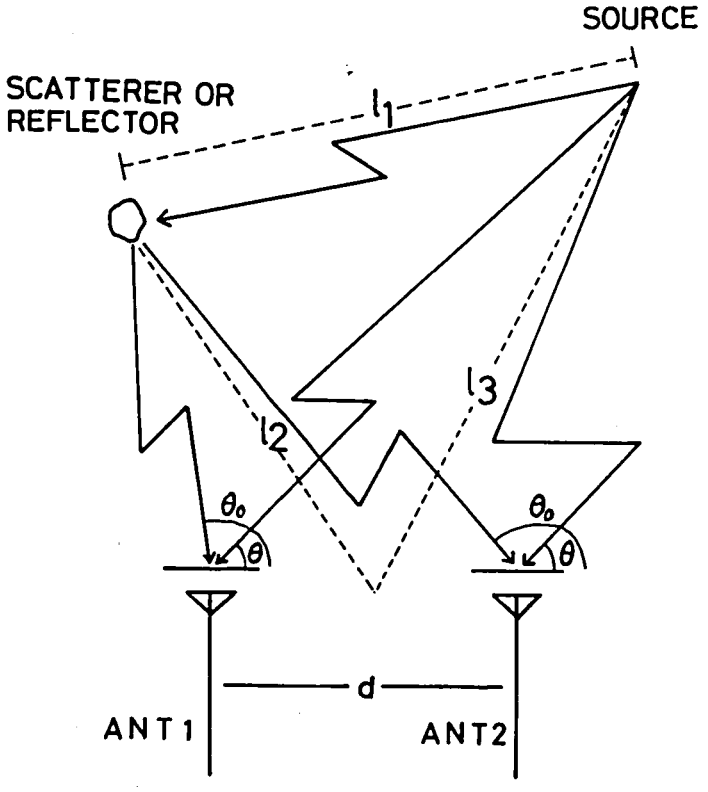

Fig.I.4.18 Effect of a secondary wave on both antennas when a secondary radiator can be considered as a point source located sufficiently far from an interferometer.

where α is expressed using (I.4.27) - (I.4.30) as

$$\alpha = \frac{2\pi d}{\lambda} (\cos\theta_s - \cos\theta_p) \qquad \text{(I.4.32)}$$

The RMS value of phase error in this case can be formulated as follows.

$$\delta_{RMS}' = \frac{1}{\sqrt{2\pi}} \{ \int_0^{2\pi} (\tan^{-1} \frac{r_1 \sin\phi_1}{1 + r_1 \cos\phi_1} - \tan^{-1} \frac{r_2 \sin(\phi_1+\alpha)}{1 + r_2 \cos(\phi_1+\alpha)})^2 d\phi_1 \}^{1/2} \qquad \text{(I.4.33)}$$

Under the assumptions that $r_1 \ll 1$ and $r_2 \ll 1$, approximated result of (I.4.33) can be written as a following equation.

$$\delta_{RMS}' \cong (\frac{r_1^2 - 2r_1 r_2 \cos\alpha + r_2^2}{2})^{1/2} \qquad \text{(I.4.34)}$$

Assuming the equal characteristics of two antennas, we can put $r_1 = r_2$ because of the plane wave assumption of the secondary wave. Under this condition, (I.4.25) and (I.4.34) can be rewritten by the following equations.

$$\delta_{RMS} = r_1 = r_2 \qquad \text{(I.4.35)}$$

$$\delta_{RMS}' = r_1 (1 - \cos\alpha)^{1/2} \qquad \text{(I.4.36)}$$

With the same secondary wave suppression ratios, the phase error for far field reflection can be expressed by that for near field reflection

multiplied by $(1 - \cos\alpha)^{1/2}$. We define a quantity γ in a following manner.

$$\gamma = \frac{\delta_{RMS}'}{\delta_{RMS}} = (1 - \cos\alpha)^{1/2} \qquad \text{(I.4.37)}$$

Though the range of γ is from 0 to $\sqrt{2}$, the value of α varied randomly according to its situation and it is impossible to estimate it. Again, therefore, we regard α as a random variable whose probability is uniform over the range of $[0, 2\pi]$. The probability that δ_{RMS}' exceeds δ_{RMS} is 0.5 and in the worst case, δ_{RMS}' is equal to square root of 2 times δ_{RMS}.

4.4 Concluding Remarks

We have presented the considerations on the problem for evaluating the phase error of an interferometer due to a secondary wave. The formulations are first made on the situation that secondary wave is retransmitted from ground above which an interferometer is located. Some results indicate that with secondary wave whose amplitude is less than -20 dB of that of the direct wave, the phase error may be neglected in comparison with that due to imperfect hardwares. In the above formulations, however, the parameters to describe the arrangement of antenna elements, the electromagnetic properties of ground and so on are included so that it is difficult to evaluate the phase error due to the secondary wave generally. To overcome this problem, the statistical

approaches are introduced to describe the influence of secondary wave generally. First, evaluations are made through probability density of phase error, which indicates that with the same secondary wave suppression ratios at two antennas, the probability that phase error has a value near zero is maximized. With different secondary wave suppression ratios, double peaks appear in the probability density whose values of phase error are determined inherently by the secondary wave suppression ratios. This result can be fully described by the RMS value of the phase error which is minimized in comparison with the maximum value of the phase error, if the secondary wave suppression ratios are equalized at two antennas.

Thus, it can be concluded that for reducing the phase error due to the secondary wave, it is important not only to reduce the secondary wave suppression ratios at two antennas but also to equalize them. In practice, equalization of the radiation pattern of each element-antenna is at first significant not only in the mainbeam region but also in the sidelobe region far apart from boresight. In addition, to uniform the condition of the ground above which the interferometer is located, covering it horizontally by the wire mesh or wave absorber is the good way to reduce the error caused by the secondary wave.

Chapter 5. SUMMARY AND CONCLUSION

In this PART 1, we have described the interferometer method for satellite tracking. Studies are carried out mainly concerning with a receiver which is used in interferometer measurements of satellite orbits and an optimal arrangement of baselines of an interferometer system. Error analysis of an interferometer due to the secondary wave retransmitted from surrounding objects is also made in a statistical manner. In the followings, summaries of each chapter are shown.

At first, a receiver for an interferometer system has been developed with PLL (phase-lock-loop) of new concept. The output level of an interferometer varies largely with time and often falls below the threshold level for locking of a PLL. It can be considered, therefore, that at this point the loop may run out of locking which results in missing the signal. To overcome this fault, sample-and-hold circuitries are inserted into the loop to cut it off during fading while holding the signal for VCO (voltage controlled oscillator). The experimental observations using this receiver attached to the test interferometer show sufficient performance.

Considerations on an interferometer system have been made in the next chapter. Prior to the discussions on baseline arrangement, problem of ambiguity resolution is described. Conventional two-element interferometer has grating lobes so that it is difficult to determine the angular position of the satellite uniquely. To overcome this fault,

four-element interferometer is proposed with the spacing of the outer pair of elements 1.5 times that of the inner pair. The design is made with considerations on the spatial frequency components of the interferometer.

Next, baseline arrangements of an interferometer system have been investigated through two methods of approach. Discussions are first made on the satellite path on the celestial sphere. A conventional interferometer system with two baselines crossed perpendicular to each other is insensitive to a certain satellite path. This fault has been understood through observations of satellite paths. To evaluate the performance of an interferometer system, the concept of tracking sensitivity is utilized. This results in the three-baseline configuration of an interferometer system for satellite tracking, in which baselines are crossed with angle of 60 degrees, in the shape of six-pointed star. The other approach for evaluation is also introduced, in which the criterion is chosen as the number a satellite crossed the array normal plane. The reason for this is accurate observation for azimuth angle can be performed in the array normal plane, for the effect of refraction exists only in the elevation angle under the assumption of concentric troposphere and ionosphere. Thus, angle measurement can be done without error. Through this evaluation, predominance of three-baseline system is also proved in the sense of cost performance. Using the prototype interferometer system of three baselines and the receiver discussed in

Chapter 2, some observations are made on the satellite paths of OGO-6 (1969-51A). These results prove that the interferometer system with three baselines has a sufficient performance even for a polar orbitting satellite such as OGO-6 and the receiver acts very well for reception of a signal from interferometers.

The phase error caused by the secondary wave has been also considered. The effect of inclined ground is analyzed to show that for high elevation angle of incidence the measurement errors for horizontal and vertical polarization are almost the same absolute values with opposite sign. To clarify the relationship between the phase error and the relative strength of the secondary wave to the direct wave, statistical treatment is introduced. Some statistical properties of phase error in terms of probability density are discussed. Through this statistical approach, phase error due to the secondary wave can be evaluated simply and effectively, and the error of the interferometer measurements may be reduced. From this, it is pointed out that RMS (root-mean-square) value of phase error is a good measure for probability density and its minimization corresponds to maximize the probability of zero error. This can be realized through equalization of secondary wave suppression ratios at two antennas. Therefore, in designing the interferometer system for satellite tracking, care must be taken not only to each element antenna to be manufactured as same as possible, but also to uniform the ground above which the interferometer will be located. To this purpose it is desirable

to cover the ground horizontally with wire mesh or wave absorber large enough compared with the size of the interferometer system.

Summarizing the results described, one desirable form of simple satellite tracking station is established. In this, three baselines are included, each of which is a four-element interferometer with spacing ratio of 1.5, which are crossed with the angle of 60 degrees with one another in the shape of six-pointed star. Wire mesh or wave absorber covers the ground horizontally above which the interferometer is located to uniform the ground condition. The outputs of three interferometers are introduced to three receivers with improved phase-lock-loop for recording the interferograms due to the travel of a satellite.

Network of many numbers of this simple station may give the ability to measure satellite orbits with high accuracy than a single large station.

PART 2.

AN ADAPTIVE ANTENNA ARRAY WITH DIRECTIONAL CONSTRAINT

Chapter 1. GENERAL INTRODUCTION

An antenna array has many advantages over a single antenna because the features of the antenna system, for example, the mainbeam direction, beamwidth, sidelobe level and pattern null directions can be easily controlled by choosing the phase and amplitude of electrical excitation of each element antenna.

In recent years, applications of the antenna arrays to a specific objective have widely been studied and the concept "Signal Processing Array"[26] has been established. A signal processing array is defined as an array of antennas (sensors) whose outputs are processed individually in the best way for a specific system objective[26]. Signal processing arrays are divided into some classes according to their modes of operation. They are, for example, synthetic arrays, correlation arrays, decision theoretic arrays, self forcusing and retrodirective arrays and adaptive arrays.

Among these systems, adaptive arrays are the most suitable for communications purpose. A term "adaptiveness" is used to describe the ability of a system to change its characteristics in accordance with the condition under which it is operating. Adaptive arrays must consist of antennas that detect the signals of interest and feedback loops that kept changing the system's operation as a function of the information obtained by the antennas.

A phase-locked array[27],[28] is a typical example of an

adaptive array. The phase-locked array has the feature that it can track a source of transmission automatically by means of the feedback control circuitry. Although, this desirable feature may be spoilt by the existence of strong interference with frequency almost equal to that of the desired signal. Not only to the phase-locked arrays, existence of interferences may generally degrade the performance of communication links.

In communication engineering, reduction of noise (which signifies the whole unwanted noise, including the interferences, the system internal noise and so on,) is one of the most significant purposes of investigations. Among them, applications of a nature of the antenna system as a spatial filter is one of the possible ways for interference rejection[29]. If the incident directions of interferences are fixed in angular coordinate, deterministic design procedures can be applicable to reject interferences by steering nulls toward them. In general, however, the incident directions and the time of occurrence of interferences may be undeterministic so that conventional procedure for array design fails to reject interference.

One solution to this problem is the adaptive arrays for interference rejection. Generally speaking, this system consists of an array of antennas followed by the tapped-delay-line filters, the processor and the feedback loops. Some systems are proposed with different performance criteria, all of which are designed to minimize the output noise power under certain protection of the desired signal

component at the output.

After investigations of the previous works on this adaptive array for interference rejection, we have proposed the adaptive array acting under the new concept, "directional constraint". In this part, we will present the concept of the system, detailed analyses of the transient behavior and steady state performance, and the results of simulation experiments by a digital computer compared with the theory.

In Chapter 2, survey of the previous works on this problem will be made from critical point of view. Based on the criticism described here, we have established a new constraint condition named "directional constraint". This concept utilizes the a priori knowledge of the incident direction and the frequency of the desired signal.

In Chapter 3, derivation of the optimal weight vector and the iterative algorithm for controlling the weight vector are presented. Method of analysis makes use of the usual Lagrange multipliers. Iterative algorithm is based on the steepest descent method with gradient projection. A modification is made for preventing the accumulation of errors which are inherent in numerical computations on digital computer[30]. The sufficient condition for convergence of the algorithm is also presented in this chapter.

Chapters 4 and 5 are devoted to the detailed analyses on single and double directional constraint system, respectively. Iterative algorithm with the form of difference equation is translated into the form of vector differential equation. This differ-

ential equation is defined in the multi-dimensional hyperspace. Therefore, orthogonal projection of the vectors are necessary for solving this equation. There is an effective method to do this and by using it, analytical solutions for several conditions of environment can be obtained in a closed form. Through the analyses in these chapters, it becomes possible to track the behavior of each weight perfectly. Inside the scope of the author's knowledge, no publications have shown such prediction of the behavior of each weight when exposed to a given environment. The analyses show that the time constant of convergence depends on the power of interferences and the angular condition between the constraint direction and the interference direction. The influence of the prediction error on the performances of the adaptive array is also analyzed, and calculated results for some examples are shown.

In Chapter 6, comparisons are made between the theory and the results of simulation experiments on computer. Analyses in the previous chapters show the mean behavior of the system because of the averaging. In practice, however, sampling feedback concept will be applied by means of a digital computer. In spite of this difference between analog and digital concept, the theory and the results of computer simulation experiments agree fairly well except for the small quantities, which may be due to the existence of internal noise simulated by Gaussian random variables and to the control of weights using the sampled data.

In Chapter 7, summary and conclusion are described to declare the performance of the present system, which are verified by the analyses and the simulation experiments on computer.

Chapter 2. A CRITICAL SURVEY OF THE PREVIOUS WORKS ON THE ADAPTIVE ARRAYS

Many authors presented some adaptive arrays for extracting the desired signal in the noisy environment which implies the isotropic noise and interferences. In these systems, tapped-delay-line (nonrecursive digital, transversal) filters with variable gain amplifiers associated with each element are generally used to obtain the combined filter in spatial and time domain, which is shown in Fig.II. 2.1. The tapped-delay-line filters are preceded with or without the spatial correction filter (this term was introduced by Griffiths[31]), which compensates the misalignment between the wavefront and the array geometry. In narrow banded applications, a phase shifter and an amplifier with variable gain can be employed in place of a tapped-delay-line filter.

In the adaptive array systems, the a priori knowledge about the desired signal, i.e. the center frequency and/or incident direction and so on, are effectively utilized for extracting the actual desired signal from noisy environment. On the other hand, it is to be noted that no a priori knowledge about the conditions of unwanted noises (interferences and isotropic noise) can be used for array design. Thus, the array system needs to learn the information of the electromagnetic environment and change its spatial and frequency characteristics to match the environment.

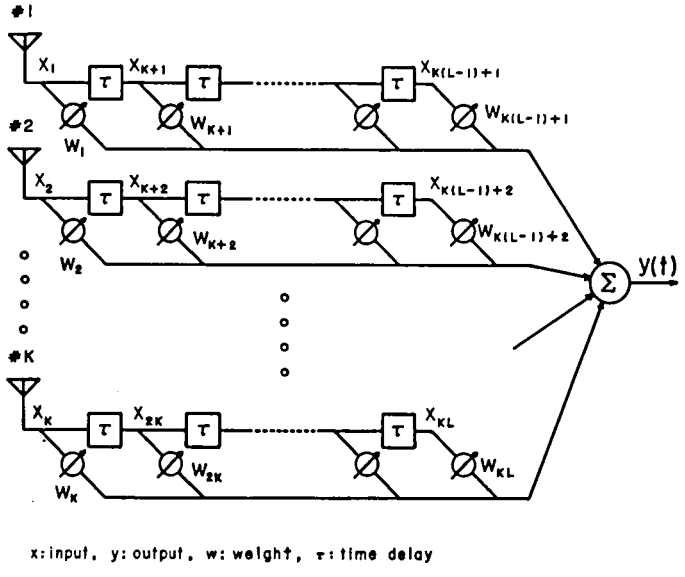

Fig.II.2.1 General configuration of an adaptive array. Each element is followed by a tapped-delay-line filter. Feedback circuitries are omitted here for simplicity.

For this purpose, array signal processing scheme based upon the least-mean-square-error (LMSE) criterion was introduced by Burg[32] in seismology. He proposed the three dimensional (time and two dimensional space) filtering and showed that his method gives higher signal-to-noise ratio (SNR) than conventional array processing technique. Alternative technique was presented by Levin[33] for obtaining the maximum-likelihood (ML) estimate of the seismic signal in the presence of seismic noise. Maximum-likelihood estimate can be provided by constraining the tapped-delay-line filters preceded by a spatial correction filter as a following manner. The sum of only one column of weights is constrained to be equal to unity and the other columns to zero, which is often called "fidelity constraint". In this system, the amplitude and phase characteristics in the direction to which the beam is steered by a spatial correction filter are constant and independent of a frequency of the incident signal, in other words the transfer of the signal can be made without distortion and this is the reason of the above naming. Under the "fidelity constraint" condition, minimization of the system output power gives the maximum-likelihood (minimum variance unbiased) estimate[34] of the seismic signal. Wiggins and Robinson[35] presented derivations of the recursive solution of the least-mean-square-error (Wiener) filter.

In seismic array applications, purpose of the processing is to extract the seismic signal from the seismometers' records which include not only the desired seismic signal but also the unknown and

undesired seismic noises. In this, off-line operations can be employed.

In communications, radar and sonar applications, however, real time processings are necessary. Therefore, a system which converges to its optimal condition through observations of an environment will be required. Shor[36] presented the adaptive technique for sonar applications which maximizes the output signal-to-noise ratio (SNR) by means of a familiar steepest descent method using the measured correlations of the desired signal and the noise (which consists of the thermal noises at each element, isotropic noise and interferences). In his method, separate measurements of the desired signal and the noise correlation were required for obtaining the desired performance. For measuring the signal correlations, strong signal with the same frequency and incident direction of the desired signal, which is generated at the receiver (this concept was utilized by Widrow et al.[38] as a pilot signal), is impinged to the array system. But measured signal correlations may include some errors caused by the unwanted noises. Noise correlations can be measured before transmitting the sonar signal. However, in general, the system characteristics are determined not only by the conditions of noises but also by the conditions of the actual desired signal, thus the system obtained by the procedure described above may not match to the actual environment. Applebaum[37] presented the alternative adaptive method for real time processing of the array system which maximizes the output signal-to-noise ratio based upon the concept of sidelobe cancellation. His

scheme is shown in Fig.II.2.2. In his method, the noise correlation matrix required for processing is approximated by the received signals at each element. And the control law can be approximated by the actual implementations only if the feedback loop gain is sufficiently high enough. As he pointed out, however, instabilities in feedback loops may occur if the loop gains are allowed to become excessively. Widrow et al.[38] presented the other adaptive scheme using the least-mean-square-error concept. Basic scheme is shown in Fig.II.2.3. The adaptive algorithm of reference (38) adjusts the weights based on a steepest descent method which is allowed to apply iteratively for converging the weights to their optimal condition in asymptotic sense. This algorithm is so designed for the purpose of a real time processing by means of a digital computer that the weight adjustments are performed to a direction of the negative gradient of the instantaneous value of squared error. Artificially generated (pilot) signal which is a replica of the desired signal is impinged to the array system as a training signal to keep the array system response as a certain value in the direction of the expected desired signal. The pilot signal is also used as a reference signal, thus the minimization of the error between the array output and the reference signal causes pattern nulls in the directions of interferences. Griffiths[31] pointed out the limitation of this method, i.e. in adaptation process, the occurrence of the actual desired signal may cause a bias of weights from their optimal (Wiener) solution. He proposed the alternative adaptive algorithm for

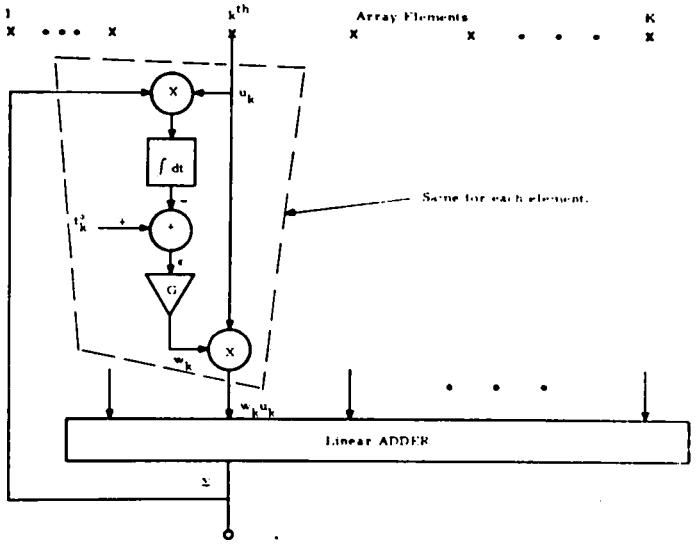

Fig.II.2.2 Weight control scheme of Applebaum's adaptive array[37].

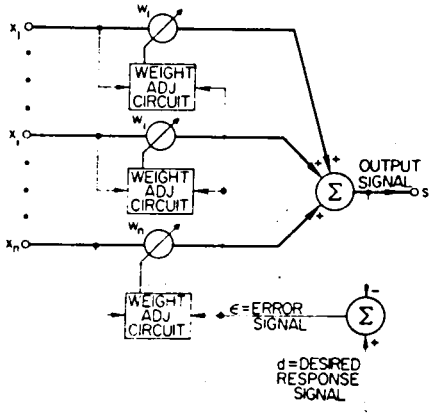

(a)

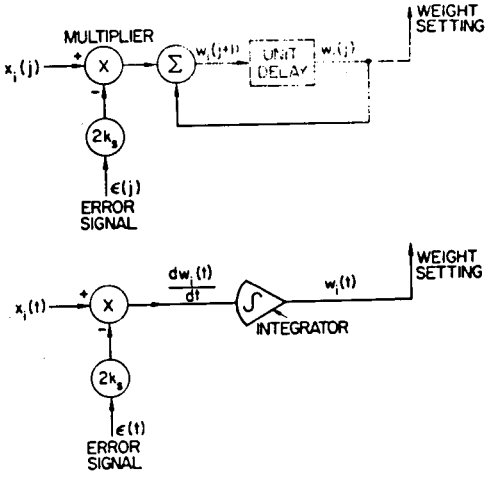

(b)

Fig.II.2.3 (a) Weight control scheme of least-mean-square-error adaptive array.
(b) Analog and digital implementation.

(after Widrow et al.[38])

least-mean-square-error processing using the estimated correlation vector between the received signals at each channel and the reference signal. Estimation of the correlation vector requires the a priori knowledge about the spectral density and the incident direction of the desired signal. Thus, his method may be effective for real time processing if the estimations could be performed easily. Zahm[39], however, pointed out that it resulted in the large amount of deteriorations in output signal-to-noise ratio if the estimation of the incident direction of the desired signal includes some errors. Griffiths[40] also proposed the adaptive algorithm based on the maximum-likelihood-ratio (MLR) criterion and the maximum-signal-to-noise ratio (MSNR) criterion. The algorithm for achieving the MLR processor is derived based on the fact that under the high signal-to-noise ratio environment, the LMSE processor may tend to it. Thus, the high power pilot signal was used for adaptation. The algorithm for achieving the MSNR processor also uses the steepest descent method as a following manner. At first, negative gradient direction of the performance measure (the output power in this case) with respect to the weights may be chosen. Then, the gradient components which minimize the desired signal may be estimated and be subtracted from the gradient to which the output power may be reduced. Detailed analysis for MSNR processor was not performed because of the complexity due to the nonlinearity of the problem. Computer simulations were carried out to compare the performances of the systems obtained by means of the

LMSE, MLR and MSNR algorithm. These results showed that the MSNR algorithm gives the higher output signal-to-noise ratio than the LMSE and MLR algorithm, however, the frequency characteristic is poorer than the others.

In the field of seismology, Capon et al.[41] proposed the procedures for designing the maximum-likelihood estimator in time domain and frequency domain. Their method is, however, so used for the seismometers' records that the off-line processing may be significant. Lacoss[42] presented the adaptive algorithm which converges to the maximum-likelihood estimator. This algorithm is designed for minimizing the system output power subject to a constraint by means of a steepest descent method with gradient projection. He also proposed the clipped gradient method for reducing the influences of significantly anomalous data on the weights of processor. His method required the occurrence of the same waveform of the desired signal at the same time at each element, thus spatial correction filter was indispensable. Claerbout[43] summarized and extended the filter design method subject to constraints. Constraint conditions described above are basically the same with Levin's condition[33]. Kobayashi[44] presented two iterative synthesis methods for a seismometer array processor. They are based on the steepest descent method with gradient projection and on the conjugate gradient method with gradient projection. In these methods, the spatial correction filter must also be included for providing the in phase condition along the array. The above described systems are all for digital

processings or simulated on a digital computer.

On the other hand, Riegler and Compton[45], Riegler[46] and Compton[47],[48] reported the experimental setups with analog feedback loops rather than computer controlled digital loops on the same concept, i.e. minimization of the mean-square-error, with Widrow et al.[38]. Thus, the basic scheme is the same with Fig.II.2.3. The experiments were performed with or without the amplitude modulated desired signal while the reference signal is only a carrier of the desired signal. They showed that the pattern null depth depends on the power of the interference, then the amplitude modulated interferences with high powers may cause the fluctuations of weights which result in the additional undesired fluctuation of the desired signal output. In addition to them, the amplitude modulated desired signal might decrease the array system response in the direction of the desired signal.

Chang and Tuteur[49] proposed the adaptive algorithm based on the least-mean-square-error method. Their method required the autocorrelation function and the incident direction of the desired signal rather than the actual reference signal. This concept resembles to Griffiths[31]. Brennan et al.[50] presented the effects of control loop noise on the performance of the adaptive array[37], i.e. the degradation of the output signal-to-noise ratio. They derived the expressions for the first and the second order loops. For reducing the effects of control loop noise, Brennan and Reed[51] introduced

the concept of hard limiting in the control loops and showed this technique does not affect the performance of the adaptive array. Booker and Ong[52] discussed the adaptive method for processing the seismometer array data subject to constraints. The examples of some constraint conditions were expressed and analyzed. They suggested the possibility of the constraint condition which utilizes the information about the expected incident direction of the desired signal. Frost[30], [53] summarized and analyzed in detail the least-mean-square-error method subject to constraints and considered some applications of this method. He presented the new constraint condition which designates the frequency characteristics of the system in digital filter form in the direction to which the beam is steered (look direction) by means of a spatial correction filter. He also presented the method to prevent the accumulation of errors in the iterative application of algorithm on digital computer due to the truncation or quantization of the projected gradient. Butcher and Sims[54] extended the works of Widrow et al.[38]. They introduced the concept of subfrequency sampling method in which the sampling and the weights adjustment are carried out sufficiently slower than the period of a signal carrier. It may be suitable for high frequency (radio frequency, RF) applications. Gabriel[55] proposed an alternative method using the fact that the eigenvectors of the input signal correlation matrix correspond to the linear combination of signal vectors along the elements due to the desired signal and the interferences. The appropriate combination of

these eigenvectors may cause pattern nulls in the directions of interferences. Zahm[56] presented the analytical method for evaluating the dynamic behavior of the adaptive array when exposed to the actual environment. He showed that the time constant of decrease of the output interference power depends on the input power of it. Brennan[57] summarized the principle of adaptive radar which maximizes the probability of detection. This method was closely related to the works of Applebaum[37] and Griffiths[31]. Baird[58] reported the recursive algorithm for minimizing the mean-square-error between the system output and the reference. Though, his method includes the direct inversion of the input signal correlation matrix, the matrix inversion lemma provides the somewhat easy implementations. The comparison of this algorithm, the algorithm based on the steepest descent method and the algorithm based on the random search method shows that the fastest convergence rate is achieved by the recursive algorithm. But, the recursive algorithm includes somewhat complicated processings, thus, the computation time for one iteration may be longer than the others. He also presented the recursive algorithm using the estimated correlations between the input signals and the reference signal. The relation between the recursive algorithm and the equation defining the Kalman filter was also discussed in detail.

Following the studies summarized briefly in this section, we proposed a new constraint condition, namely "directional constraint"[59]. In the following chapters, we will present the detailed analysis on this

directional constraint system and some simulation results on digital computer for demonstrating the performance of this system.

Chapter 3. ADAPTIVE OPTIMIZATION OF AN ARRAY SUBJECT TO CONSTRAINTS

3.1 Introduction

In this chapter, we will present the adaptive optimization procedure of an array system when exposed to a noisy environment. As reviewed in Chapter 2, several performance criteria were proposed. Among them, we paid our attentions to the least-mean-square-error method and to the constraint optimization procedures.

A least-mean-square-error method requires the reference signal which must be synchronized with carrier of the desired signal. If this requirement might not be satisfied, normal operation of the adaptive array system may not be achieved by this method. And if the desired signal is frequency modulated, the array system response toward the desired signal direction may become unstable due to the lack of synchronization.

On the contrary, the constrained optimization procedures do not require the detailed information, i.e. the waveform, of the desired signal. Constrained optimization methods were widely used in seismology for obtaining the maximum-likelihood estimate of the seismic signal using the fidelity constraint (see Chapter 2). Frost[30],[53] proposed the alternative constraint condition which designates the frequency characteristics in the look direction toward which the array beam is steered. The constrained optimization procedures described previously must include the spatial correction filter followed by the

processor. Thus, these systems consist of two processing stages, i.e. the beam steering stage and the interference rejection stage, in other words these systems are redundant.

Thus, we will propose the new constraint condition named "directional constraint" and demonstrate the performance of the adaptive array with this concept. In this system, two processing stages (beam steering stage and interference rejection stage) can be merged into one in which two processing operations are provided.

3.2 Description of the Concept

3.2.1 Receiving System of an Array and Processor

Prior to the main discussion on the new system, descriptions of the receiving system are given here. Typical configuration of an adaptive array is shown in Fig.II.3.1. In this figure, it is to be noted that the feedback loops are not depicted for simplicity. The amount of time delay which is symbolized by τ in Fig.II.3.1 is chosen to be equal to one quarter of the period of the center frequency of the desired signal. Thus, the phase of the desired signal is lagged through the time delay element with the amount of $\pi/2$, so that delayed and undelayed signal are orthogonal to each other.

The w_k(k=1, 2,..., K) represents the gain of each amplifier in Fig.II.3.1 which shall be called weight. The points to which the weights are connected are named as tap points. The x_k(k=1, 2,..., K) represents the signal at each tap point as depicted in Fig.II.3.1.

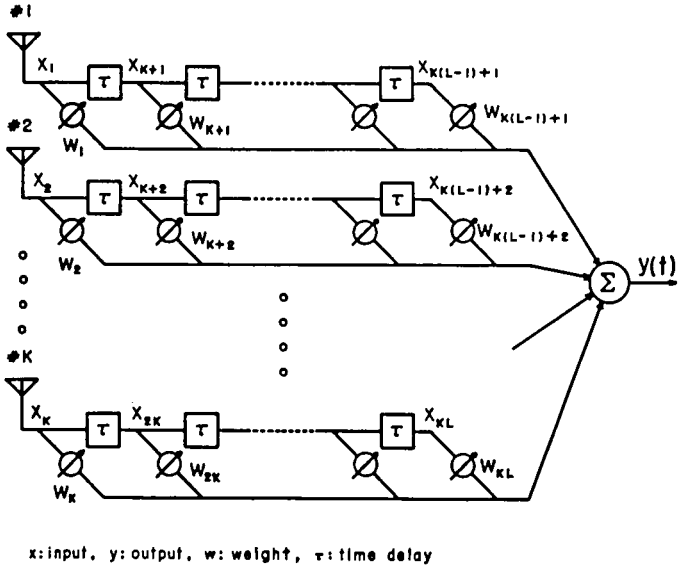

Fig.II.3.1 Configuration of an adaptive array under consideration except for the feedback loops.

Undelayed and delayed signal at each tap point are weighted and added to produce the array system output, y. For simplicity of formulations, weights are written in vector form as a following manner.

$$W^T = (w_1, w_2, \ldots, w_{KL}) \qquad \text{(II.3.1)}$$

Signals are also written in vector form as,

$$X^T = (x_1, x_2, \ldots, x_{KL}) \qquad \text{(II.3.2)}$$

where superscript T denotes the transpose. This notation will be used commonly in this part.

Using the vector notations described above, array system output, y, can be expressed by the inner product of the weight vector by the signal vector, i.e.,

$$y = X^T W = W^T X \qquad \text{(II.3.3)}$$

The above descriptions are free from the arrangement of the antenna elements so that we make no reference to the antenna array itself.

3.2.2 Expression of Signals

The signals x_k at each tap point consist of the desired signal component s_k and the undesired noise component n_k as,

$$x_k = s_k + n_k \quad , \quad k = 1, 2, \ldots, KL \qquad \text{(II.3.4)}$$

The undesired signal component generally consists of three

kinds, the interferences and isotropic noise coming from the external sources and the internal noise generated in the system. Again, vector forms are adopted as follows.

$$S^T = (s_1, s_2, \ldots, s_{KL}) \tag{II.3.5}$$

$$N^T = (n_1, n_2, \ldots, n_{KL}) \tag{II.3.6}$$

(II.3.4) can also be expressed in a vector form, as,

$$X = S + N \tag{II.3.7}$$

The correlation matrix of the tap-point signals is defined as follows.

$$R_{XX} = E[X\ X^T] \tag{II.3.8}$$

where E[ ] denotes the expected value. It is to be noted that R_{XX} is a KL-dimensional symmetric matrix, which can be easily proved by the direct application of transpose operation on (II.3.8). It may be duly assumed that the desired signal does not correlate with the undesired noise. The assumption is made that the internal noise does not correlate not only with the desired signal but also with the interferences. Then, we obtain,

$$R_{XX} = E[S\ S^T] + E[N\ N^T] \tag{II.3.9}$$

It is to be noted that $E[S\ S^T]$ is a correlation matrix of the desired signal vector so that it is positive semidefinite and $E[N\ N^T]$ consists

of the interference and internal noises which are independent to each other so that it is positive definite. Summarizing the above discussions, correlation matrix R_{XX} is positive definite.

3.3 Constraint Condition and Optimal Solution

Here, we will introduce the "directional constraint" condition. The condition aims to guarantee the response of the array system to the desired signal input that is coming from a specified direction at a certain frequency. The general form of constraint with regards to the weights may be expressed as follows[30),(53)].

$$C^T W = H \qquad \text{(II.3.10)}$$

where C is a $(KL \times M)$ matrix called the "constraint matrix" and H is an M-th order column vector, which will be called the "response vector" hereafter. M is an integer equal to or greater than L and equal to or smaller than KL. (II.3.10) defines the M-dimensional hyperplane in KL-dimensional hyperspace for W that will be called "constraint plane".

In the following analysis, we consider a simple system that has only two taps for each channel (the case L = 2 in Fig.II.3.1). It is also assumed that the antenna elements are located linearly with equal spacing of a half wavelength and the element factor is isotropic. It should be noted, however, that these assumptions are made in order to simplify the physical meanings of the results and do not essentially affect the validity of the analysis.

The complex (i.e. amplitude and phase) response $Y_h(\theta)$ of the array system under consideration to the signal with normalized amplitude and the angle of arrival, θ, can be expressed by the following formula.

$$Y_h(\theta) = \sum_{k=1}^{K} \{w_k \exp[j\psi_k(\theta)] + w_{k+K} \exp[j\{\psi_k(\theta)+\pi/2\}]\} \tag{II.3.11}$$

where

$$\psi_k(\theta) = \pi(k - \frac{K+1}{2}) \cos\theta \quad , \quad k=1, 2,\ldots,K \tag{II.3.12}$$

which denotes the phase of the signal arriving from the direction θ at each element with the phase reference taken at the center of the array. These phase differences result from the angle between the wavefront and the array baseline. Then, the complex response of the array system to a certain direction θ_c (which will be called the "constraint direction") is set under the constraint as follows.

$$Y_h(\theta_c) = 1 \tag{II.3.13}$$

This constraint specifies the transfer function of the system to be unity to the signal with the specified angle of arrival and frequency. Using (II.3.11), real and imaginary part of the constraint condition (II.3.13) can be expressed by the following equations.

$$\mathrm{Re}[Y_h(\theta_c)] = \sum_{k=1}^{K} \{w_k \cos\psi_k(\theta_c) - w_{k+K} \sin\psi_k(\theta_c)\} = 1 \tag{II.3.14}$$

$$\mathrm{Im}[Y_h(\theta_c)] = \sum_{k=1}^{K} \{w_k \sin\psi_k(\theta_c) + w_{k+K} \cos\psi_k(\theta_c)\} = 0 \qquad \text{(II.3.15)}$$

where Re[ ] and Im[ ] denote the real and the imaginary part of the value in brackets, respectively. (II.3.14) and (II.3.15) can be re-written in a vector product form as follows.

$$\mathrm{Re}[Y_h(\theta_c)] = (w_1, w_2, \ldots, w_K, w_{K+1}, w_{K+2}, \ldots, w_{2K}) \begin{pmatrix} \cos\psi_1(\theta_c) \\ \cos\psi_2(\theta_c) \\ \vdots \\ \cos\psi_K(\theta_c) \\ -\sin\psi_1(\theta_c) \\ -\sin\psi_2(\theta_c) \\ \vdots \\ -\sin\psi_K(\theta_c) \end{pmatrix} = 1 \qquad \text{(II.3.16)}$$

$$\mathrm{Im}[Y_h(\theta_c)] = (w_1, w_2, \ldots, w_K, w_{K+1}, w_{K+2}, \ldots, w_{2K}) \begin{pmatrix} \sin\psi_1(\theta_c) \\ \sin\psi_2(\theta_c) \\ \vdots \\ \sin\psi_K(\theta_c) \\ \cos\psi_1(\theta_c) \\ \cos\psi_2(\theta_c) \\ \vdots \\ \cos\psi_K(\theta_c) \end{pmatrix} = 0 \qquad \text{(II.3.17)}$$

Thus, with regard to (II.3.10), (II.3.16) and (II.3.17), C^T and H^T are given by (II.3.18) and (II.3.19), respectively.

$$C^T = \begin{vmatrix} \cos\psi_1(\theta_c),\ldots, \cos\psi_K(\theta_c), & -\sin\psi_1(\theta_c),\ldots, & -\sin\psi_K(\theta_c) \\ \sin\psi_1(\theta_c),\ldots, \sin\psi_K(\theta_c), & \cos\psi_1(\theta_c),\ldots, & \cos\psi_K(\theta_c) \end{vmatrix} \tag{II.3.18}$$

$$H^T = (1,\ 0) \tag{II.3.19}$$

In the same manner, extension to multiple directional constraints system can be easily performed in a straightforward manner.

If the output power of this array system is minimized under the condition of the above constraint, the noise component tends to be nullified while the signal component is maintained, with the result of maximum signal-to-noise ratio.

Mean output power of an array system, Q, is given by,

$$Q = E[W^T X X^T W] = W^T R_{XX} W \tag{II.3.20}$$

Q of (II.3.20) is a quadratic function with respect to W. As R_{XX} is positive definite, Q grows up when every term of W increases.

Now, the problem is to find W which minimizes the system output power Q of (II.3.20) subject to the constraint condition of (II.3.10). Geometrical interpretation of minimization of output power subject to the constraint is shown in Fig.II.3.2. Constrained minimization problem can be solved by means of the well known method of Lagrange multipliers. The following analysis is after Frost[30),(53].

The cost function A(W) is defined as follows by introducing M-th order column vector of undetermined Lagrange multipliers, Λ.

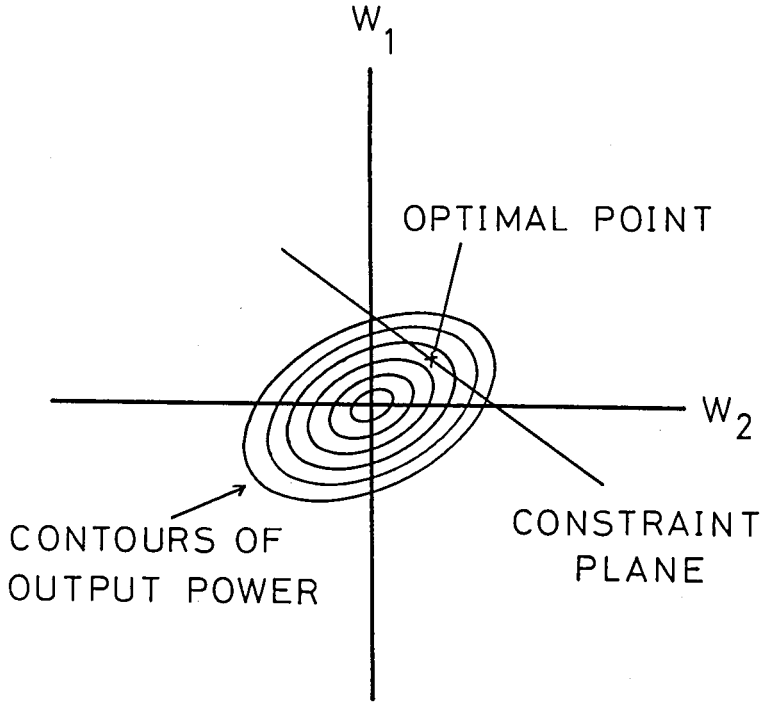

Fig.II.3.2 Geometrical interpretation of minimization of output power subject to constraint. The weight vector is assumed to be two dimensional for illustration. The optimal solution is shown by × on the constraint plane.

$$A(W) = \frac{1}{2} W^T R_{XX} W + \Lambda^T (C^T W - H) \qquad \text{(II.3.21)}$$

where coefficient $\frac{1}{2}$ is introduced for mathematical simplicity. Taking the gradient of $A(W)$ with respect to W, thus,

$$\nabla_W A(W) = R_{XX} W + C \Lambda \qquad \text{(II.3.22)}$$

(II.3.22) represents the gradient of the system output power with respect to W in the constraint plane. (II.3.21) is a quadratic function of W with positive definite matrix coefficient so that it has unique minima. Thus, the optimal weight vector, W_{opt}, can be obtained by equating (II.3.22) to zero. As discussed previously, R_{XX} is positive definite so that R_{XX}^{-1} exists. The W_{opt} can be written as follows.

$$W_{opt} = - R_{XX}^{-1} C \Lambda \qquad \text{(II.3.23)}$$

Then, we must determine the expression of Λ in terms of the previously defined vectors and matrices. The optimal weight vector W_{opt} must also satisfy the constraint condition of (II.3.10). Substituting (II.3.23) into (II.3.10), following expression is obtained.

$$C^T W_{opt} = - C^T R_{XX}^{-1} C \Lambda = H \qquad \text{(II.3.24)}$$

Solving (II.3.24) with respect to Λ, we can determine the Lagrange multipliers vector which is written as follows.

$$\Lambda = -(C^T R_{XX}^{-1} C)^{-1} H \qquad \text{(II.3.25)}$$

The existence of $(C^T R_{XX}^{-1} C)^{-1}$ can be proved easily because of the fact that R_{XX} is positive definite and C has full ranks.

Thus, substituting (II.3.25) into (II.3.23), we can obtain the expression of W_{opt} as follows.

$$W_{opt} = R_{XX}^{-1} C (C^T R_{XX}^{-1} C)^{-1} H \qquad \text{(II.3.26)}$$

If, the environment condition, i.e. R_{XX} is perfectly known or can be estimated with sufficient accuracy, direct calculation of (II.3.26) may be performed. These informations are, however in general, inavailable. Then, we must develop the alternative method in which weight vector is updated through observations of the environment and converges to its optimal which matches to the environment.

3.4 Iterative Algorithm for Sampling Feedback Loop

Renewal of the weight vector subject to constraints is generally performed by means of the steepest descent method with gradient projection. This technique was adopted by many authors. We suppose the computer controlled feedback loops for changing the weight vector so that the iterative algorithm is required to converge the weight vector to its optimal. In the steepest descent method, changing of the weight vector is performed toward the direction to which the gradient of the cost function with respect to the weight vector is steepest. Thus, the basic algorithm can be expressed as follows. The temporary assumptions are made that R_{XX} is known.

$$W(m+1) = W(m) - \mu \nabla_W A[W(m)] \qquad \text{(II.3.27)}$$

where μ is called a step size which determines the amount of increments of weights and m is an iteration number. In the following analysis, also the method of Lagrange multipliers is employed for the formulation. Cost function is a function of W, and W varies with iteration so that Lagrange multipliers are functions of iteration number.

Thus, cost function is expressed in place of (II.3.21) as follows.

$$A[W(m)] = \frac{1}{2} W^T(m) R_{XX} W(m) + \Lambda^T(m) [C^T W(m) - H] \qquad \text{(II.3.28)}$$

where $\Lambda(m)$ is the undetermined vector of Lagrange multipliers at m-th iteration. Gradient of (II.3.28) with respect to W(m) can be thus obtained as follows.

$$\nabla_W A[W(m)] = R_{XX} W(m) + C \Lambda(m) \qquad \text{(II.3.29)}$$

Substitution of (II.3.29) into (II.3.27) gives the following adaptive algorithm, yet, which includes the undetermined Lagrange multipliers vector.

$$W(m+1) = W(m) - \mu[R_{XX} W(m) + C \Lambda(m)] \qquad \text{(II.3.30)}$$

The constraint condition must be satisfied not only for W(m) but also for W(m+1). Thus,

$$C^T W(m+1) = C^T W(m) - \mu[C^T R_{XX} W(m) + C^T C \Lambda(m)] = H \quad \text{(II.3.31)}$$

and

$$C^T W(m) = H \quad \text{(II.3.32)}$$

Then, we have,

$$C^T R_{XX} W(m) + C^T C \Lambda(m) = 0 \quad \text{(II.3.33)}$$

Solving (II.3.33) with respect to $\Lambda(m)$ gives the following expression. It is to be noted that $(C^T C)^{-1}$ exists because of the fact that C has full ranks.

$$\Lambda(m) = -(C^T C)^{-1} C^T R_{XX} W(m) \quad \text{(II.3.34)}$$

Iterative algorithm for constrained optimization can be expressed thus by substituting (II.3.34) into (II.3.30) as follows.

$$W(m+1) = W(m) - \mu P R_{XX} W(m) \quad \text{(II.3.35)}$$

with

$$P = U - C (C^T C)^{-1} C^T \quad \text{(II.3.36)}$$

P is a projection operator which projects a vector onto the constraint plane and U is a unit matrix. The algorithm of (II.3.35) which is a steepest descent algorithm with gradient projection was used by Lacoss [42], Winkler and Schwartz [60] and others. But, as pointed out by

Frost[30],[53], small computation error may occur at each iteration because of the truncation, round off or quantization error in an implementation of this algorithm on digital computer. Thus, a large number of the iterative applications of this algorithm may accumulate the computation errors causing the deviation of the weight vector from a constraint plane. These faults become more serious if a processor may adopt a short bit computer. Frost proposed a constrained least-mean-square algorithm which has the error correction feature. Referring to (II.3.32), formulation of a gradient projection algorithm (II.3.35) is based on a premise that $W(m)$ is satisfying the constraint condition.

However, if once the weight vector does not satisfy the constraint condition because of the computation error, the weight vector of following iterations may run away from a constraint plane. To avoid this fault , the algorithm with error correction feature was proposed by Frost that Lagrange multipliers vector must be determined from the following equation rather than (II.3.33).

$$C^T W(m) - \mu[C^T R_{XX} W(m) + C^T C \Lambda(m)] = H \qquad \text{(II.3.37)}$$

Solving (II.3.37) with respect to $\Lambda(m)$, the following equation is obtained.

$$\Lambda(m) = \frac{1}{\mu} (C^T C)^{-1} C^T W(m) - (C^T C)^{-1} C^T R_{XX} W(m) - \frac{1}{\mu} (C^T C)^{-1} H \qquad \text{(II.3.38)}$$

Substituting (II.3.38) into (II.3.30) and making some arithmetical manipulations, the constrained least-mean-square algorithm can be obtained as a following manner[30),(53)].

$$W(m+1) = P[W(m) - \mu R_{XX} W(m)] + F \qquad \text{(II.3.39)}$$

with

$$F = C (C^T C)^{-1} H \qquad \text{(II.3.40)}$$

The vector F of (II.3.40) is the shortest one, in other words perpendicular to a constraint plane, which satisfies the constraint condition. The proof is given as follows.[61] The vector W_s is assumed to be the shortest vector which satisfies the constraint condition. For obtaining the expression of W_s, we make use of the method of Lagrange multipliers. Thus, the cost function for W_s is defined as,

$$M(W_s) = \frac{1}{2} W_s^T W_s + \Lambda^T (C^T W_s - H) \qquad \text{(II.3.41)}$$

Apparently, (II.3.41) is a quadratic function of W_s having unique minima. From the definition on W_s, gradient of (II.3.41) with respect to the weight vector must be zero. Thus,

$$\nabla_W M(W_s) = W_s + C \Lambda = 0 \qquad \text{(II.3.42)}$$

Therefore, W_s can be written as follows.

$$W_s = - C \Lambda \qquad \text{(II.3.43)}$$

W_s must also satisfy the constraint condition, then,

$$C^T W_s = - C^T C \Lambda = H \qquad \text{(II.3.44)}$$

From (II.3.44), undetermined vector of Lagrange multipliers can be solved as follows.

$$\Lambda = -(C^T C)^{-1} H \qquad \text{(II.3.45)}$$

Existence of $(C^T C)^{-1}$ is discussed previously. Substituting (II.3.45) into (II.3.43) gives the expression of W_s, the shortest vector which satisfies the constraint condition.

$$W_s = C (C^T C)^{-1} H \qquad \text{(II.3.46)}$$

which is the same with (II.3.40). Therefore, F of (II.3.40) is proved as the shortest vector which satisfies the constraint condition.

Though, in (II.3.39), correlation matrix R_{XX} is included, in practice, R_{XX} may be inavailable. Then, we approximate R_{XX} by the outer product of the instantaneous value of the signals at each tap point, namely, $X(m)\ X^T(m)$. The practical form of the algorithm is thus written as follows.

$$W(m+1) = P[W(m) - \mu\ X(m)\ y(m)] + F \qquad \text{(II.3.47)}$$

where

$$y(m) = X^T(m)\ W(m) = W^T(m)\ X(m) \qquad \text{(II.3.48)}$$

which is an instantaneous output of the array system. Block diagram representation of the operation of (II.3.47) is shown in Fig.II.3.3.

The constrained least-mean-square algorithm (II.3.39) is the same with gradient projection algorithm (II.3.35), if

$$W(m) = P\, W(m) + F \tag{II.3.49}$$

is satisfied, which indicates that $W(m)$ is in a constraint plane. Here, we present the proof of (II.3.49) when $W(m)$ satisfies the constraint condition. We assume that $W(m)$ satisfies the constraint condition, namely,

$$C^T W(m) = H \tag{II.3.50}$$

Using (II.3.36) and (II.3.50), projection operation with P on $W(m)$ gives the following equation.

$$\begin{aligned} P\, W(m) &= [U - C\, (C^T C)^{-1} C^T]\, W(m) \\ &= W(m) - C\, (C^T C)^{-1} H \end{aligned} \tag{II.3.51}$$

The vector F is given by (II.3.40) and is the same with the second term of the right hand side of (II.3.51). After substituting (II.3.40) into (II.3.51) and rearranging the equation, it yiels the same expression with (II.3.49). Geometrical representation is given in Fig.II.3.4. From Fig.II.3.4, the weight vector which satisfies the constraint condition can be divided into two parts; one of them is the component which is

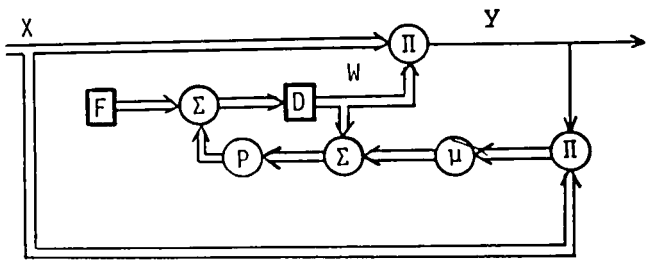

Fig.II.3.3 Block diagram representation of the constrained least-mean-square algorithm. In this figure, Σ, Π and D represent the sum, multiplication and time delay operation, respectively. The double line denotes the flow of vectors and single line denotes the flow of scalars.

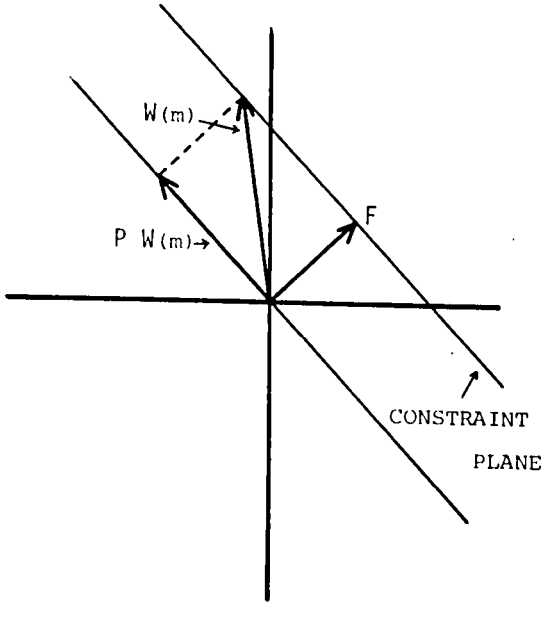

Fig.II.3.4 Division of a weight vector into the components parallel to and perpendicular to the constraint plane.

parallel to the constraint plane and the other is a perpendicular vector which satisfies the constraint condition.

The next, for demonstrating the feature of the constrained least-mean-square algorithm in comparison with the gradient projection algorithm, geometrical interpretations are made in Figs.II.3.5 and II.3.6. As shown in Fig.II.3.5, if W(m) might deviate from a constraint plane because of the computation errors, the constrained least-mean-square algorithm can correct the errors in the next step, that is W(m+1) will satisfy the constraint condition. But, in the gradient projection algorithm (see Fig.II.3.6), projection operation is applied only to the additional term, and W(m+1) can not satisfy the constraint condition if W(m) might deviate from a constraint plane. Taking into consideration of the above discussions, we will adopt the constrained least-mean-square algorithm hereafter.

In a digital loop, the problem of stability may occur. The loop stability in a digital loop depends on the loop gain which corresponds to a step size μ in our problem. After Frost[30],[53], for the proof of convergence of the algorithm, the behavior of the Euclidian norm between the weight vector and the optimal weight vector is examined which must decrease according to the increment of iteration numbers.

Taking the expected value of both sides of (II.3.47) gives the following equation.

$$E[W(m+1)] = P\{E[W(m) - \mu R_{XX} E[W(m)]\} + F \quad \text{(II.3.52)}$$

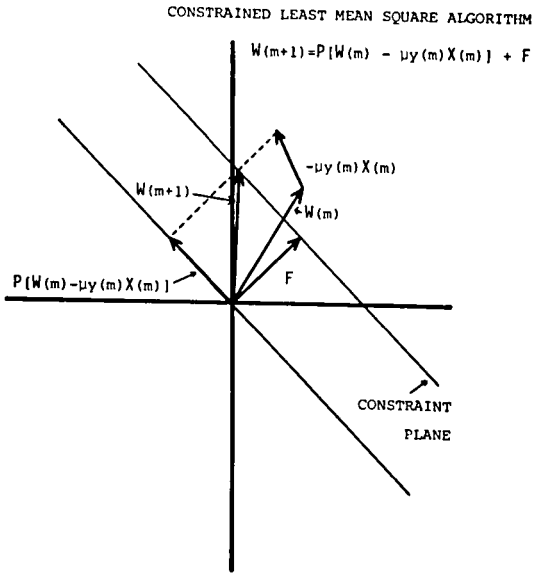

Fig.II.3.5 Error correcting feature of the constrained least-mean-square algorithm.

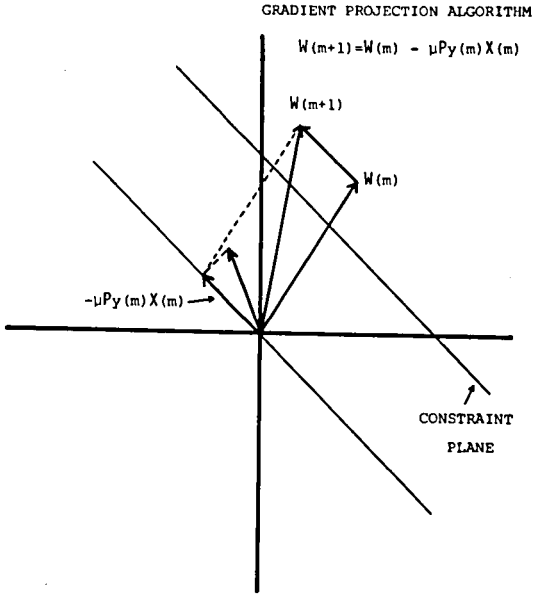

Fig.II.3.6 Error propagation feature of the gradient projection algorithm.

We define the vector $V(m)$ as a following manner.

$$V(m) = E[W(m)] - W_{opt} \qquad \text{(II.3.53)}$$

Subtracting the optimal weight vector from both sides of (II.3.52) and using (II.3.49) and (II.3.53) give the following equation in terms of $V(m)$.

$$\begin{aligned} V(m+1) &= [U - \mu P R_{XX} P] V(m) \\ &= [U - \mu P R_{XX} P]^{m+1} V(0) \end{aligned} \qquad \text{(II.3.54)}$$

The initial difference vector $V(0)$ can be expressed by a linear combination of the eigenvectors of $P R_{XX} P$ whose associated eigenvalues are nonzero. Then, $V(0)$ is expressed by the following form.

$$V(0) = \sum_{k=1}^{2K'} a_k G_k \qquad \text{(II.3.55)}$$

where G_k (k=1, 2,..., 2K') is an eigenvector of $P R_{XX} P$ with nonzero eigenvalue. a_k (k=1, 2,..., 2K') is an undetermined coefficient and K' is a number equal to or smaller than K. Substituting (II.3.55) into (II.3.54) and operating some arithmetical manipulations yield the following expression.

$$V(m+1) = \sum_{k=1}^{2K'} a_k (1 - \mu \lambda_k)^{m+1} G_k \qquad \text{(II.3.56)}$$

where λ_k is an eigenvalue associated to the eigenvector G_k. If we

choose μ to satisfy the relation $0 < 1 - \mu \lambda_k < 1$ for all k, convergence of (II.3.47) to the optimal weight vector in an expected value sense, may be guaranteed. Thus, μ must be chosen as follows for convergence of the algorithm.

$$0 < \mu < \frac{1}{\lambda_{max}} \qquad \text{(II.3.57)}$$

where λ_{max} is the maximum eigenvalue of $P\ R_{XX}\ P$.

Chapter 4. TRANSIENT BEHAVIOR AND STEADY STATE PERFORMANCE OF THE ADAPTIVE ARRAY WITH SINGLE DIRECTIONAL CONSTRAINT

4.1 Introduction

As discussed in Chapter 3, Frost's analysis gives only the sufficient condition that the step size μ must be satisfied for convergence of the algorithm and also shows that the convergence rate depends on the product of the step size and the eigenvalue of the matrix $P\ R_{XX}\ P$. In this chapter, for clarifying the behavior of each weight in terms of time, we will analyze the expected behavior of the system in detail and discuss the convergence properties of the system in terms of the conditions of the environment. For convenience of the analysis, adaptive algorithm of (II.3.47) developed in Chapter 3 is reformulated to the algorithm with the form of vector differential equation with matrix coefficient. Thus, for solving such vector differential equation, diagonalization of matrix coefficient must be required.

As to the detailed dynamic behavior, Zahm[56] presented an effective method to solve a vector differential equation. His objective, however, aimed at the adaptive array of the least-mean-square-error style. Thus, we will utilize his method to analyze in detail the convergence properties of our system of directional constraint when it is exposed to a certain environment. In Zahm's analysis, as the eigenvectors concerned with the internal noise components can not be evaluated explicitly, the perfect prediction of the behavior of the weight

is impossible generally. But, in the applications of this method to our problem, practical and reasonable choice of the initial weight vector makes it possible to evaluate the change of the weight vector.

4.2 Governing Equation

For utilizing Zahm's method, we must reformulate the adaptive algorithm of (II.3.47) to a form of vector differential equation.

First, we take the expectation of (II.3.47) with the aid of (II.3.49).

$$E[W(m+1)] = E[W(m)] - \mu P R_{XX} P E[W(m)] - \mu P R_{XX} F \tag{II.4.1}$$

With T_s as the notation for the sampling interval, (II.4.1) can be rewritten as follows.

$$\frac{E[W(m+1)] - E[W(m)]}{T_s} + \frac{\mu}{T_s} P R_{XX} P E[W(m)] = -\frac{\mu}{T_s} P R_{XX} F \tag{II.4.2}$$

We return from the discrete quantity to the continuous quantity and obtain a differential equation by tending T_s to zero in (II.4.2). For simplicity of the expression, $E[W(m)]$ is rewritten as $W(t)$.

$$\frac{dW(t)}{dt} + q P R_{XX} P W(t) = -q P R_{XX} F \tag{II.4.3}$$

where q is the equivalent step size per unit time (μ/T_s) and always positive. By solving (II.4.3), behavior of the weight vector in terms

of time, t, can be predicted when exposed to a given environment. The informations about the environment are included in the correlation matrix R_{XX} and about the constraint condition in the projection operator P and the vector F. As (II.4.3) has a form of linear first order differential equation, it is expected that time constant of the convergence may be governed by the eigenvalues of $P\ R_{XX}\ P$. As discussed previously, P and R_{XX} are symmetric matrices so that $P\ R_{XX}\ P$ is a symmetric one. Thus, 2K eigenvectors exist which are orthogonal to each other. Using these eigenvectors, we can divide the vector differential equation of (II.4.3) into 2K scalar differential equations. Solving these equations and again recomposing the weight vector give the solution of (II.4.3).

4.3 Analysis on the Case with Accurate Prediction of the Desired Signal Direction

For convenience of the following analysis, complex notation is introduced. Then, matrices W, C and H must be modified as,

$$W^T = (w_1+jw_{1+K},\ w_2+jw_{2+K},\ldots,\ w_K+jw_{2K}) \qquad \text{(II.4.4)}$$

$$C^T = (z_{c1},\ z_{c2},\ldots,\ z_{cK}) \qquad \text{(II.4.5)}$$

$$H^T = 1\ \underline{/0°} \qquad \text{(II.4.6)}$$

where

$$z_{ck} = \exp[j\psi_k(\theta_c)] \quad , \quad k = 1,\ 2,\ldots,K \qquad \text{(II.4.7)}$$

The constraint condition of (II.3.10) is thus modified as,

$$C^* W = H \qquad \text{(II.4.8)}$$

where superscript (*) denotes the complex conjugate transpose. It is to be noted that the value of H can be chosen arbitrary, however, we put H equal to be $1\underline{/0°}$ for the ease of the analysis. Using the expression of (II.4.5), (II.3.36) and (II.3.40) are also reformulated as follows. It is to be noted that the complex conjugate transpose operation of matrices must be employed in place of the transpose operation in (II.3.36) and (II.3.40)

$$P = U - \frac{1}{K} C C^* \qquad \text{(II.4.9)}$$

$$F = \frac{1}{K} C \qquad \text{(II.4.10)}$$

The k-th channel of the adaptive array under consideration is shown in Fig.II.4.1. The desired signal component and the interference component at each channel can be expressed in a vector form using the familiar complex envelope notation[62].

$$S^T(t) = s(t)\ Z_s^T = s(t)\ (z_{s1}, z_{s2}, \ldots, z_{sK}) \qquad \text{(II.4.11)}$$

$$B^T(t) = b(t)\ Z_b^T = b(t)\ (z_{b1}, z_{b2}, \ldots, z_{bK}) \qquad \text{(II.4.12)}$$

$$z_{sk} = \exp[j\psi_k(\theta_s)] \quad , \quad k=1, 2, \ldots, K \qquad \text{(II.4.13)}$$

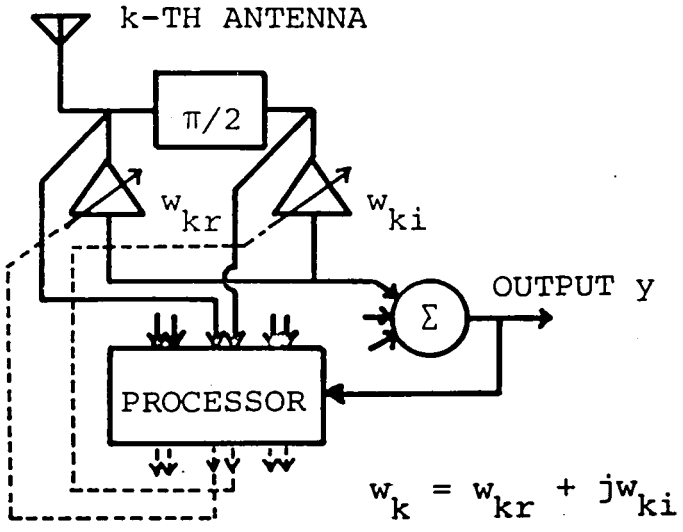

Fig.II.4.1 Block diagram of the feedback loop associated to the k-th element.

$$z_{bk} = \exp[j\psi_k(\theta_b)] \quad , \quad k = 1, 2, \ldots, K \qquad \text{(II.4.14)}$$

where s(t) and b(t) are the complex envelopes of the desired signal and the interference, respectively. z_{sk} and z_{bk} are the phasors at the k-th element corresponding to the desired signal and the interference, respectively, which in turn are arriving from the angles θ_s and θ_b, respectively. The internal noise component is assumed to be random and independent at each channel. Its average power per channel is denoted by P_r. The complex correlation matrix R_{XX} can, therefore, be expressed in the following manner by using (II.3.9), (II.4.11) and (II.4.12).

$$R_{XX} = P_r U + P_s Z_s Z_s^* + P_b Z_b Z_b^* \qquad \text{(II.4.15)}$$

where P_s and P_b are the average powers of the desired signal and the interference and given by the following equations. (The desired signal and the interference are assumed to be ergodic.)

$$P_s = \lim_{T\to\infty} \frac{1}{T} \int_0^T |s(t)|^2 \, dt \qquad \text{(II.4.16)}$$

$$P_b = \lim_{T\to\infty} \frac{1}{T} \int_0^T |b(t)|^2 \, dt \qquad \text{(II.4.17)}$$

Though, in the analysis, only one interference is assumed to exist, extensions to multiple interferences can be performed in a straightforward manner. R_{XX} is Hermitian because of the following relationship of (II.4.18) and (II.4.19).

$$(Z_s Z_s^*)^* = Z_s Z_s^* \qquad \text{(II.4.18)}$$

$$(Z_b Z_b^*)^* = Z_b Z_b^* \qquad \text{(II.4.19)}$$

Thus, K eigenvectors exist which are orthogonal one another. It is to be noted that the eigenvalues of Hermitian are all real values. In addition to them, as discussed previously, R_{XX} is positive definite. First, we assume that the angle of the desired signal falls on the constraint direction, which means $\theta_s = \theta_c$ ($Z_s = C$). Using (II.4.9), (II.4.10) and (II.4.15), expression of the forced term of (II.4.3) except for q can be written as follows.

$$P R_{XX} F = - \frac{P_b |C^* Z_b|^2}{K^2} C + \frac{P_b C^* Z_b}{K} Z_b \qquad \text{(II.4.20)}$$

In order to solve (II.4.3), we must find the eigenvectors of $P R_{XX} P$. By (II.4.9) and (II.4.15), we obtain the next formula.

$$P R_{XX} P = P_r U - \frac{P_r}{K} Z_s Z_s^* + \frac{P_b}{K^2} (Z_s^* Z_b)^2 Z_s Z_s^* + P_b Z_b Z_b^*$$

$$- \frac{P_b}{K} (Z_s^* Z_b) Z_s Z_b^* - \frac{P_b}{K} (Z_b^* Z_s) Z_b Z_s^* \qquad \text{(II.4.21)}$$

From the assumption that the array is linear with equal spacing of a half wavelength, $Z_s^* Z_b$ is a real function and the same with $Z_b^* Z_s$. Direct operation of the complex conjugate transpose on (II.4.21) shows

that $P\ R_{XX}\ P$ is Hermitian. Thus, $P\ R_{XX}\ P$ of (II.4.21) has K eigenvectors which are orthogonal one another. Frost proved that the constraint vector C is one of these eigenvectors whose associated eigenvalue is zero. This fact can be easily interpreted as follows; each row vector of $P\ R_{XX}\ P$ is in the constraint plane so that the inner product of the constraint vector and each row vector of $P\ R_{XX}\ P$ is zero which results in the zero eigenvalue. We will denote this eigenvector as G_1 and eigenvalue as λ_1 as follows.

$$G_1 = C \tag{II.4.22}$$

$$\lambda_1 = 0 \tag{II.4.23}$$

Next, we assume another eigenvector as a linear combination of C and Z_b as,

$$G_2 = a\ C + b\ Z_b \tag{II.4.24}$$

For obtaining the expressions of the coefficients a and b, (II.4.24) is substituted into a characteristic equation for $P\ R_{XX}\ P$ of (II.4.21). It is to be noted that C and Z_s are the same vectors because of the assumption, $\theta_c = \theta_s$.

$$P\ R_{XX}\ P\ (aC + bZ_b) = \{\frac{bP_b}{aK^2}\ (C^*\ Z_b)^3 - \frac{bP_r}{aK}\ C^*\ Z_b - \frac{bP_b}{a}\ C^*\ Z_b\}\ aC$$

$$+\{P_r + K P_b - \frac{P_b}{K} (C^* Z_b)^2\} b Z_b = \lambda_2 (aC + bZ_b) \qquad \text{(II.4.25)}$$

Equating the coefficients of aC and bZ_b in (II.4.25), $\frac{b}{a}$ can be determined as a following manner.

$$\frac{b}{a} = - \frac{K}{C^* Z_b} \qquad \text{(II.4.26)}$$

The eigenvalue λ_2 can be, thus, obtained as follows.

$$\lambda_2 = P_r + K P_b (1 - A_{cb}^2) \qquad \text{(II.4.27)}$$

where we have introduced a new notation as,

$$A_{cb} = \frac{C^* Z_b}{K} = \frac{\sin[\frac{K\pi}{2} (\cos \theta_c - \cos \theta_b)]}{K \sin[\frac{\pi}{2} (\cos \theta_c - \cos \theta_b)]} = \frac{Z_b^* C}{K} = A_{bc} \qquad \text{(II.4.28)}$$

We put b equal to 1 so that the eigenvector G_2 can be expressed as a following manner.

$$G_2 = - A_{cb} C + Z_b \qquad \text{(II.4.29)}$$

A_{cb} or A_{bc} in (II.4.28) happens to be the value in the direction of the interference (θ_b) of the radiation pattern of a uniformly excited array whose main beam is steered to the direction of the desired signal (θ_s) that is equal to the constraint direction (θ_c) under the present assumption. The remaining eigenvectors G_i (i=3, 4,..., K) must be in the constraint plane and may be chosen to be orthogonal to G_2. These facts

can be approved through considerations about the K-dimensional hyperspace. Orthogonality between G_i (i=3, 4,..., K) and G_j (j=3, 4,..., K, $i \neq j$) can be also approved through the same reason. It can be derived from (II.4.21) that all of their associated eigenvalues λ_i (i=3, 4,..., K) have the same value of P_r. Arbitrary weight vector can now be expressed by a linear combination of these eigenvectors as,

$$W(t) = \sum_{i=1}^{K} a_i(t)\, G_i \qquad \text{(II.4.30)}$$

where $a_i(t)$ (i=1, 2,..., K) are the undetermined coefficients for each eigenspace spanned by G_i (i=1, 2,..., K). It is to be noted that the coefficients $a_i(t)$ are varying with time which correspond to the change of weights in terms of time.

At first, for determining the coefficients of each eigenvector for the initial weight vector W_0, following considerations are made. W_0 can be written from (II.4.30) as,

$$W_0 = \sum_{i=1}^{K} a_i(0)\, G_i \qquad \text{(II.4.31)}$$

Making the inner products of each eigenvector by (II.4.31), following equations are obtained.

$$G_i^{*}\, W_0 = a_i(0)\, G_i^{*}\, G_i \quad , \quad i=1, 2,..., K \qquad \text{(II.4.32)}$$

Thus,

$$a_i(0) = \frac{G_i^{*}\, W_0}{G_i^{*}\, G_i} \quad , \quad i=1, 2,..., K \qquad \text{(II.4.33)}$$

Giving our mind to the results of the above, we turn our attention to the problem for solving (II.4.3).

Substituting (II.4.30) into (II.4.3) gives the following equation.

$$\frac{d \sum_{i=1}^{K} a_i(t)\, G_i}{dt} + q\, P\, R_{XX}\, P \sum_{i=1}^{K} a_i(t)\, G_i = -\, q\, P\, R_{XX}\, F \qquad \text{(II.4.34)}$$

Thus, the behavior of the weight in the eigenspace spanned by G_i (i=1, 2,...,K) can be obtained by operating the complex conjugate transpose of G_i to (II.4.34) from the left hand side of it as,

$$\frac{d\, a_i(t)}{dt} + q\, \lambda_i\, a_i(t) = -\, q\, G_i^{*}\, P\, R_{XX}\, F \quad , \qquad i=1,\ 2,\ldots,\ K \qquad \text{(II.4.35)}$$

It is to be noted that G_i (i=3, 4,...,K) are in the constraint plane and orthogonal to the vector Z_b so that they are orthogonal to $P\, R_{XX}\, F$. Thus, (II.4.35) can be written as follows.

$$\frac{d\, a_1(t)}{dt} = 0 \qquad \text{(II.4.36)}$$

$$\frac{d\, a_2(t)}{dt} + q\, \lambda_2\, a_2(t) = -\, q\, G_2^{*}\, P\, R_{XX}\, F \qquad \text{(II.4.37)}$$

$$\frac{d\, a_i(t)}{dt} + q\, \lambda_i\, a_i(t) = 0 \quad , \qquad i=3,\ 4,\ldots,\ K \qquad \text{(II.4.38)}$$

Solving the above equations, following expressions can be obtained using the results of (II.4.33).

$$a_1(t) = \frac{G_1^* W_0}{G_1^* G_1} \qquad \text{(II.4.39)}$$

$$a_2(t) = \frac{G_2^* W_0}{G_2^* G_2} \exp(-q\lambda_2 t) - \frac{1}{\lambda_2}\{1 - \exp(-q\lambda_2 t)\}\frac{G_2^* P R_{XX} F}{G_2^* G_2} \qquad \text{(II.4.40)}$$

$$a_i(t) = \frac{G_i^* W_0}{G_i^* G_i} \exp(-q\lambda_i t) \quad , \quad i=3, 4, \ldots, K \qquad \text{(II.4.41)}$$

Using (II.4.30), (II.4.39), (II.4.40) and (II.4.41), solution of (II.4.3) can be written as follows.

$$W(t) = \frac{G_1^* W_0}{G_1^* G_1} G_i - \frac{1}{\lambda_2}\{1 - \exp(-q\lambda_2 t)\} \frac{G_2^* P R_{XX} F}{G_2^* G_2} G_2 + \sum_{i=2}^{K} \frac{G_i^* W_0}{G_i^* G_i} G_i \exp(-q\lambda_i t) \qquad \text{(II.4.42)}$$

Initial weight vector W_0 must be chosen to satisfy the constraint condition. Thus,

$$C^* W_0 = H \qquad \text{(II.4.43)}$$

In order to verify the constraint condition, we make the inner product

of (II.4.42) by the constraint vector C. As the constraint vector C is equal to G_1 and is orthogonal to the eigenvector G_i (i=2, 3,..., K), (because the eigenvector G_i (i=2, 3,..., K) is in the constraint plane), the following equation is obtained.

$$C^* W(t) = G_1^* W_0 = C^* W_0 = H \qquad \text{(II.4.44)}$$

Thus, it is proved that the weight vector which is the solution of (II. 4.3) satisfies the constraint condition in every time. Since all λ_i are zero or positive so that the weight vector of (II.4.42) converges as time elapses, resulting in,

$$\lim_{t\to\infty} W(t) = \frac{1}{K} G_1 - \frac{1}{P_r + K P_b (1 - A_{cb}^2)} P_b A_{cb} G_2 \qquad \text{(II.4.45)}$$

where A_{cb} is given in (II.4.28).

Now, the proof that (II.4.45) gives the minimum output noise power is presented. Arbitrary weight vector W_a can also be expressed by the linear combination of the eigenvectors G_i (i=1, 2,...,K) as follows.

$$W_a = \sum_{i=1}^{K} b_i G_i \qquad \text{(II.4.46)}$$

where b_i is the undetermined coefficient and G_i is the eigenvector derived previously. W_a of (II.4.46) must satisfy the constraint condition. Thus,

$$C^* W_a = \sum_{i=1}^{K} b_i C^* G_i = H \qquad \text{(II.4.47)}$$

As C is equal to G_1 and is orthogonal to G_i (i=2, 3,..., K), b_1 can be obtained as,

$$b_1 = \frac{1}{K} \qquad \text{(II.4.48)}$$

The array system response toward the interference direction can be obtained by making the inner product of (II.4.46) by Z_b as follows.

$$Z_b^* W_a = b_1 Z_b^* C + b_2 K (1 - A_{cb}^2) \qquad \text{(II.4.49)}$$

Thus, the output interference power is given by,

$$P_b (Z_b^* W_a)^2 = P_b \{A_{cb} + K b_2 (1 - A_{cb}^2)\}^2 \qquad \text{(II.4.50)}$$

In addition, the output internal noise power can be written as a following manner.

$$P_r W_a^* W_a = P_r \sum_{i=1}^{K} b_i^2 G_i^* G_i \qquad \text{(II.4.51)}$$

Substituting (II.4.22), (II.4.29) and (II.4.48) into (II.4.49) and (II.4.50) and rearranging terms, we get the following expression for the total output noise power, P_t.

$$P_t = \frac{P_r}{K} + P_b A_{cb}^2 + P_r \sum_{i=3}^{K} b_i^2 G_i^* G_i + 2b_2 K P_b A_{cb}(1 - A_{cb}^2)$$

$$+ b_2^2 K (1 - A_{cb}^2) \{P_r + K P_b (1 - A_{cb}^2)\} \qquad \text{(II.4.52)}$$

(II.4.52) can be interpreted as a quadratic function of b_2 whose second order coefficient is positive, because the A_{cb} is always less than 1 except for the condition that the interference direction is coincident with the constraint direction. In addition to them, (II.4.52) expresses the total output noise "power", thus, which is positive in all cases through dimensional considerations. For finding the coefficient b_2 which gives the minimum output noise power, differentiating (II.4.52) with respect to b_2 and equating to zero, the following equation is obtained.

$$P_b A_{cb} + b_2 \{P_r + K P_b (1 - A_{cb}^2)\} = 0 \qquad \text{(II.4.53)}$$

Therefore, we have,

$$b_2 = - \frac{P_b A_{cb}}{P_r + K P_b (1 - A_{cb}^2)} \qquad \text{(II.4.54)}$$

(II.4.48) and (II.4.54) are the coefficients of G_1 and G_2 of (II.4.45) themselves, respectively. Under the conditions of (II.4.48) and (II.4.54), total output noise power P_t can be written as follows.

$$P_t = \frac{P_r (P_r + K P_b)}{K \{P_r + K P_b (1 - A_{cb}^2)\}} + P_r \sum_{i=3}^{K} b_i^2 G_i^* G_i \qquad \text{(II.4.55)}$$

As G_i (i=3, 4,..., K) is orthogonal to Z_b, they do not influence the function to reduce the output interference power. They only relate with the output internal noise power. Referring to (II.4.55), minimization of output noise power can be provided by choosing b_i (i=3, 4,..., K) as,

$$b_i = 0 \quad , \quad i=3, 4,..., K \tag{II.4.56}$$

Summarizing the results of the above considerations, it is proved that (II.4.45) gives the minimum output noise power. The output desired signal power is guaranteed by the constraint condition so that minimization of the output noise power corresponds to maximize the output signal-to-noise ratio.

The array system response toward the interference direction converges to the following value.

$$Y(\theta_b) = \frac{P_r A_{cb}}{P_r + K P_b (1 - A_{cb}^2)} \tag{II.4.57}$$

In Fig.II.4.2, the array system response toward the interference direction is shown in terms of the interference direction with parameter of the ratio of the interference power to the internal noise power. In the calculations, constraint direction is chosen toward the array normal direction, i.e. θ_c (= θ_s) = 90°, and four element-antenna system is assumed. Referring to this figure, the array system response decreases as the interference direction removes from the constraint di-

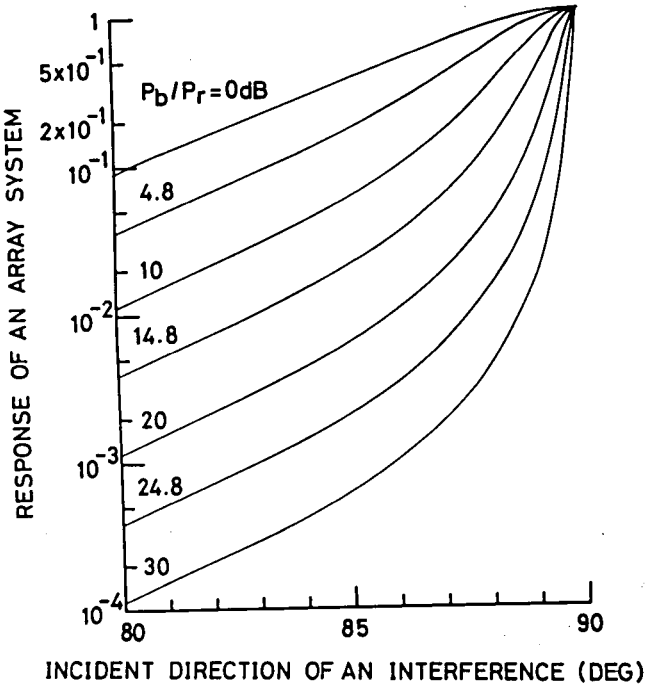

Fig.II.4.2 Response of an array system toward the interference direction. (constraint direction, desired signal direction : 90°)

rection. This result suggests us that the effect of the constraint decreases with the increment of the difference between the constraint direction and the interference direction. It is to be noted, referring to (II.4.57), that if the internal noise power might be zero, the array system response would fall to zero. Null depth toward the interference direction is determined also by the ratio of the interference power to the internal noise power. Also referring to Fig.II.4.2, higher the ratio of the interference power to the internal noise power is, lower the array system response toward the interference is, with the same angular conditions of the constraint, the desired signal and the interference direction. In addition, the interference rejection function of this system is not affected by the existence of the desired signal, and it is related only to the internal noise.

The output interference power $P_{b_{out}}$ and the output internal noise power $P_{r_{out}}$ under the optimal weight vector can be derived from (II.4.45) and (II.4.57) as follows, respectively.

$$P_{b_{out}} = \frac{P_r^2 P_b A_{cb}^2}{\{P_r + K P_b (1 - A_{cb}^2)\}^2} \qquad \text{(II.4.58)}$$

$$P_{r_{out}} = \frac{P_r}{K} + \frac{K P_r P_b^2 A_{cb}^2 (1 - A_{cb}^2)}{\{P_r + K P_b (1 - A_{cb}^2)\}^2} \qquad \text{(II.4.59)}$$

$P_{b_{out}}$ and $P_{r_{out}}$ are determined only by the interference power, the internal noise power and the angular condition of the interference di-

rection and the constraint direction. The output internal noise power, $P_{r_{out}}$, is greater than that under the equal weight condition, which had been called "maximal ratio condition"[63]. Under the maximal ratio condition, the output internal noise power shall be $\frac{P_r}{K}$ and the second term of the right hand side of (II.4.59) is the additional one which is introduced by the deviation of weights from the maximal ratio condition for rejecting the interference. It must be noted, however, the existence of the internal noise prevents the system to fall into the condition similar to the super gain antenna.

The output signal-to-noise ratio SNR_{out} can now be derived using (II.4.58) and (II.4.59) as follows.

$$SNR_{out} = \frac{P_s}{\frac{P_r (P_r + K P_b)}{K \{P_r + K P_b (1 - A_{cb}^2)\}}} \qquad \text{(II.4.60)}$$

As the output desired signal power is guaranteed by the constraint condition, it is not affected by the interference and the internal noise. Since, the interference direction differs generally from the constraint direction, therefore referring to (II.4.28), we have,

$$A_{cb}^2 < 1 \qquad \text{(II.4.61)}$$

Therefore, the denominator of (II.4.60) is bounded as a following manner.

$$\frac{P_r (P_r + K P_b)}{K \{P_r + K P_b (1 - A_{cb}^2)\}} > \frac{P_r}{K} \qquad \text{(II.4.62)}$$

From the fact of (II.4.62), maximum obtainable signal-to-noise ratio using the adaptive antenna array under the directional constraint is bounded by the internal noise component as follows.

$$SNR_{out} < \frac{K P_s}{P_r} \qquad \text{(II.4.63)}$$

Although (II.4.42) represents the dynamic behavior of the weight vector, the eigenvectors G_i (i=3, 4,..., K) are not given in closed forms. Now, the initial weight vector W_0 may be chosen coincident with the vector F. As proved in (II.3.41) to (II.3.46), the vector F satisfies the constraint condition. This choice is very practical and reasonable, for it corresponds to the uniform excitation of the array with its beam steered to the constraint direction. Since F is orthogonal to the constraint plane, its inner products by G_i (i=2, 3,..., K) must vanish. With (II.4.10), (II.4.20), (II.4.22) and (II.4.29), (II.4.42) will become simplified as follows.

$$W(t) = \frac{1}{K} G_1 - \frac{1}{\lambda_2} \{1 - \exp(-q\lambda_2 t)\} P_b A_{cb} G_2 \qquad \text{(II.4.64)}$$

This equation shows that the weight vector changes in an exponential manner whose time constant depends on the product of the equivalent step size by the eigenvalue of $P R_{XX} P$ which in turn is affected by the radio environment where the system is located. As all terms of (II.4.64) can be expressed in closed forms, we can track the change of the weight vector explicitly. The response of the system toward the directions of

the desired signal and the interference are given by,

$$Z_s^* W(t) = G_1^* W(t) = 1 \tag{II.4.65}$$

$$Z_b^* W(t) = A_{cb} - \frac{1}{\lambda_2} K P_b A_{cb} (1 - A_{cb}^2)\{1 - \exp(-q\lambda_2 t)\} \tag{II.4.66}$$

In most cases, the internal noise power, P_r, is much smaller than the interference power, P_b, and can be neglected. Then, the eigenvalue λ_2 in (II.4.27) may be approximated as,

$$\lambda_2 \cong K P_b (1 - A_{cb}^2) \tag{II.4.67}$$

which results in that (II.4.66) tends to vanish as time elapses, i.e. cancellation of the interference. (II.4.67) also shows that the convergence rate of either (II.4.64) or (II.4.66) is approximately proportional to the number of elements K and the interference power P_b. The latter means that the system acts faster to the stronger interference, which is preferable property of the adaptive system. The term A_{cb} of (II.4.66) is, as described in (II.4.28), a normalized array factor, which is much smaller than unity when the difference between the constraint direction and the direction of the interference $|\theta_c - \theta_b|$ is larger than the beamwidth. More specifically, A_{cb} does not exceed 0.25 for the array with more than four elements. Therefore, the term $(1 - A_{cb}^2)$ in (II.4.67) is greater than 0.93.

Using (II.3.3), (II.3.7), (II.4.11), (II.4.12), (II.4.16) and (II.4.17), the signal-to-noise ratio at the output of the system is ex-

pressed as follows.

$$SNR_{out}(t) = \frac{P_s}{P_b \left| Z_b^* W(t) \right|^2 + P_r \left| W(t)^* W(t) \right|} \quad \text{(II.4.68)}$$

Some calculated results based on the formula derived previously are shown in the followings. The array system under considerations is again assumed to have four elements located linearly with equal spacing of a half wavelength. Parameters used in the examples are summarized in Table II.4.1. The directional parameters for EN (example number) 1 are chosen for corresponding to the condition that the interference is impinging to the sidelobe region. EN 2 corresponds to the condition the interference is inside of the mainbeam and EN 3 to the condition that the constraint direction is off from the array normal direction. The changes of the real and the imaginary part of each weight for EN 1 are shown in Figs.II.4.3 and II.4.4, respectively. As the constraint direction is the array normal direction, in other words 90°, no phasing operation is required for setting the initial condition so that all of the imaginary parts of the weights take the same value of zero. From the constraint condition, all of the real parts of the weights are 0.25. As time elapses, the weights change exponentially and converge to their optimal values. History of the output powers from each source and the output signal-to-noise ratio during adaptation are shown in Figs.II.4.5 and II.4.6, respectively. According to the change of the weights, output interference power decreases exponentially,

	θ_c	θ_s	θ_b	P_s/P_r	P_b/P_r	q
EN 1	90°	90°	45°	10^2	10^4	10^{-5}
EN 2	90°	90°	75°	10^2	10^4	2×10^{-5}
EN 3	45°	45°	90°	10^2	10^4	10^{-5}

Table II.4.1 Parameters for computations of a transient behavior of the adaptive array.

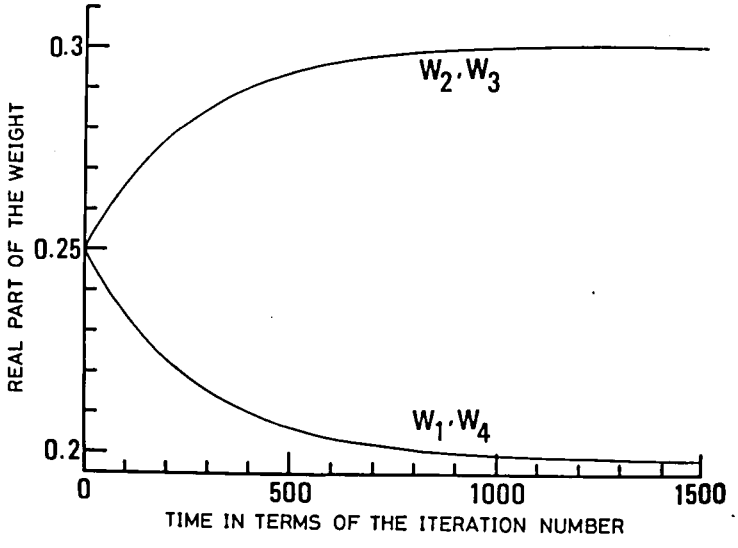

Fig.II.4.3 Transient behavior of the real parts of the weights for EN 1.

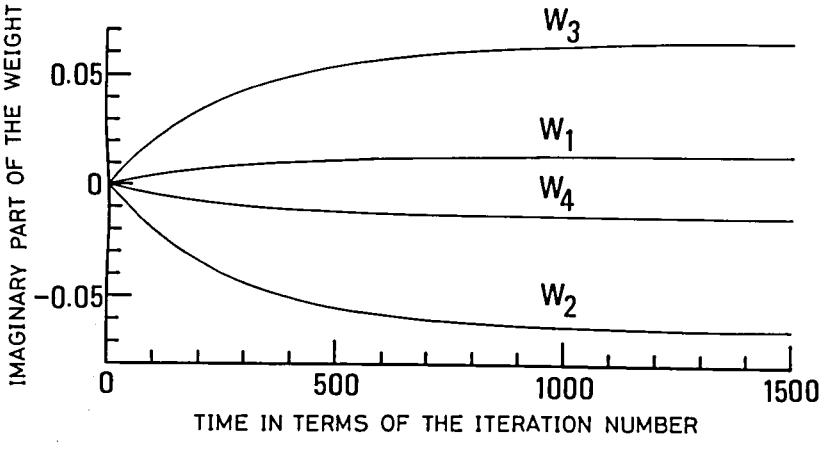

Fig.II.4.4 Transient behavior of the imaginary parts of the weights for EN 1.

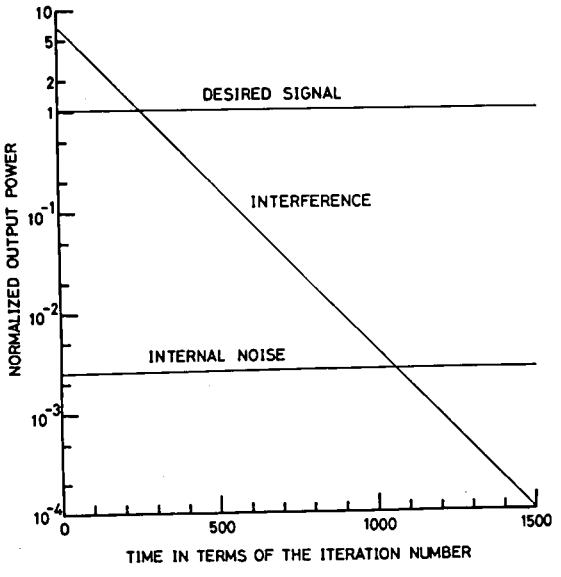

Fig.II.4.5 History of the output powers from each source for EN 1.

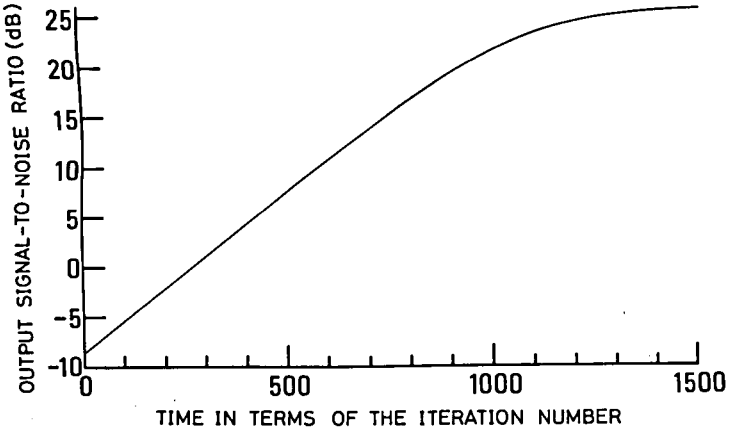

Fig.II.4.6 Transient behavior of the output signal-to-noise ratio for EN 1.

however, the output desired signal power is maintained as a constant value. On the other hand, the output internal noise power increases in accordance with the deviation of the weights from the equal weighting condition. Thus, minimization of the output interference power is provided with sacrifice of the increment of the output internal noise power. As the incident direction of the interference, i.e. the direction toward which the pattern null must be steered, is toward the sidelobe of the initial array system pattern, the absolute values of the inner pair of the weights increase and the outer pair decrease for widening the mainbeam. (see Table II.4.2)

Figs.II.4.7 and II.4.8 show the change of the weights under the condition corresponding to EN 2 in terms of time. As the constraint direction is 90°, the initial weights are also the same with those of EN 1. In this case, however, the incident direction of the interference is 75°, namely toward inside of the initial mainbeam. Thus, A_{cb} of (II.4.23) for EN 2 is smaller than that for EN 1 so that the time constant for convergence for EN 2 is larger than that for EN 1. It is to be expected that long time is required for convergence. In Figs. II.4.9 and II.4.10, history of the output powers from each source and the history of the output signal-to-noise ratio are shown, respectively. The decrement of the output interference power is also exponential and the output desired signal power is also maintained as a constant value, but, the increment of the output internal noise power is larger than that of EN 1. This is due to the fact that the steering

	EN 1	EN 2	EN 3
$\|w_1\|$	0.1990	0.4081	0.1990
$\|w_2\|$	0.3084	0.2031	0.3084
$\|w_3\|$	0.3084	0.2031	0.3084
$\|w_4\|$	0.1990	0.4081	0.1990
$\angle w_1$	3.95°	37.13°	165.15°
$\angle w_2$	-12.11°	30.71°	-51.53°
$\angle w_3$	12.11°	-30.71°	51.53°
$\angle w_4$	-3.95°	-37.13°	-165.15°

Table II.4.2 Final values of the weights of tha adaptive array. (absolute value and phase)

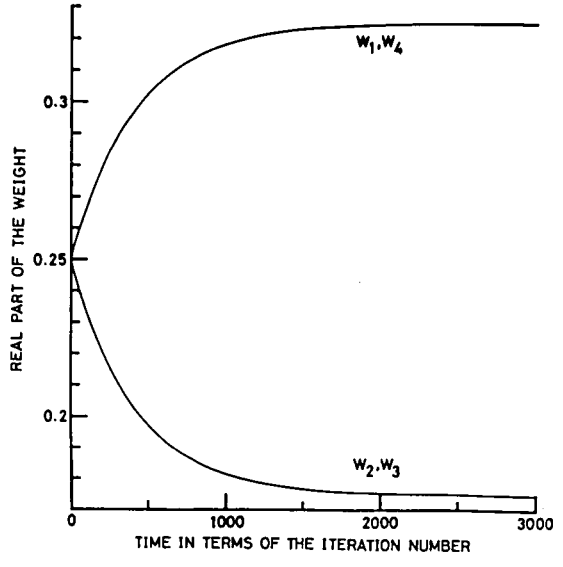

Fig.II.4.7 Transient behavior of the real parts of the weights for EN 2.

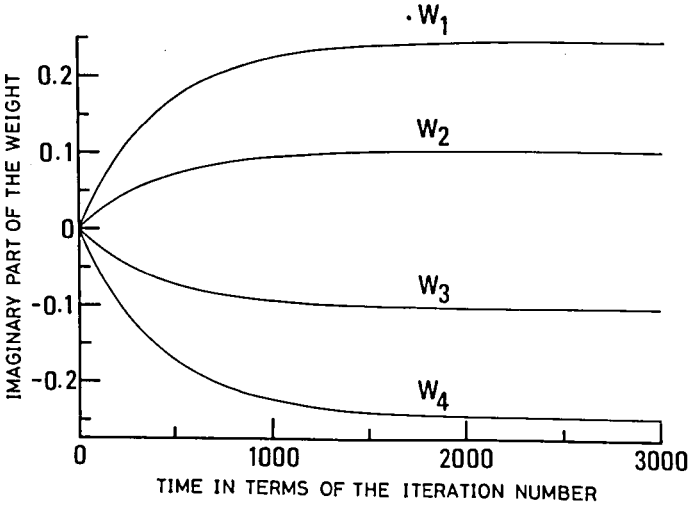

Fig.II.4.8 Transient behavior of the imaginary parts of the weights for EN 2.

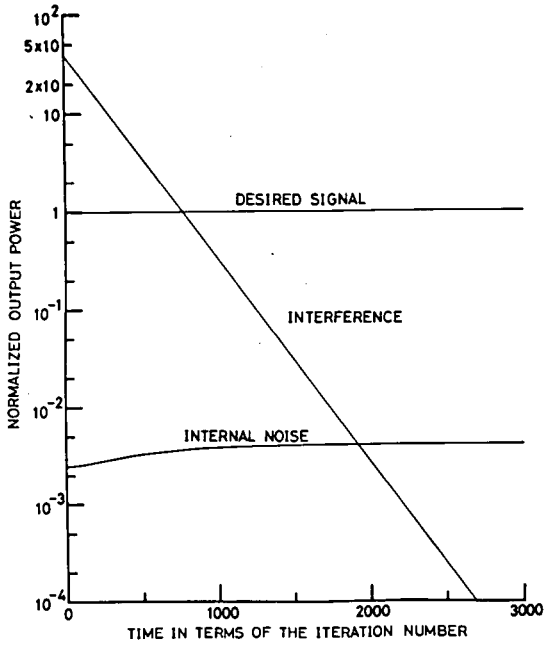

Fig.II.4.9 History of the output powers from each source for EN 2.

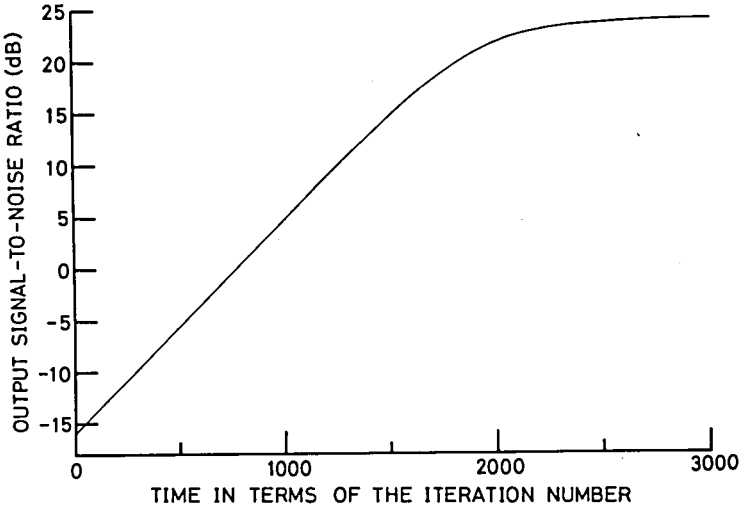

Fig.II.4.10 Transient behavior of the output signal-to-noise ratio for EN 2.

null toward the direction near the constraint direction causes the shift of mainbeam peak from the constraint direction having a larger directional response than the initial one because of the limitation of the beamwidth. In addition to them, for narrowing the beamwidth, as shown in Table II.4.2, absolute values of the outer pair of the weights increase and the inner pair decrease. The output signal-to-noise ratio obtained in the converged state is thus less than that of EN 1.

In Figs.II.4.11 and II.4.12, the histories of the weights under the condition corresponding to EN 3 are shown for the real and the imaginary part, respectively. Setting of the constraint and the interference direction for EN 3 is reversely provided compared with that for EN 1, i.e. the constraint direction for EN 3 is the same with the interference direction for EN 1 and the interference direction for EN 3 is the same with the constraint direction for EN 1. As the constraint direction is off from the array normal direction, the initial weights are set to steer the mainbeam toward the constraint direction so that the absolute values of each initial weight have the same value of 0.25, but the real and the imaginary part of each weight provide the phase shift for steering. It is to be noted that as the direction setting condition for EN 3 is reversed for EN 1, A_{cb} for EN 3 is the same with A_{cb} for EN 1 from (II.4.28). Therefore, under the conditions of EN 1 and EN 3 of Table II.4.1, the convergence properties of the output powers of each source and the output signal-to-noise ratio for EN 1 and EN 3 are the same with each other.

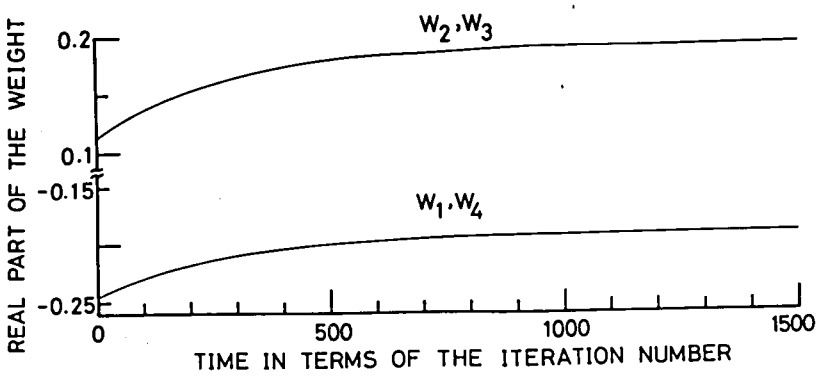

Fig.II.4.11 Transient behavior of the real parts of the weights for EN 3.

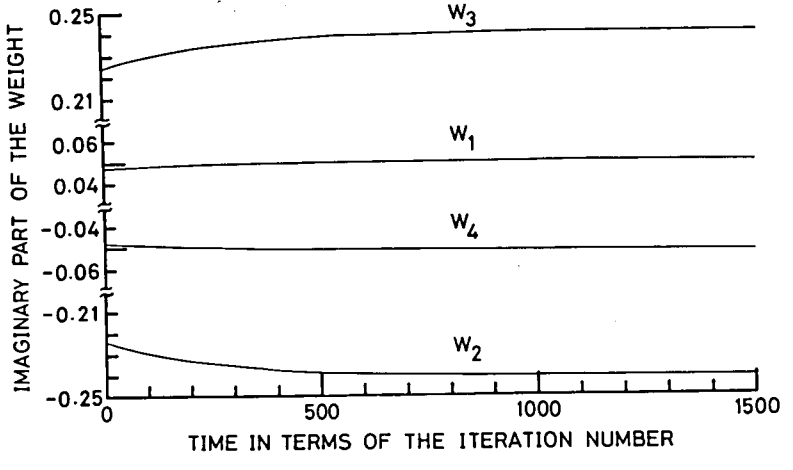

Fig.II.4.12 Transient behavior of the imaginary parts of the weights for EN 3.

As shown in the above examples, the transient properties of the adaptive antenna array with single directional constraint can be predicted perfectly when exposed to a certain environment.

4.4 Analysis on the Case with Prediction Error of the Desired Signal Direction

In the preceding analysis, the constraint direction is assumed to coincide with the direction of the desired signal. In other words, it is assumed that the angle of arrival of the desired signal is predicted accurately. In practice, however, the prediction usually involves some slight error (see Fig.II.4.13). This situation will be treated in this section. In this situation, however, the differential equation (II.4.3) is still valid except for the forms of the matrices $P\,R_{XX}\,P$ and $P\,R_{XX}\,F$. The matrix $P\,R_{XX}\,P$ which is slightly different from (II.4.21) can be derived using (II.4.9) and (II.4.15) as,

$$P\,R_{XX}\,P = P_r\,U - \frac{P_r}{K}\,C\,C^* + P_s\,A_{cs}^2\,C\,C^* + P_b\,A_{cb}^2\,C\,C^* + P_s\,Z_s\,Z_s^* + P_b\,Z_b\,Z_b^* - P_s\,A_{cs}\,C\,Z_s^* - P_s\,A_{cs}\,Z_s\,C^* - P_b\,A_{cb}\,C\,Z_b^* - P_b\,A_{cb}\,Z_b\,C^* \qquad \text{(II.4.69)}$$

where

$$A_{cs} = \frac{C^*\,Z_s}{K} = \frac{\sin[\frac{K\pi}{2}\,(\cos\theta_c - \cos\theta_s)]}{K\,\sin[\frac{\pi}{2}\,(\cos\theta_c - \cos\theta_s)]} \qquad \text{(II.4.70)}$$

and A_{cb} has been given by (II.4.28). (II.4.69) is also Hermitian which can be proved through the direct operation of the complex conjugate transpose on (II.4.69). The constraint vector C is again one of the eigenvectors of $P\ R_{XX}\ P$ whose associated eigenvalue is zero. Without sacrificing generality, it may be assumed that two of the remaining eigenvectors are expressed by the forms of linear combination of the constraint vector C, the desired signal phase vector Z_s and the interference phase vector Z_b. Then, the assumed eigenvector is substituted into the characteristic equation with (II.4.69) as follows.

$$P\ R_{XX}\ P\ (C + aZ_s + bZ_b) = \lambda(C + aZ_s + bZ_b) \qquad \text{(II.4.71)}$$

where a and b are the undetermined coefficients and λ is the eigenvalue associated to the eigenvector $(C + aZ_s + bZ_b)$. Calculating and equating terms of both sides of (II.4.71), we obtain the following eigenvectors and their associated eigenvalues.

$$\begin{matrix} G_2 \\ \text{or} \\ G_3 \end{matrix} = C + \frac{2\alpha_3\alpha_5 + \alpha_6^2 \pm (2\alpha_3 + \alpha_5)\alpha_6}{2\alpha_1(\alpha_5 \pm \alpha_6) + 2\alpha_2\alpha_4} Z_s + \frac{2\alpha_3\alpha_4 \pm \alpha_4\alpha_6}{2\alpha_1(\alpha_5 \pm \alpha_6) + 2\alpha_2\alpha_4} Z_b \qquad \text{(II.4.72)}$$

$$\begin{matrix} \lambda_2 \\ \text{or} \\ \lambda_3 \end{matrix} = \alpha_3 \pm \frac{1}{2}\alpha_6 \qquad \text{(II.4.73)}$$

where double signs in the right hand sides are in order, corresponding to the two quantities on the left hand sides of each equation. The new notations in the above equations are shown below.

$$\alpha_1 = - P_r A_{cs} - K P_s A_{cs} (1 - A_{cs}^2) - K P_b A_{cb} A_{sb} + K P_b A_{cb}^2 A_{cs} \tag{II.4.74}$$

$$\alpha_2 = - P_r A_{cb} - K P_b A_{cb} (1 - A_{cb}^2) - K P_s A_{cs} A_{sb} + K P_s A_{cs}^2 A_{cb} \tag{II.4.75}$$

$$\alpha_3 = P_r + \frac{KP_s}{2} (1 - A_{cs}^2) + \frac{KP_b}{2} (1 - A_{cb}^2) \tag{II.4.76}$$

$$\alpha_4 = 2P_b (A_{sb} - \frac{A_{cs} A_{cb}}{K}) \tag{II.4.77}$$

$$\alpha_5 = K P_s (1 - A_{cs}^2) - K P_b (1 - A_{cb}^2) \tag{II.4.78}$$

$$\alpha_6 = (\alpha_5^2 + \frac{P_s}{P_b} \alpha_4^2) \tag{II.4.79}$$

where

$$A_{sb} = \frac{Z_s^* Z_b}{K} = \frac{\sin[\frac{K\pi}{2} (\cos \theta_s - \cos \theta_b)]}{K \sin[\frac{\pi}{2} (\cos \theta_s - \cos \theta_b)]} \tag{II.4.80}$$

The orthogonality between the eigenvectors G_1, G_2 and G_3 can be easily confirmed by making the inner products on each other. From the considerations on the degrees of freedom in the hyperspace, the rest of the eigenvectors G_i (i=4, 5,..., K) must be in the constraint plane and also perpendicular to Z_s and Z_b, as well. Thus, all of their associ-

ated eigenvalues are P_r, similar to the previous section. Using the eigenvalues and the eigenvectors derived here, the solution of (II.4.3) for the weight vector under the condition considered here can be written as follows with initial weight vector W_0 which satisfies the constraint condition.

$$W(t) = \frac{G_1^* W_0}{G_1^* G_1} G_1 - \frac{1}{\lambda_2} \{1 - \exp(-q\lambda_2 t)\} \frac{G_2^* (P R_{XX} F)}{G_2^* G_2} G_2$$

$$- \frac{1}{\lambda_3} \{1 - \exp(-q\lambda_3 t)\} \frac{G_3^* (P R_{XX} F)}{G_3^* G_3} G_3$$

$$+ \sum_{i=2}^{K} \frac{G_i^* W_0}{G_i^* G_i} G_i \exp(-q\lambda_i t) \qquad \text{(II.4.81)}$$

where

$$P R_{XX} F = - (P_s A_{cs}^2 + P_b A_{cb}^2) C + P_s A_{cs} Z_s + P_b A_{cb} Z_b \qquad \text{(II.4.82)}$$

As the initial weight vector W_0 is chosen to satisfy the constraint condition, thus,

$$G_1^* W_0 = C^* W_0 = 1 \qquad \text{(II.4.83)}$$

The eigenvalues λ_i (i=2, 3,..., K) are all positive and q is chosen to be positive so that (II.4.81) may converge to the following vector after an infinite time of operation.

$$W(\infty) = \frac{1}{K} G_1 - \frac{1}{\lambda_2} \frac{G_2^* (P R_{XX} F)}{G_2^* G_2} G_2 - \frac{1}{\lambda_3} \frac{G_3^* (P R_{XX} F)}{G_3^* G_3} G_3 \qquad \text{(II.4.84)}$$

Because of the same reason in the preceding section, the initial weight vector is chosen as F which is given by (II.4.10). Thus, (II.4.81) is simplified as a following manner.

$$W(t) = \frac{1}{K} G_1 - \frac{1}{\lambda_2} \{1 - \exp(-q\lambda_2 t)\} \frac{G_2^* (P R_{XX} F)}{G_2^* G_2} G_2$$

$$- \frac{1}{\lambda_3} \{1 - \exp(-q\lambda_3 t)\} \frac{G_3^* (P R_{XX} F)}{G_3^* G_3} G_3 \qquad \text{(II.4.85)}$$

Apparently, (II.4.85) converges to (II.4.84). By using (II.4.85), we find the responses of the system in the directions of the constraint, the desired signal and the interference as follows, respectively.

$$C^* W(t) = 1 \qquad \text{(II.4.86)}$$

$$Z_s^* W(t) = A_{cs} - \frac{1}{\lambda_2} \{1 - \exp(-q\lambda_2 t)\} \frac{(G_2^* P R_{XX} F) (Z_s^* G_2)}{G_2^* G_2}$$

$$- \frac{1}{\lambda_3} \{1 - \exp(-q\lambda_3 t)\} \frac{(G_3^* P R_{XX} F) (Z_s^* G_3)}{G_3^* G_3}$$

(II.4.87)

$$Z_b^* W(t) = A_{cb} - \frac{1}{\lambda_2}\{1 - \exp(-q\lambda_2 t)\} \frac{(G_2^* P R_{XX} F)(Z_b^* G_2)}{G_2^* G_2}$$

$$- \frac{1}{\lambda_3}\{1 - \exp(-q\lambda_3 t)\} \frac{(G_3^* P R_{XX} F)(Z_b^* G_3)}{G_3^* G_3} \quad \text{(II.4.88)}$$

The convergence rate of the system is also governed by the eigenvalues of $P R_{XX} P$. As shown in (II.4.86), the constraint condition is also satisfied in such a case. Not only the response toward the interference direction but also toward the desired signal direction decrease as time elapses. Since the exact calculations of the above equations would be much complicated, we adopt the following approximations. The first one is based on the small prediction error, i.e. that the angle of arrival of the actual desired signal is very close to the constraint direction. Thus, in place of (II.4.70) and (II.4.80), we have,

$$A_{cs} = \frac{C^* Z_s}{K} \cong 1 - \varepsilon \quad \text{(II.4.89)}$$

$$A_{sb} = \frac{Z_s^* Z_b}{K} \cong \frac{C^* Z_b}{K}(1 + \delta) = A_{cb}(1 + \delta) \quad \text{(II.4.90)}$$

where ε and δ are much smaller than unity. Second, the internal noise is assumed to be small so that,

$$K P_s > P_r \tag{II.4.91}$$

The last approximation assumes an adverse radio environment where;

$$P_b >> P_s \tag{II.4.92}$$

With these, we can obtain the results as follows.

$$\lambda_2 \cong P_r + K P_b (1 - A_{cb}^2) + \frac{K P_s A_{cb}^2}{1 - A_{cb}^2} (\varepsilon + \delta)^2 \tag{II.4.93}$$

$$\lambda_3 \cong P_r + K P_s (2\varepsilon - \varepsilon^2) - \frac{K P_s A_{cb}^2}{1 - A_{cb}^2} (\varepsilon + \delta)^2 \tag{II.4.94}$$

$$Z_s^* W(t) \cong 1 - \varepsilon - \frac{1}{\lambda_2} \{K P_b A_{cb}^2 - \frac{K^2 P_b^2}{P_r + K P_b (1 - A_{cb}^2)} \} (\varepsilon + \delta) \times$$

$$\{1 - \exp(-q\lambda_2 t)\} - \frac{K^2 P_b^2 A_{cb}^2}{2\lambda_3 P_r} [\{1 + \frac{\delta}{2\varepsilon} + \frac{A_{cb}^2}{2} +$$

$$(\varepsilon + \delta) \frac{K P_b A_{cb}^2}{4\varepsilon r}\} (1 - A_{cb}^2) - \frac{A_{cb}^2}{2\varepsilon} (\varepsilon + \delta)] (\varepsilon + \delta) \times$$

$$\{1 - \exp(-q\lambda_3 t)\} \tag{II.4.95}$$

$$Z_b^* W(t) \cong A_{cb} - \frac{1}{\lambda_2}[KP_bA_{cb}(1 - A_{cb}^2) + \{KP_sA_{cb}(1 + A_{cb}^2)$$

$$- \frac{K^2P_b^2A_{cb}^3}{P_r + KP_b(1 - A_{cb}^2)}\}(\varepsilon + \delta)]\{1 - \exp(-q\lambda_2 t)\}$$

$$- \frac{1}{\lambda_3}[KP_sA_{cb}(1 + A_{cb}^2)\varepsilon + 2KP_sA_{cb}\delta + \{\frac{KP_bA_{cb}^3}{2}(1 + A_{cb}^2)$$

$$+ \frac{KP_bA_{cb}^3}{\varepsilon}\delta + \frac{K^2P_b^2A_{cb}^3(1 - A_{cb}^4)}{4P_r} + \frac{K^2P_b^2A_{cb}^3\delta(1 - A_{cb}^2)}{2\varepsilon P_r}\}$$

$$\times(\varepsilon + \delta)]\{1 - \exp(-q\lambda_3 t)\} \qquad \text{(II.4.96)}$$

Approximated value of λ_2 of (II.4.93) is different from (II.4.27) only in the third term of (II.4.93) which is negligibly small because of (II. 4.92) and the second order term of ε and δ. The new variable in this section, λ_3, given by (II.4.94) is very small which is consisting of such small quantities as P_r, ε and δ. It is to be considered that this quantity corresponds to the eigenvalue of P_r for the case in the preceding section. This results in that the new time-dependent term varies very slowly and scarcely affects the transient behavior of the adaptation process.

For evaluating the approximated array system response toward

the desired signal direction and toward the interference direction, we must perform the order estimation of each term of (II.4.95) and (II.4.96). A quantity in the first braces of the third term of the right hand side of (II.4.95) has the order of $K P_b$ because of (II.4.91) and (II.4.92) which is the same order of λ_2 so that the third term is very small compared with unity. The coefficient of $\{1 - \exp(-q\lambda_3 t)\}$ of the fourth term is large compared with that of $\{1 - \exp(-q\lambda_2 t)\}$ of the third term, but as discussed previously, λ_3 is very small so that its contribution can be neglected in a normal operation. Summarizing the above discussions, the array system response toward the desired signal direction decreases scarcely from the initial value under the assumptions from (II.4.89) to (II.4.92). As for the array system response toward the interference direction, the first term in the brackets of the second term of the right hand side of (II.4.96) is the same with that of (II.4.66) and which is much greater than the remaining terms because of the existence of $\varepsilon + \delta$. It is, however, difficult to estimate the order of the coefficient of $\{1 - \exp(-q\lambda_3 t)\}$ in the third term of the right hand side of (II.4.96) because of the existence of ε/λ_3 and δ/λ_3. But, as discussed for the case of (II.4.95), the third term of (II.4.96) varies very slowly compared with the second term, its contribution affects scarcely the convergence property of the array system response toward the interference direction. As above, the behavior of the adaptive antenna array with directional constraint under the conditions from (II.4.89) to (II.4.92) is almost identical with the case without prediction

error of the desired signal direction and can be approximated by it.

In the followings, the examples of the behavior of the adaptive antenna array with directional constraint under the condition with slight prediction error of the desired signal direction are given. The computations are carried out using (II.4.85), (II.4.87) and (II.4.88). The parameters used in the computations are listed in Table II.4.3. It is to be noted that these parameters for EN4, EN 5 and EN 6 are chosen correspondingly to EN 1, EN 2 and EN 3, respectively. Computed results for the behavior of weights are almost the same with those for EN 1, EN 2 and EN 3, respectively. Difference between the corresponding two examples hides behind the lines to denote the behavior of weights so that the figures are omitted here. Figs.II.4.3, II.4.4, II.4.7, II.4.8, II.4.11 and II.4.12 should be refered for understanding the behavior of weights. Apparently, the approximations under the conditions from (II.4.89) to (II.4.92) are valid. The histories of the output powers from each source for EN4, EN 5 and EN 6 are also agreed with those for EN 1, EN 2 and EN 3, respectively, and thus the histories of the output signal-to-noise ratio are agreed with them. Therefore, the figures to show these quantities are also omitted here. Summarizing the results described above, it is proved and verified that the adaptive antenna array with directional constraint operates satisfactory even if the prediction of the desired signal direction includes some slight error under the condition of low signal-to-noise ratio of the field strength. But, in the high signal-to-noise ratio of the field strength, the ap-

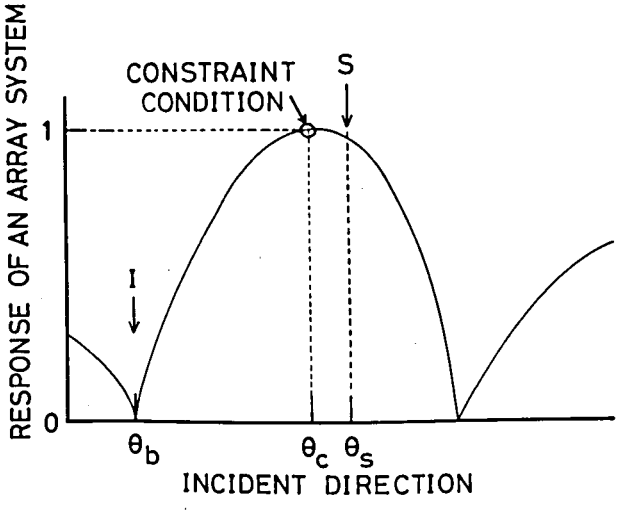

Fig.II.4.13 A sketch showing the setting error of the constraint condition.

	θ_c	θ_s	θ_b	P_s/P_r	P_b/P_r	q	remarks
EN 4	90°	91°	45°	10^2	10^4	10^{-5}	EN 1
EN 5	90°	91°	75°	10^2	10^4	2×10^{-5}	EN 2
EN 6	45°	44°	90°	10^2	10^4	10^{-5}	EN 3

Table II.4.3 Parameters for computations of a transient behavior of the adaptive array.

proximations from (II.4.93) to (II.4.96) are no longer valid and it is not expected to improve the output signal-to-noise ratio by means of the adaptive antenna array with directional constraint under prediction error of the desired signal direction. To verify the above considerations, calculations are carried out using (II.4.85), (II.4.87) and (II.4.88). The parameters for calculation are shown in Table II.4.4. Calculated results of the history of the output powers from each source and of the output signal-to-noise ratio are shown in Figs.II.4.14 and II.4.15, respectively. Referring To Fig.II.4.14, The remarkable feature of this example is the large amount of increment of the internal noise power at the output. This is due to the fact that, in this case, the desired signal is regarded as an interference rather than the real interference so that the operation is performed for reducing the output desired signal power at the sacrifice of increment of the output internal noise power. This effect is like a super gain antenna. But, the guiding principle of this system, i.e. minimization of the output power subject to the directional constraint, is still satisfied, as shown in Fig.II.4.14 (the history of the total output power). Corresponding to the decrease of the desired signal power and the increase of the internal noise power, the output signal-to-noise ratio decreases and finally the desired signal hides behind the internal noise as shown in Fig.II.4.15. At the initial stage, however, the output signal-to-noise ratio increases temporarily. This is caused by the difference of time constants of convergence in each term. But, after the output

	θ_c	θ_s	θ_b	P_s/P_r	P_b/P_r	q
EN 7	90°	87°	45°	5×10	1.25×10	10^{-2}

Table II.4.4 Parameters for computations of a transient behavior of the adaptive array. (high signal-to-noise ratio case of a field strength)

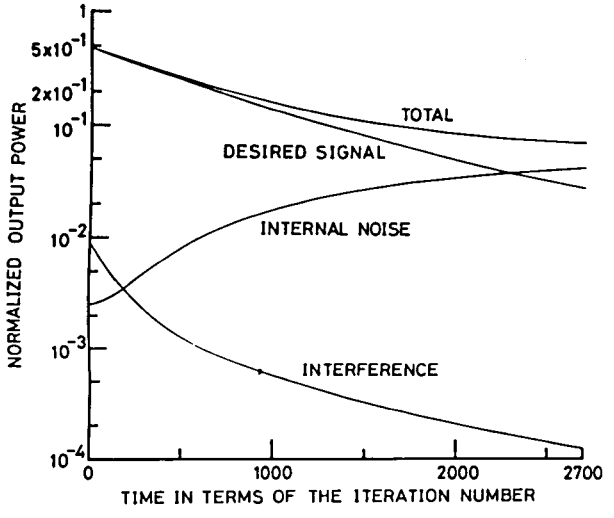

Fig.II.4.14 History of the output powers from each source for EN 7.

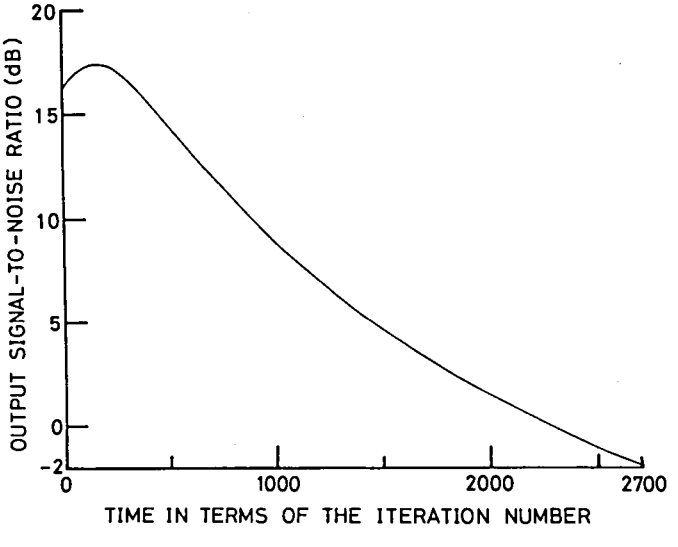

Fig.II.4.15 Transient behavior of the output signal-to-noise ratio for EN 7.

internal noise power exceeds the output interference power, the output signal-to-noise ratio decreases monotonously which results in the unacceptable steady state performance. However, under such condition described above, the applications of the adaptive antenna array are not required. Thus, the adaptive antenna array with single directional constraint is effective in practice.

In addition to them, it is to be noted that (II.4.85) can be regarded as the behavior of weights on the case including two interferences with accurate prediction of the desired signal direction, i.e. the constraint direction is coincident with the desired signal direction. Thus, for clarifying the physical meanings of this situation, some variables written in Table II.4.5 are used for rewriting the equation for weights and so on as follows.

$$W(t) = \frac{1}{K} G_1 - \frac{1}{\lambda_2} \{1 - \exp(-q\lambda_2 t)\} \frac{G_2^* (P R_{XX} F)}{G_2^* G_2} G_2$$

$$- \frac{1}{\lambda_3} \{1 - \exp(-q\lambda_3 t)\} \frac{G_3^* (P R_{XX} F)}{G_3^* G_3} G_3 \qquad \text{(II.4.97)}$$

where

$$G_1 = C \qquad \text{(II.4.98)}$$

$$\begin{matrix} G_2 \\ \text{or} \\ G_3 \end{matrix} = C + \frac{2\alpha_3\alpha_5 + \alpha_6^2 \pm (2\alpha_3 + \alpha_5)\alpha_6}{2\alpha_1 (\alpha_5 \pm \alpha_6) + 2\alpha_2\alpha_4} Z_{b_1}$$

$$+ \frac{2\alpha_3\alpha_4 \pm \alpha_4\alpha_6}{2\alpha_1(\alpha_5 \pm \alpha_6) + 2\alpha_2\alpha_4} Z_{b_2} \qquad \text{(II.4.99)}$$

$$\begin{matrix}\lambda_2 \\ \text{or} \\ \lambda_3\end{matrix} = \alpha_3 \pm \frac{1}{2}\alpha_6 \qquad \text{(II.4.100)}$$

$$\alpha_1 = -P_r A_{cb_1} - KP_{b_1} A_{cb_1}(1 - A_{cb_1}^2) - KP_{b_2} A_{cb_2} A_{b_1b_2} + KP_{b_2} A_{cb_2}^2 A_{cb_1} \qquad \text{(II.4.101)}$$

$$\alpha_2 = -P_r A_{cb_2} - KP_{b_2} A_{cb_2}(1 - A_{cb_2}^2) - KP_{b_1} A_{cb_1} A_{b_1b_2} + KP_{b_1} A_{cb_1}^2 A_{cb_2} \qquad \text{(II.4.102)}$$

$$\alpha_3 = P_r + \frac{K P_{b_1}}{2}(1 - A_{cb_1}^2) + \frac{K P_{b_2}}{2}(1 - A_{cb_2}^2) \qquad \text{(II.4.103)}$$

$$\alpha_4 = 2P_{b_2}\left(A_{b_1b_2} - \frac{A_{cb_1} A_{cb_2}}{K}\right) \qquad \text{(II.4.104)}$$

$$\alpha_5 = KP_{b_1}(1 - A_{cb_1}^2) - KP_{b_2}(1 - A_{cb_2}^2) \qquad \text{(II.4.105)}$$

$$\alpha_6 = \left(\alpha_5^2 + \frac{P_{b_1}}{P_{b_2}}\alpha_4^2\right)^{1/2} \qquad \text{(II.4.106)}$$

$$P\, R_{XX}\, F = -(P_{b_1} A_{cb_1}^2 + P_{b_2} A_{cb_2}^2)\, C + P_{b_1} A_{cb_1} Z_{b_1} + P_{b_2} A_{cb_2} Z_{b_2} \qquad \text{(II.4.107)}$$

	old	new
angle	θ_c	$\theta_c (=\theta_s)$
	θ_s	θ_{b_1}
	θ_b	θ_{b_2}
power	P_s	P_{b_1}
	P_b	P_{b_2}
Phase vector	C	$C (=Z_s)$
	Z_s	Z_{b_1}
	Z_b	Z_{b_2}
variable	A_{cs}	A_{cb_1}
	A_{cb}	A_{cb_2}
	A_{sb}	$A_{b_1 b_2}$

Table II.4.5 Guide for understanding the new variables with renewed concept of double interferences case

	θ_c	θ_s	θ_{b_1}	θ_{b_2}	P_s/P_r	P_{b_1}/P_r	P_{b_2}/P_r	q
EN 8	90°	90°	70°	110°	10^2	5×10^3	5×10^3	5×10^{-5}
EN 9	90°	90°	70°	130°	10^2	5×10^3	5×10^3	5×10^{-5}

Table II.4.6 Parameters for computations of a transient behavior of the adaptive array under the condition with double interferences case.

Using (II.4.97) - (II.4.107), behavior of the weights under two interferences condition and the history of the output powers from each source and of the output signal-to-noise ratio can be calculated. Parameters used in the following two examples are shown in Table II.4.6. In Figs. II.4.16 and II.4.17, the history of the output powers from each source and of the output signal-to-noise ratio are given, respectively, corresponding to EN 8 in Table II.4.6. Referring to Fig.II.4.16, output interference powers decrease in an exponential manner. It is to be noted that two interferences are impinging to the array toward the directions which are symmetric to each other with respect to the constraint direction. In addition to them, the powers of two interferences are chosen to be the same value so that the eigenvalues, in other word the time constants of convergence, take the same value. Thus, the histories of the output powers from two interferences are just coincident with each other. As in the preceding section, the output internal noise power increases because the weights differ from the uniform excitation condition. The output signal-to-noise ratio is, as shown in Fig. II.4.17, improved also in an exponential manner and converges to the value which is almost determined by the desired signal-to-internal noise power ratio.

The same kinds of figures with parameters given in Table II. 4.6 of EN 9 are shown in Figs.II.4.18 and II.4.19. In this case, as two interference directions are not symmetrical in spite of the same interference power, output powers from two interfering sources take

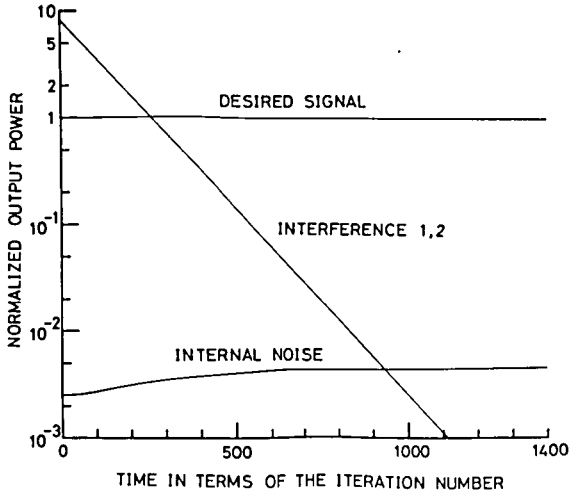

Fig.II.4.16 History of the output powers from each source for EN 8.

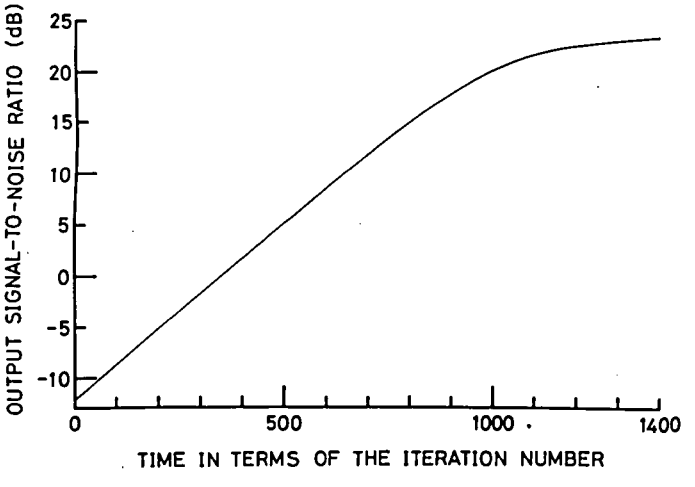

Fig.II.4.17 Transient behavior of the output signal-to-noise ratio for EN 8.

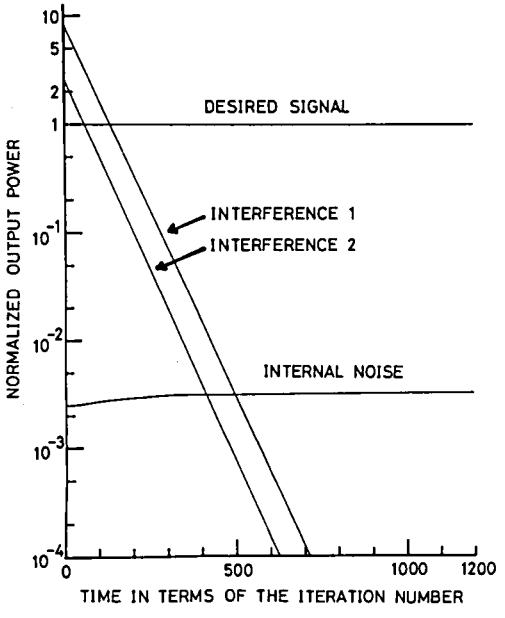

Fig.II.4.18 History of the output powers from each source for EN 9.

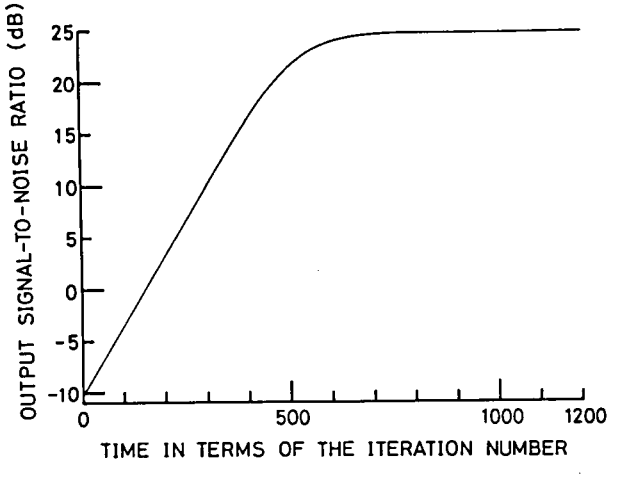

Fig.II.4.19 Transient behavior of the output signal-to-noise ratio for EN 9.

different values so that two lines are drawn for interferences. The time constants for these two lines are almost equal so that they are regarded as parallel to each other in the range of this figure. The output signal-to-noise ratio is also improved in an exponential manner.

Comparing with Figs.II.4.17 and II.4.19, the case for EN 9 converges faster than for EN 8. This difference is caused by the fact that one interference direction of EN 9 is far apart from the constraint direction compared with that of EN 8, so that, in qualitative sense, the eigenvalues of EN 9 are larger than those of EN 8. Thus, faster convergence is provided for EN 9 than for EN 8.

4.5 Concluding Remarks

Transient behavior and steady state performance of the adaptive antenna array with single directional constraint have been investigated in detail. The adaptive algorithm written in the form of difference equation is translated into the form of differential equation and which is solved by means of the method utilizing the concept of multi-dimensional hyperspace with orthogonal projection. Analytical results show the convergence property of the system is governed by the eigenvalues of $P\,R_{XX}\,P$. Practical and reasonable choice of the initial weight vector makes the transient behavior of the weight vector predictable in a given environment. As a result, history of the output powers from each sources and of the output signal-to-noise ratio can be written in a closed form. It is also proved that the maximum ob-

tainable output signal-to-noise ratio is limited by the ratio of the desired signal power to the internal noise power.

The effect of error in setting the constraint condition is also investigated. Approximated results and calculated results from the rigorous solution show that such error does not affect the good performance of the adaptive system under consideration if the error is small compared to the beamwidth of the antenna array and the interference power is large enough compared to the desired signal power. In the high signal-to-noise ratio environment, however, output signal-to-noise ratio decreases because the system regards the desired signal as an interference and steers null toward its direction which results in the effect like a super gain antenna so that large amount of increment of the output internal noise power may be obtained. In practice, however, the adaptive antenna may not required under such environment.

It is also pointed out that the analytical results on the case with setting error in the constraint direction can be regarded as for the case without setting error of the constraint and including two interferences as it is, by regarding physical meanings of some variables from the standpoint of new situation. Two examples are shown which are calculated using rigorous analytical results and discussions are given by comparing two cases.

Throughout this chapter except for the final case of discussion, the number of interferences is assumed to be one, however, the analysis can be extended to the case with much more number of interfer-

ences. But, if the number of interferences exceeds the number of remaining degrees of freedom of the system, the problem changes in quality to find the suboptimal solution. This problem exceeds the sight of this thesis and the discussions on which are not included here.

Chapter 5. TRANSIENT BEHAVIOR AND STEADY STATE PERFORMANCE OF THE ADAPTIVE ARRAY WITH DOUBLE DIRECTIONAL CONSTRAINTS

5.1 Introduction

In the preceding chapter, detailed analysis on the adaptive antenna array with single directional constraint is given. The analysis and some examples show that single directional constraint system acts well to reject the interferences while the desired signal component is almost guaranteed from decrement if the prediction error of the desired signal direction is small compared with the beamwidth and the signal-to-noise ratio of the incident field strength is very low. But, under the condition with high signal-to-noise ratio, the system may fall in the poor performance even if the prediction error of the desired signal direction is small. This is due to the fact that the desired signal cannot hide behind the interference and suffer elimination.

One method to prevent this difficulty would be to insert a strong external noise intentionally to assure low signal-to-noise ratio situation of the incident field strength. The shortcoming of this method is that it deteriorates the output signal-to-noise ratio unless another set of processor is prepared for signal transmission without the intentional noise (a set of master-slave system). Here, we develop the another flexible system for solving this problem.

5.2 Analysis

In circuit theory, wide-bandwidth frequency characteristics can be realized by the staggered tuning technique. Thus, in analogy to the circuit theory, multiple constraints are applied toward the directions which are closely arranged surrounding the predicted incident direction of the desired signal. It is to be considered that serious degradation of the reception performance of the desired signal may not be introduced because of the constraints surrounding the desired signal direction. This property can be predicted from the fact that it is impossible to steer a null toward the direction near, and especially between, the constraint directions because of the limitations of resolving power of the antenna system. In addition to them, algorithm to minimize the output power prevents the system from falling into the effect like a super-gain antenna.

In the following analysis, only the double directional constraints system is treated, because this choice may be sufficient for small angular ambiguity of the desired signal. However, extension to much more constraints system can be performed in a straightforward manner. In almost all the cases, it is favourable to prepare the double directional constraints system rather than the system with much more directional constraints to remain the degrees of freedom for rejecting interferences. The sketch showing the concept of the double directional constraints is shown in Fig.II.5.1.

For the double directional constraints system, the adaptive

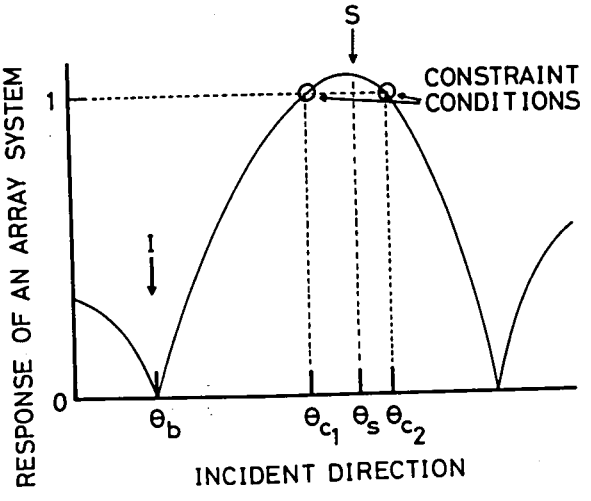

Fig.II.5.1 Concept of double directional constraint system.

algorithm of (II.4.3) is still valid, but the constraint matrix and the response vector must be modified as follows.

$$C = \begin{pmatrix} \cos\psi_1(\theta_{c_1}), & \sin\psi_1(\theta_{c_1}), & \cos\psi_1(\theta_{c_2}), & \sin\psi_1(\theta_{c_2}) \\ \circ & \circ & \circ & \circ \\ \cos\psi_K(\theta_{c_1}), & \sin\psi_K(\theta_{c_1}), & \cos\psi_K(\theta_{c_2}), & \sin\psi_K(\theta_{c_2}) \\ -\sin\psi_1(\theta_{c_1}), & \cos\psi_1(\theta_{c_1}), & -\sin\psi_1(\theta_{c_2}), & \cos\psi_1(\theta_{c_2}) \\ \circ & \circ & \circ & \circ \\ -\sin\psi_K(\theta_{c_1}), & \cos\psi_K(\theta_{c_1}), & -\sin\psi_K(\theta_{c_2}), & \cos\psi_K(\theta_{c_2}) \end{pmatrix} \qquad \text{(II.5.1)}$$

$$H = (1, 0, 1, 0) \qquad \text{(II.5.2)}$$

where θ_{c_1} and θ_{c_2} are the constraint directions. For extending to much more constraints system, one pair of row vectors must be added to the constraint matrix C for one constraint direction, also to the response vector H, real and imaginary part of the array system response must be added.

Similar to the single directional constraint system, a vector differential equation is formulated for this problem. For this, (II.5.1) and (II.5.2) are rewritten in complex forms as,

$$C^T = \begin{vmatrix} 1 \\ 0 \end{vmatrix} C_1^T + \begin{vmatrix} 0 \\ 1 \end{vmatrix} C_2^T \qquad \text{(II.5.3)}$$

$$C_1^T = (z_{c_1 1}, z_{c_1 2}, \ldots\ldots, z_{c_1 K}) \qquad \text{(II.5.4)}$$

$$C_2^T = (z_{c_2 1}, z_{c_2 2}, \ldots\ldots, z_{c_2 K}) \qquad \text{(II.5.5)}$$

where

$$z_{c_1 k} = \exp[j\psi_k(\theta_{c_1})] \quad , \quad k=1, 2, \ldots, K \qquad \text{(II.5.6)}$$

$$z_{c_2 k} = \exp[j\psi_k(\theta_{c_2})] \quad , \quad k=1, 2, \ldots, K \qquad \text{(II.5.7)}$$

and

$$H^T = (1 \angle 0° \ , \ 1 \angle 0°) \qquad \text{(II.5.8)}$$

Using (II.3.36), (II.3.40), (II.5.3), (II.5.4), (II.5.5) and (II.5.8), the complex form of projection operator and of the shortest vector to the constraint plane are derived as follows.

$$P = U - \frac{1}{K\,(1 - A_{c_1 c_2}{}^2)} [C_1 C_1^* + C_2 C_2^* - A_{c_1 c_2} (C_1 C_2^* + C_2 C_1^*)] \qquad \text{(II.5.9)}$$

$$F = \frac{1}{K\,(1 + A_{c_1 c_2})}(C_1 + C_2) \qquad \text{(II.5.10)}$$

where

$$A_{c_1c_2} = \frac{C_1^* C_2}{K} = \frac{\sin[\frac{K\pi}{2}(\cos\theta_{c_1} - \cos\theta_{c_2})]}{K \sin[\frac{\pi}{2}(\cos\theta_{c_1} - \cos\theta_{c_2})]} \qquad \text{(II.5.11)}$$

It is to be noted that $A_{c_1c_2}$ of (II.5.11) denotes the normalized array system response toward one constraint direction when an antenna array is steered toward the other constraint direction with uniform amplitude excitation.

At first, for clarifying the reception performance for the desired signal of the double directional constraints system, we consider the radio environment including the desired signal only. Thus, following the procedures described in the preceding chapter, the correlation matrix R_{XX} can be written as follows.

$$R_{XX} = P_r U + P_s Z_s Z_s^* \qquad \text{(II.5.12)}$$

where the variables in (II.5.12) denote the same meanings as appeared precedingly. Thus, the matrix coefficient of (II.4.3) can be derived by using (II.5.9) and (II.5.12) as follows.

$$P R_{XX} P = P_r U + P_s Z_s Z_s^* - \frac{P_s(A_{c_1s} - A_{c_2s}A_{c_1c_2})}{K(1 - A_{c_1c_2}^2)} (Z_s C_1^* + C_1 Z_s^*) - \frac{P_s(A_{c_2s} - A_{c_1s}A_{c_1c_2})}{K(1 - A_{c_1c_2}^2)} (Z_s C_2^* + C_2 Z_s^*)$$

$$+ \frac{1}{1 - A_{c_1c_2}^{\ 2}} [C_1 C_1^* \{- \frac{P_r}{K} + \frac{P_s (A_{c_1s} - A_{c_2s} A_{c_1c_2})^2}{1 - A_{c_1c_2}^{\ 2}}\}$$

$$+ C_2 C_2^* \{- \frac{P_r}{K} + \frac{P_s (A_{c_2s} - A_{c_1s} A_{c_1c_2})^2}{1 - A_{c_1c_2}^{\ 2}}\}] \qquad \text{(II.5.13)}$$

For evaluating the behavior of the system, eigenvalues and their associated eigenvectors must be derived. As discussed by Frost, each column vector of the constraint matrix is the eigenvector of $P\ R_{XX}\ P$ whose associated eigenvalue is zero. The vectors C_1 and C_2 are thus the eigenvectors of $P\ R_{XX}\ P$ with associated eigenvalues of zero. As (II.5.13) is Hermitian so that the eigenvectors can be chosen orthogonal with each other. Using C_1 and C_2, we derive two eigenvectors and their eigenvalues by the next equations.

$$G_1 = C_1 + C_2 \qquad \text{(II.5.14)}$$

$$G_2 = C_1 - C_2 \qquad \text{(II.5.15)}$$

$$\lambda_1 = \lambda_2 = 0 \qquad \text{(II.5.16)}$$

In order to determine the one of the remaining eigenvectors, we form a set of linear combination of C_1, C_2 and Z_s. By substituting it into the characteristic equation for $P\ R_{XX}\ P$ of (II.5.13), we obtain the following eigenvector G_3 and its eigenvalue λ_3.

$$G_3 = Z_s - \frac{1}{1 - A_{c_1c_2}^2}\left[(A_{c_1s} - A_{c_2s}A_{c_1c_2})\,C_1 + (A_{c_2s} - A_{c_1s}A_{c_1c_2})\,C_2\right] \qquad \text{(II.5.17)}$$

$$\lambda_3 = P_r + K\,P_s - \frac{P_s}{1 - A_{c_1c_2}^2}\left[(A_{c_1s} - A_{c_2s}A_{c_1c_2})\,A_{c_1s} + (A_{c_2s} - A_{c_1s}A_{c_1c_2})\,A_{c_2s}\right] \qquad \text{(II.5.18)}$$

where

$$A_{c_1s} = \frac{C_1^{*}\,Z_s}{K} = \frac{\sin[\frac{K\pi}{2}(\cos\theta_{c_1} - \cos\theta_s)]}{K\sin[\frac{\pi}{2}(\cos\theta_{c_1} - \cos\theta_s)]} \qquad \text{(II.5.19)}$$

$$A_{c_2s} = \frac{C_2^{*}\,Z_s}{K} = \frac{\sin[\frac{K\pi}{2}(\cos\theta_{c_2} - \cos\theta_s)]}{K\sin[\frac{\pi}{2}(\cos\theta_{c_2} - \cos\theta_s)]} \qquad \text{(II.5.20)}$$

The other eigenvectors G_i (i=4, 5,....., K) are chosen to be in the constraint plane and to be orthogonal to C_1, C_2 and G_3, so that their associated eigenvalues take the same value of P_r. Thus, the solution of (II.4.3) for the present case can be written as follows.

$$W(t) = \frac{G_1^{*}\,W_0}{G_1^{*}\,G_1}\,G_1 + \sum_{i=3}^{K}\exp(-q\lambda_i t)\,\frac{G_i^{*}\,W_0}{G_i^{*}\,G_i}\,G_i - \frac{1}{\lambda_3}\{1$$

$$- \exp(-q\lambda_3 t)\} \frac{G_3^* (P R_{XX} F)}{G_3^* G_3} G_3 \qquad \text{(II.5.21)}$$

where

$$P R_{XX} F = \frac{P_s (A_{c_1 s} + A_{c_2 s})}{1 + A_{c_1 c_2}} [Z_s - \frac{1}{(1 - A_{c_1 c_2}^2)} \{(A_{c_1 s}$$

$$- A_{c_2 s} A_{c_1 c_2}) C_1 + (A_{c_2 s} - A_{c_1 s} A_{c_1 c_2}) C_2\}] \qquad \text{(II.5.22)}$$

and W_0 is the initial weight vector which is chosen to satisfy the constraint condition. As the eigenvector G_2 is orthogonal to the weight vector which satisfies the constraint condition, the term concerned with G_2 has vanished in (II.5.21).

Since, the eigenvalue λ_i (i=3, 4,..., K) is positive and the equivalent step size q is chosen to be positive, (II.5.21) converges to the following equation.

$$\lim_{t \to \infty} W(t) = \frac{1}{K (1 + A_{c_1 c_2})} (C_1 + C_2) - \frac{1}{\lambda_3} \frac{P_s (A_{c_1 s} + A_{c_2 s})}{1 + A_{c_1 c_2}} Z_s \qquad \text{(II.5.23)}$$

The array system response toward the desired signal direction can be derived by making the inner product of (II.5.23) by the desired signal phase vector Z_s as follows.

$$\lim_{t\to\infty} Z_s^* W(t) = \frac{A_{c_1 s} + A_{c_2 s}}{1 + A_{c_1 c_2}}$$

$$\times \left\{ \frac{P_r}{P_r + K^3 P_s (1 - A_{c_1 s}^2 - A_{c_2 s}^2 - A_{c_1 c_2}^2 + 2 A_{c_1 s} A_{c_2 s} A_{c_1 c_2})} \right\} \quad \text{(II.5.24)}$$

Calculated results of the array system response toward the desired signal direction using (II.5.24) are shown in Figs.II.5.2 and II.5.3. In Fig.II.5.2, array system response toward the desired signal direction is shown in terms of its direction with parameters of the constraint directions. For clarifying the physical meanings, the constraint directions are chosen to be symmetric with respect to the array normal direction. Apparently, as the angular separation between two constraint directions increases, the array system response at the midpoint of the constraints decreases seriously. But, near the constraint directions, the response is almost equal to unity. On the other hand, if double constraints are applied nearer in angular separation, decrement of the array system response is small even if its direction is outside of the double constraints. This condition can be interpreted that the interference rejection performance is affected due to the applications of the double directional constraints near to each other. In Fig.II.5.3, the array system response is also shown with parameter of the ratio between the desired signal power to the internal noise power.

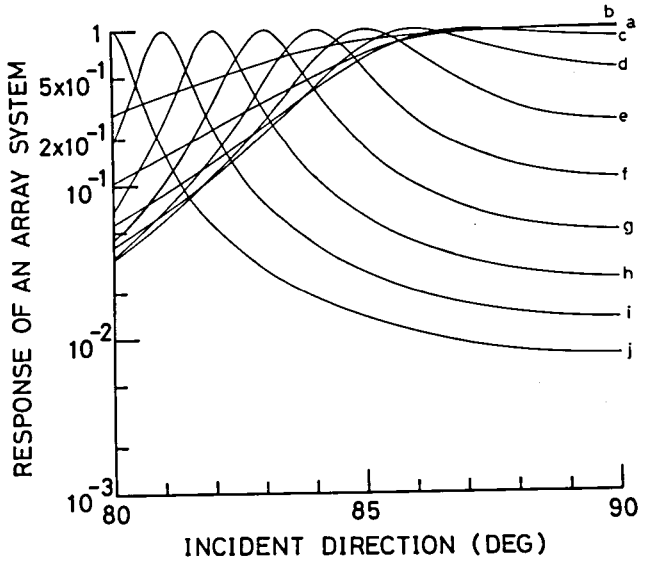

Fig.II.5.2 Array system response toward the desired signal direction.

(constraint directions)

a : 89°, 91°
b : 88°, 92°
c : 87°, 93°
d : 86°, 94°
e : 85°, 95°
f : 84°, 96°
g : 83°, 97°
h : 82°, 98°
i : 81°, 99°
j : 80°, 100°

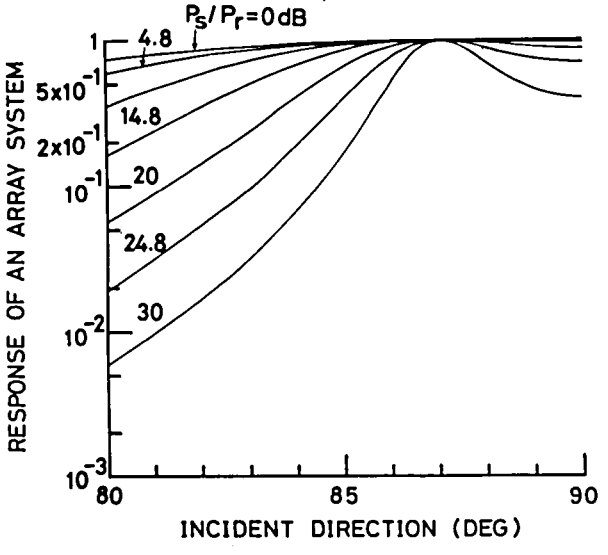

Fig.II.5.3 Array system response toward the desired signal direction. Constraint directions are chosen as 87° and 93°

As increasing the ratio between the desired signal power to the internal noise power is, the array system response is decreasing. This is due to the fact that for minimizing the output power of the array system, it is effective to reduce the array system response toward the desired signal direction with high power desired signal than small amount of increment of the internal noise power introduced by the deviation of the weight vector from uniform excitation condition. Referring to Fig.II.5.3, even if the desired signal power-to-internal noise power ratio is 30 dB, the decrement of the array system response at the midpoint of constraints is only 4 dB.

Summarizing the above discussions, new double constraints system may acts well for interference rejection and for guaranteeing the desired signal component. In addition to them, it is adequate from the qualitative considerations to choose the angular separation of double constraints to be equal to about one tenth of the beamwidth of the array system with uniform excitation.

Now, we will consider the radio environment including the desired signal and one interference. Using the same notations as in the preceding chapter, the correlation matrix R_{XX} is given as follows.

$$R_{XX} = P_r U + P_s Z_s Z_s^* + P_b Z_b Z_b^* \qquad \text{(II.5.25)}$$

Thus, the matrix coefficient $P R_{XX} P$ can be calculated using (II.5.9) and (II.5.25) and which can be given as follows.

$$P\,R_{XX}\,P = P_r\,U + P_s\,Z_s\,Z_s^* + P_b\,Z_b\,Z_b^* + \frac{1}{1 - A_{c_1c_2}^{\;2}}\,[C_1\,C_1^*$$

$$\times\{-\frac{P_r}{K} + \frac{P_s(A_{c_1s}-A_{c_1c_2}A_{c_2s})^2 + P_b(A_{c_1b}-A_{c_1c_2}A_{c_2b})^2}{1 - A_{c_1c_2}^{\;2}}\} + C_2\,C_2^*$$

$$\times\{-\frac{P_r}{K} + \frac{P_s(A_{c_2s}-A_{c_1c_2}A_{c_1s})^2 + P_b(A_{c_2b}-A_{c_1c_2}A_{c_1b})^2}{1 - A_{c_1c_2}^{\;2}}\} + (C_1\,C_2^*$$

$$+ C_2\,C_1^*)\,[\{P_s(A_{c_1s}-A_{c_1c_2}A_{c_2s})(A_{c_2s}-A_{c_1c_2}A_{c_1s}) + P_b(A_{c_1b}-A_{c_1c_2}$$

$$\times A_{c_2b})(A_{c_2b}-A_{c_1c_2}A_{c_1b})\}\,\frac{1}{1 - A_{c_1c_2}^{\;2}} + \frac{P_r\,A_{c_1c_2}}{K}] - (Z_s\,C_1^*$$

$$+ C_1\,Z_s^*)P_s(A_{c_1s}-A_{c_1c_2}A_{c_2s}) - (Z_s\,C_2^* + C_2\,Z_s^*)P_s(A_{c_2s}-A_{c_1c_2}$$

$$\times A_{c_1s}) - (Z_b\,C_1^* + C_1\,Z_b^*)P_b(A_{c_1b}-A_{c_1c_2}A_{c_2b}) - (Z_b\,C_2^* + C_2\,Z_b^*)$$

$$\times P_b(A_{c_2b}-A_{c_1c_2}A_{c_1b})\} \qquad \text{(II.5.26)}$$

where

$$A_{c_1 b} = \frac{C_1^* Z_b}{K} = \frac{\sin[\frac{K\pi}{2}(\cos\theta_{c_1} - \cos\theta_b)]}{K \sin[\frac{\pi}{2}(\cos\theta_{c_1} - \cos\theta_b)]} \qquad \text{(II.5.27)}$$

$$A_{c_2 b} = \frac{C_2^* Z_b}{K} = \frac{\sin[\frac{K\pi}{2}(\cos\theta_{c_2} - \cos\theta_b)]}{K \sin[\frac{\pi}{2}(\cos\theta_{c_2} - \cos\theta_b)]} \qquad \text{(II.5.28)}$$

As discussed by Frost[30],[53], again the column vectors of the constraint matrix, i.e. C_1 and C_2, are two of the eigenvectors of the matrix $P\,R_{XX}\,P$, both of which have the associated eigenvalues of zero. Since the matrix is Hermitian, K eigenvectors can be chosen to be orthogonal with each other. Using C_1 and C_2, we can derive two of such eigenvectors and their eigenvalues shown by the following equations.

$$G_1 = C_1 + C_2 \qquad \text{(II.5.29)}$$

$$G_2 = C_1 - C_2 \qquad \text{(II.5.30)}$$

$$\lambda_1 = \lambda_2 = 0 \qquad \text{(II.5.31)}$$

In order to determine two of the remaining eigenvectors, we form a set of linear combination of C_1, C_2, Z_s and Z_b. By substituting it into the characteristic equation for $P\,R_{XX}\,P$ of (II.5.26), we obtain the following eigenvectors G_3 and G_4 and their associated eigenvalues λ_3 and λ_4.

$$G_3 \text{ or } G_4 = Z_s + \beta_1 C_1 + \beta_2 C_2 + \beta_3 Z_b \qquad \text{(II.5.32)}$$

$$\lambda_3 \text{ or } \lambda_4 = P_r + \beta_5 + \beta_3 \beta_4 \qquad \text{(II.5.33)}$$

where

$$\beta_1 = \frac{A_{c_1c_2} A_{c_2s} - A_{c_1s} + \beta_3 (A_{c_1c_2} A_{c_2b} - A_{c_1b})}{1 - A_{c_1c_2}^2} \qquad \text{(II.5.34)}$$

$$\beta_2 = \frac{A_{c_1c_2} A_{c_1s} - A_{c_2s} + \beta_3 (A_{c_1c_2} A_{c_1b} - A_{c_2b})}{1 - A_{c_1c_2}^2} \qquad \text{(II.5.35)}$$

$$\beta_3 = \frac{-\beta_5 - \beta_6 \pm [(\beta_5 + \beta_6)^2 - 4 \beta_4 \beta_7]^{1/2}}{2 \beta_4} \qquad \text{(II.5.36)}$$

$$\beta_4 = KP_s \left[A_{sb} - \frac{A_{c_1b}(A_{c_1s} - A_{c_1c_2} A_{c_2s}) + A_{c_2b}(A_{c_2s} - A_{c_1c_2} A_{c_1s})}{1 - A_{c_1c_2}^2}\right] \qquad \text{(II.5.37)}$$

$$\beta_5 = KP_s \left[1 - \frac{A_{c_1s}(A_{c_1s} - A_{c_1c_2} A_{c_2s}) + A_{c_2s}(A_{c_2s} - A_{c_1c_2} A_{c_1s})}{1 - A_{c_1c_2}^2}\right] \qquad \text{(II.5.38)}$$

$$\beta_6 = KP_b \left[1 - \frac{A_{c_1s}(A_{c_1b} - A_{c_1c_2} A_{c_2b}) + A_{c_2s}(A_{c_2b} - A_{c_1c_2} A_{c_1b})}{1 - A_{c_1c_2}^2}\right] \qquad \text{(II.5.39)}$$

$$\beta_7 = KP_b[A_{sb} - \frac{A_{c_1b}(A_{c_1b} - A_{c_1c_2}A_{c_2b}) + A_{c_2b}(A_{c_2b} - A_{c_1c_2}A_{c_1b})}{1 - A_{c_1c_2}^2}] \qquad \text{(II.5.40)}$$

where the double signs in the right hand side of (II.5.36) are in order, according to the left hand sides of (II.5.32) and (II.5.33) with corrospoinding values of (II.5.34) and (II.5.35) which depend on (II.5.36). The remaining eigenvectors can be chosen within the constraint plane and orthogonal to Z_s and Z_b because of the properties of the eigenvectors of Hermitian. Following the same procedures discussed in the preceding chapter, the solution of the differential equation of W(t) of (II.4.3) for the double directional constraints system is given by the following equation. The initial weight vector is chosen to be equal to F in accordance with the fact discussed previously.

$$W(t) = \frac{1}{K(1 + A_{c_1c_2})} G_1 - \frac{1}{\lambda_3}\{1 - \exp(-q\lambda_3 t)\} \frac{G_3^* P R_{XX} F}{G_3^* G_3} G_3$$

$$- \frac{1}{\lambda_4}\{1 - \exp(-q\lambda_4 t)\} \frac{G_4^* P R_{XX} F}{G_4^* G_4} G_4 \qquad \text{(II.5.41)}$$

with

$$P R_{XX} F = \frac{P_s(A_{c_1s} + A_{c_2s})}{1 + A_{c_1c_2}} Z_s - \frac{1}{(1 + A_{c_1c_2})^2(1 - A_{c_1c_2})}[P_s(A_{c_1s}^2$$

$$- A_{c_1c_2}A_{c_1s}A_{c_2s} - A_{c_1c_2}A_{c_2s}^2 + A_{c_1s}A_{c_2s}) + P_b(A_{c_1b}^2 - A_{c_1c_2}$$

$$\times A_{c_1b}A_{c_2b} - A_{c_1c_2}A_{c_2b}^2 + A_{c_1b}A_{c_2b})]\ C_1$$

$$- \frac{1}{(1 + A_{c_1c_2})^2(1 - A_{c_1c_2})} [P_s(A_{c_2s}^2 - A_{c_1c_2}A_{c_1s}A_{c_2s} - A_{c_1c_2}$$

$$\times A_{c_1s}^2 + A_{c_1s}A_{c_2s}) + P_b(A_{c_2b}^2 - A_{c_1c_2}A_{c_1b}A_{c_2b} - A_{c_1c_2}A_{c_1b}^2$$

$$+ A_{c_1b}A_{c_2b})]\ C_2 + \frac{P_b(A_{c_1b} + A_{c_2b})}{1 + A_{c_1c_2}} Z_b \qquad \text{(II.5.42)}$$

In (II.5.41), there is no term corresponding to the eigenvector G_2 because G_2 is orthogonal to F and its contribution has vanished.

To clarify the double directional constraints condition, inner products of (II.5.41) by C_1 and C_2, which are column vectors of the constraint matrix, are calculated with the aid of the orthogonal properties of the eigenvectors as,

$$C_1^* W(t) = 1 \qquad \text{(II.5.43)}$$

$$C_2^* W(t) = 1 \qquad \text{(II.5.44)}$$

These results can be derived in accordance with the fact that C_1 and C_2

are orthogonal to both of G_3 and G_4. It is proved that at any time, the double directional constraints condition is satisfied. In the same fashion, the array system response toward the desired signal direction and toward the interference direction can be calculated as follows.

$$Z_s^* W(t) = \frac{1}{K(1 + A_{c_1 c_2})} Z_s^* G_1 - \frac{1}{\lambda_3}\{1 - \exp(-q\lambda_3 t)\} \frac{G_3^* P R_{XX} F}{G_3^* G_3}$$

$$\times Z_s^* G_3 - \frac{1}{\lambda_4}\{1 - \exp(-q\lambda_4 t)\} \frac{G_4^* P R_{XX} F}{G_4^* G_4} Z_s^* G_4 \qquad \text{(II.5.45)}$$

$$Z_b^* W(t) = \frac{1}{K(1 + A_{c_1 c_2})} Z_b^* G_1 - \frac{1}{\lambda_3}\{1 - \exp(-q\lambda_3 t)\} \frac{G_3^* P R_{XX} F}{G_3^* G_3}$$

$$\times Z_b^* G_3 - \frac{1}{\lambda_4}\{1 - \exp(-q\lambda_4 t)\} \frac{G_4^* P R_{XX} F}{G_4^* G_4} Z_b^* G_4 \qquad \text{(II.5.46)}$$

Closed forms of (II.5.45) and (II.5.46) can be obtained by using some equations derived previously, however, they are too much complicated and can not clearly indicate their physical meanings so that they are omitted here.

In order to evaluate the transient behavior of the system,

some computations are carried out by use of (II.5.41). First of all, the condition discussed in the preceding chapter in which the output signal-to-noise ratio is seriously affected due to the prediction error of the desired signal direction is treated to verify the performance of double directional constraints system. The parameters are the same with those of the preceding case except for the constraint condition which are summarized in Table II.5.1.

In Figs.II.5.4, II.5.5 and II.5.6, transient behavior of the weights, the output signal-to-noise ratio at the array output and the history of the output powers from each source during adaptation are shown. Fig.II.5.6 indicates clearly the performance of the double directional constraints system to reject the interference component at the array output while maintaining the desired signal. In accordance with the reduction of the noise power at the output of the system, the output signal-to-noise ratio increases to its saturation level as shown in Fig.II.5.5.

Summarizing the results described above, the double directional constraints system acts well compared with the signal directional constraint system under the condition with prediction error of the desired signal direction in the high signal-to-noise ratio environment of the field strength.

Additional calculations are made with parameters shown in Table II.5.2. Transient behavior of the weights, the output signal-to-noise ratio and the history of the desired signal, the interference and the in-

	θ_{c_1}	θ_{c_2}	θ_s	θ_b	P_s/P_r	P_b/P_r	q
EN 10	90°	84°	87°	45°	5×10	1.25×10	10^{-2}

Table II.5.1 Parameters for computation of a transient behavior of the adaptive array. (high signal-to-noise ratio of a field strength)

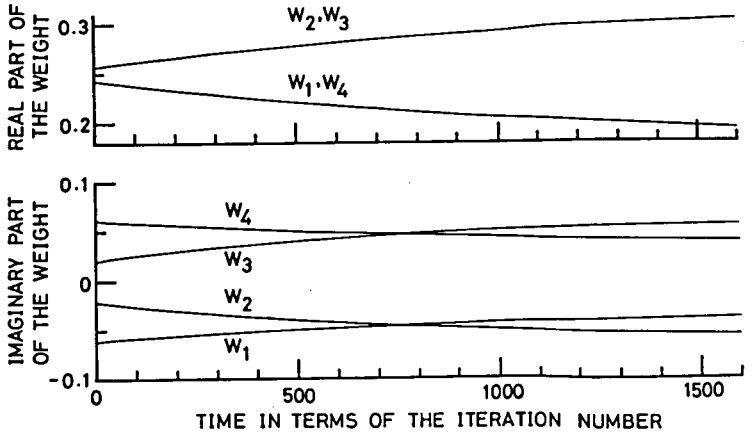

Fig.II.5.4 Transient behavior of the weights for EN 10.

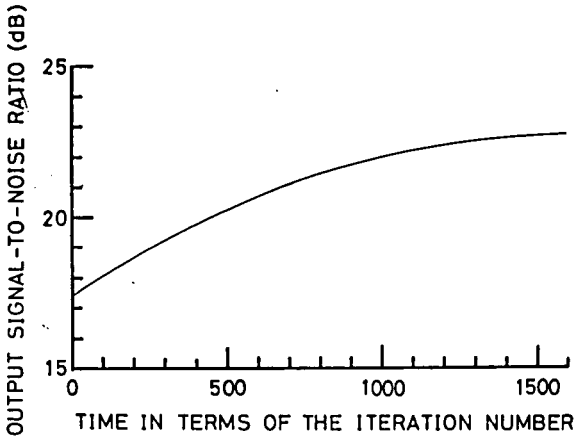

Fig.II.5.5 Transient behavior of the output signal-to-noise ratio for EN 10.

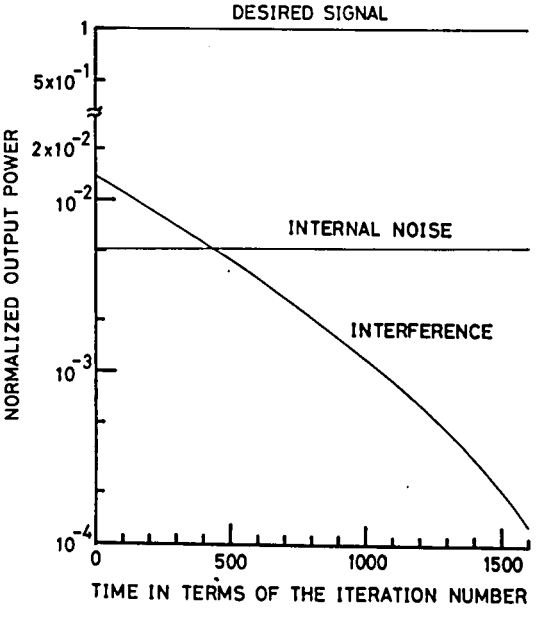

Fig.II.5.6 History of the output powers from each source for EN 10.

ternal noise of the output powers are shown in Figs.II.5.7, II.5.8, II.5.9 and II.5.10 for EN 11 of Table II.5.2 and in Figs.II.5.11, II.5.12, II.5.13 and II.5.14 for EN 12 of Table II.5.2, respectively. Comparing the results in this chapter with those of the corresponding cases appeared in the preceding chapter, the double directional constraints system acts almost the same with the single directional constraint system under the condition with low signal-to-noise ratio of the field strength.

5.3 Concluding Remarks

The transient behavior of the double directional constraints system is analyzed in comparison with the single directional constraint system by use of the method discussed in the preceding chapter. The analysis shows the array system responses toward each of double constraint direction are maintained as unity in the process of adaptation. At the same time, in the interference direction the array system response decreases in an exponential manner while in the desired signal direction, in spite of the deviation from the constraint directions, the array system response is supported almost equal to unity by the double directional constraints which results in the increment of the output signal-to-noise ratio.

This performance is suitable not only under the condition with low signal-to-noise ratio environment but also with high signal-to-noise ratio environment under which the prediction error of the desired signal direction for the single directional constraint system may cause a

	θ_{c_1}	θ_{c_2}	θ_s	θ_b	P_s/P_r	P_b/P_r	q	remarks
EN 11	87°	93°	90°	45°	10^2	10^4	5×10^{-5}	EN 1
EN 12	42°	48°	45°	90°	10^2	10^4	5×10^{-5}	EN 3

Table II.5.2 Parameters for computation of a transient behavior of the adaptive array.

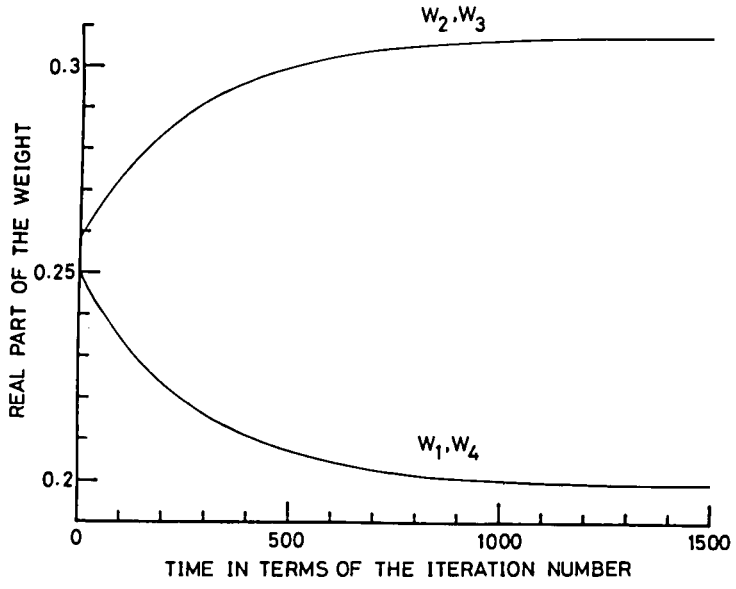

Fig.II.5.7 Transient behavior of the real parts of the weights for EN 11.

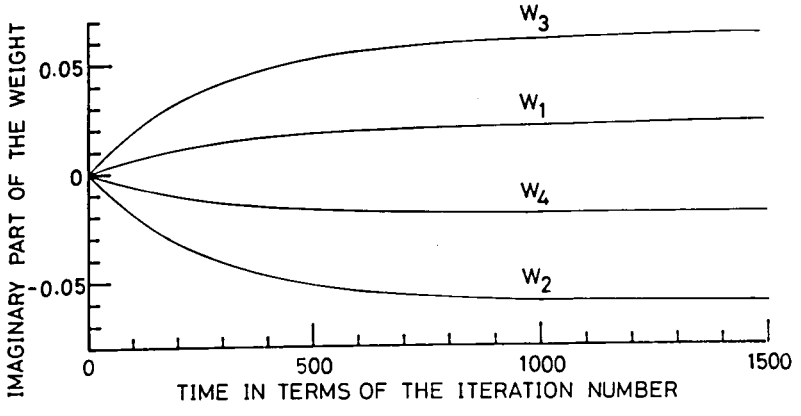

Fig.II.5.8 Transient behavior of the imaginary parts of the weights for EN 11.

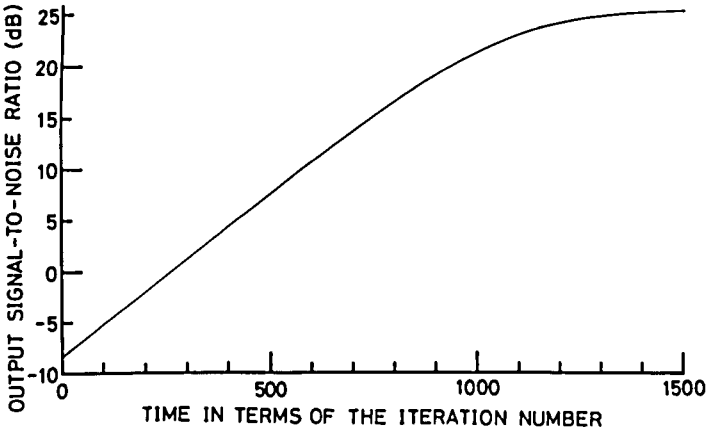

Fig.II.5.9 Transient behavior of the output signal-to-noise ratio for EN 11.

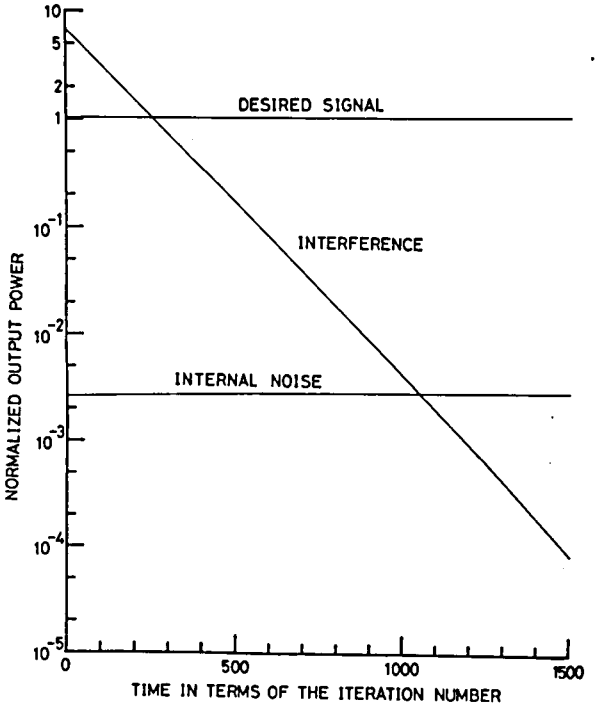

Fig.II.5.10 History of the output powers from each source for EN 11.

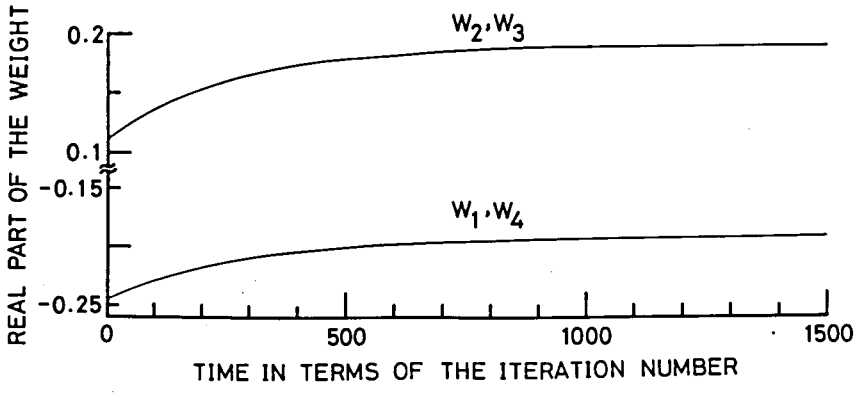

Fig.II.5.11 Transient behavior of the real parts of the weights for EN 12.

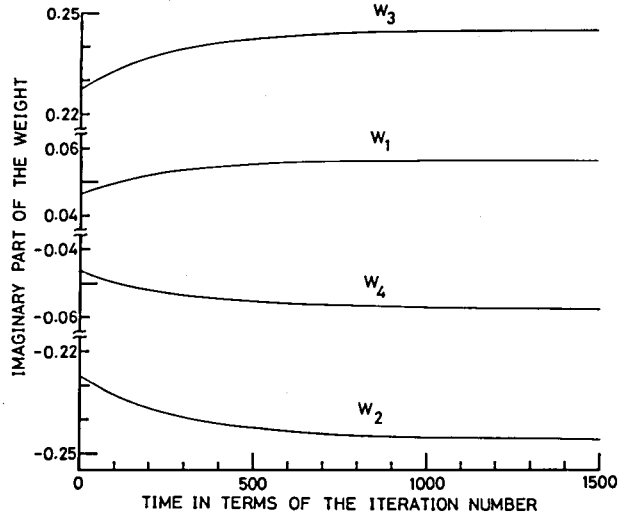

Fig.II.5.12 Transient behavior of the imaginary parts of the weights for EN 12.

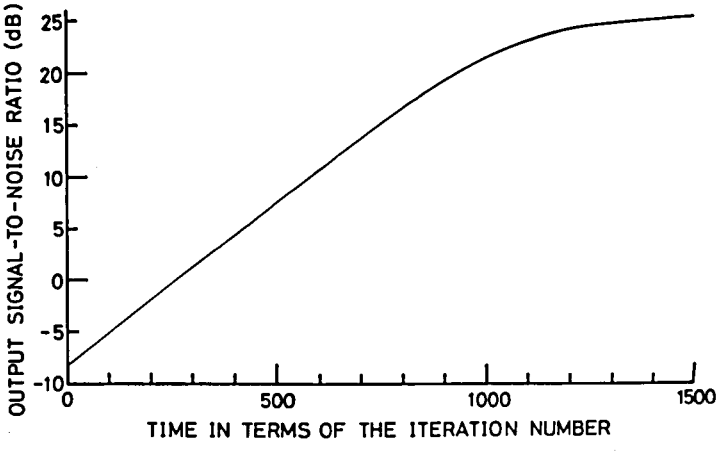

Fig.II.5.13 Transient behavior of the output signal-to noise ratio for EN 12.

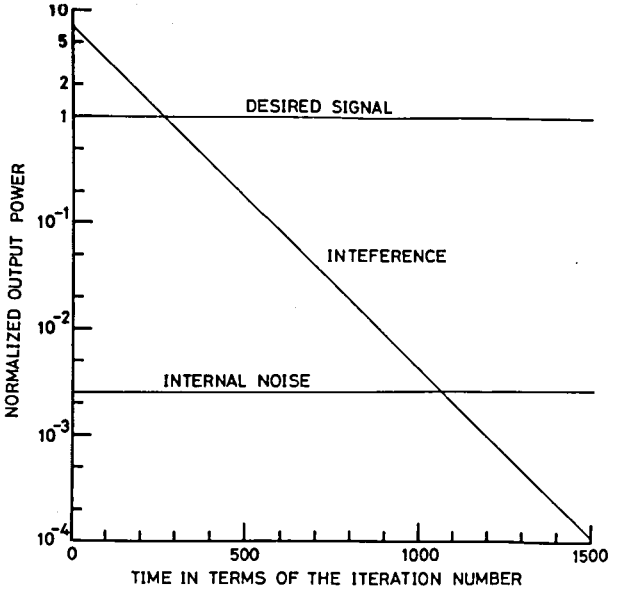

Fig.II.5.14 History of the output powers from each source for EN 12.

large amount of degradation of the output signal-to-noise ratio.

The one shortcoming of the double directional constraints system is the degradation of the interference rejection property compared with the single directional constraint system when interference direction approaches to the constraint directions. However, this property relates closely to the guaranty of the desired signal component whose incident direction is off from the constraint directions.

Therefore, the selection of the system must be performed in accordance with the conditions under which the system should be operated, i.e. the conditions of the signal-to-noise ratio and/or expected ambiguity of the direction of the desired signal.

Chapter 6. COMPUTER SIMULATION EXPERIMENTS

6.1 Introduction

The detailed analyses on the single and the double directional constraint system are given in Chapters 4 and 5. These analyses give the expected mean behavior of the systems based on the analog feedback circuitry concept. On the contrary, the practical system may adopt the signal processor implemented on digital computer so that signals for processings must be in digital forms. Thus, sampling feedback is significant for the practical applications.

Digital feedback loop may generally include the problems, for example, the loop stability, rather than analog feedback loops as discussed in Chapter 3. In addition to them, practical system will utilize the instantaneous values of the received signal rather than the correlation matrix of the received signal so that it will be expected that the system behaves with some differences from the theoretical results. In order to verify the above described points, some experiments by means of computer simulations are carried out.

It is to be noted, however, in the following computer experiments only signal generations are simulated by computer, as the signal processor is supposed to implement on computer.

6.2 Description of Simulation Experiments

The antenna array system used in the computer simulations

includes four element-antennas located linearly with spacing of a half wavelength of the desired signal between adjacent elements. Though, an element factor of each antenna is assumed to be isotropic, this assumption does not affect the generality of the results discussed in this chapter, because the effect of an element factor relates only to the signal amplitudes so that the results here can be easily interpreted to such situations by weighting appropriately the signal amplitudes.

The tapped delay lines for processor are supposed to consist of one time delay element and two weights (variable gain amplifiers) which are connected to both arms of time delay element. The amount of time delay is one quarter of the period of the center frequency of the desired signal which produces the quadrature components of the desired signal at each arm of the time delay element. This type of tapped delay line acts as an amplitude control device and a phase shifter. Referring to Fig.II.6.1, the gain, A, and the amount of phase shift, ϕ, through a tapped delay line with two taps can be written as follows.

$$A = (w_r^2 + w_i^2)^{1/2} \qquad \text{(II.6.1)}$$

$$\phi = \tan^{-1} \frac{w_i}{w_r} \qquad \text{(II.6.2)}$$

Fig.II.6.2 shows the conceptual diagram of the adaptive array used in the computer simulation experiments. This figure does not include the feedback circuitry for controlling each weight. The weights shown in

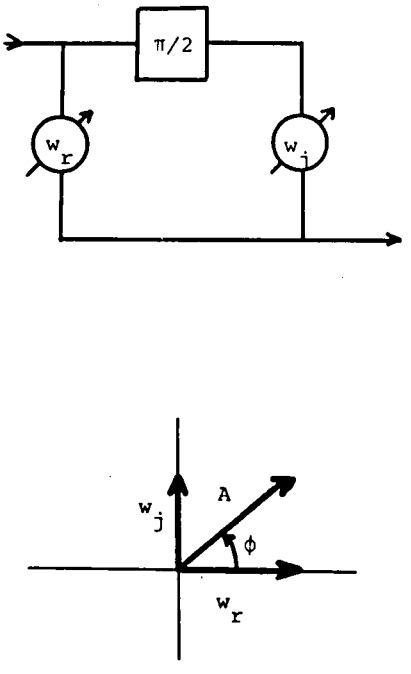

Fig.II.6.1 Tapped-delay-line filter with two taps as an amplifier and a phase shifter.

Fig.II.6.2 should be controlled as (II.3.47) through observations of the radio environment.

The desired signal and the interferences are designed to be sinusoidal waves whose phases are randomly fluctuated over 0 to 2π with respect to the sampling clock for observing the radio environment and for controlling the weights. This feature accomodates a situation in which the lack of synchronization between oscillators and/or a certain modulation such as frequency or phase modulation is supposed. The phase difference between adjacent elements, however, is determined only by the frequency, the spacing between elements and the incident angle of arrival of a signal. The frequency of the interference is not exactly the same with that of the desired signal, but the deviation is not so large as to cause any different response of the system. The internal noise at each tap point is independent random variable with Gaussian distribution which is generated by the computer.

The iteration (of sampling and feedback) period is taken to be longer than that of the signals to provide the applications of this system to a radio frequency range and care was taken not to cause any beat frequency phenomenon[54].

Under such conditions, some computer simulations are carried out by changing the parameters such as the powers and the incident directions of the desired signal and the interferences. The results of computer simulations are discussed in detail in the following section compared with the theory.

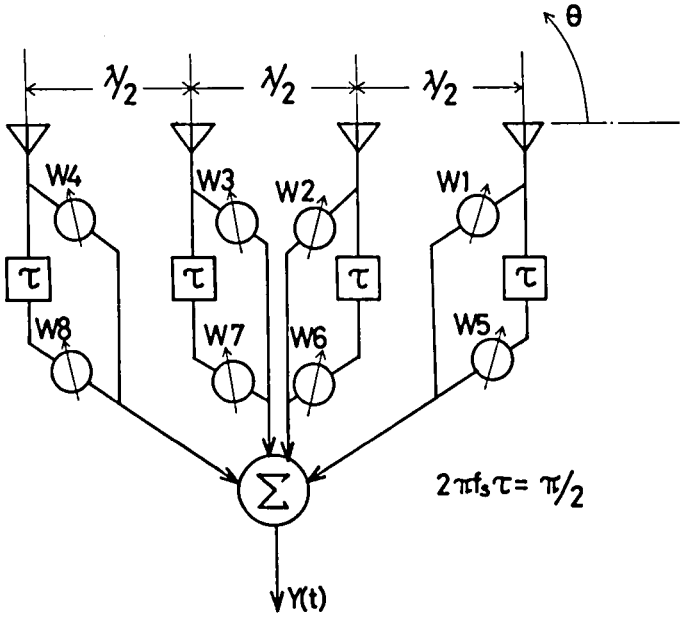

Fig.II.6.2 An array system used in the computer simulation experiments.

6.3 Comparison between the Theory and the Results of Simulation

In the following figures indicating the adaptation process, solid lines and symbolized dots signify the theory and the results of simulations, respectively. First of all, we will pay our attention to the simplest case in which accurate prediction of the desired signal direction can be provided, that is, this condition implies the case of $\theta_c = \theta_s$. Typical example of this case is shown in Figs.II.6.3 to II.6.6 with respect to the real and the imaginary parts of each weight, the output powers from each source and the output signal-to-noise ratio, respectively. As shown in Fig.II.6.3 and II.6.4, the data points for each weight by the experiment agree well with the theory except for those of negligible small values. According to this fact, not only the history of the output powers caused by the interference and the internal noise but also of the output signal-to-noise ratio fits so well with the theory. It is to be noted that the desired signal power at the output is guaranteed as a constant value by means of the constraint condition so that it is not depicted in Fig.II.6.5. Slight deviations of the data points by the experiment from the theoretical curves may be introduced by approximation of the correlation matrix R_{XX} by the instantaneous valued matrix $X X^T$ and application of the sampling feedback concept. In addition, though, variations of the influence of the internal noise may cause such deviations, which may introduce only minor effect under the conditions considered here. For reducing such deviations, as discussed by Widrow et al.[38] as a misadjustment, it is sufficient to choose the

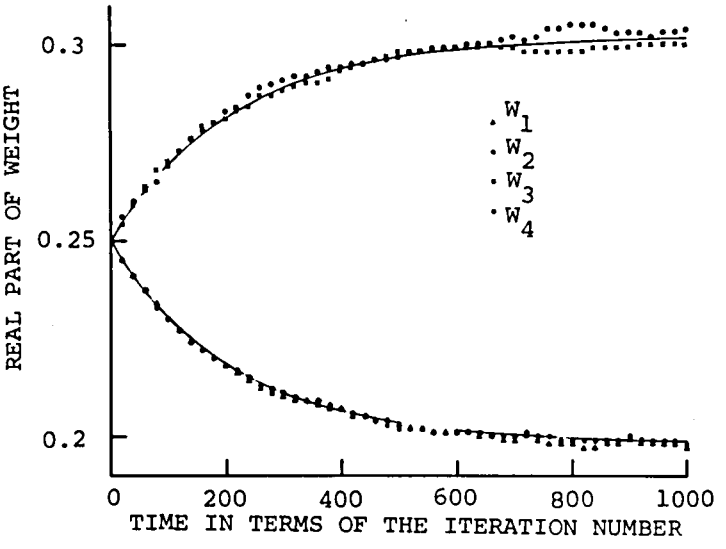

Fig.II.6.3 Transient behavior of the real parts of the weights. Solid lines show the theoretical results and symbolized dots show the results of computer simulation experiment, respectively.

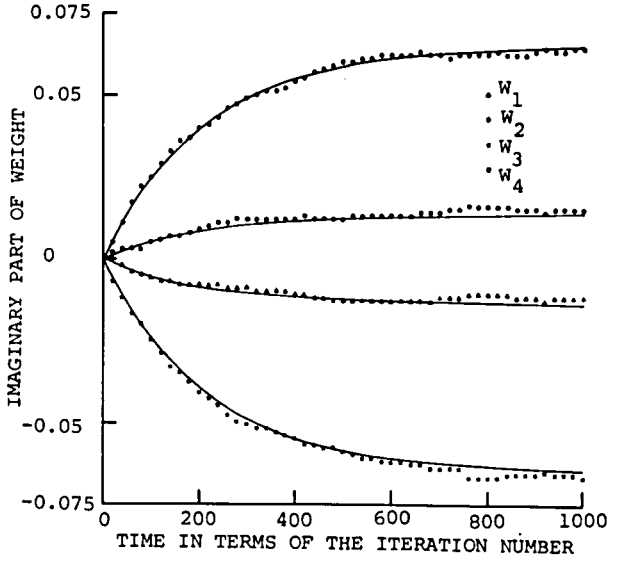

Fig.II.6.4 Transient behavior of the imaginary parts of the weights. Solid lines show the theoretical results and symbolized dots show the results of computer simulation experiments, respectively.

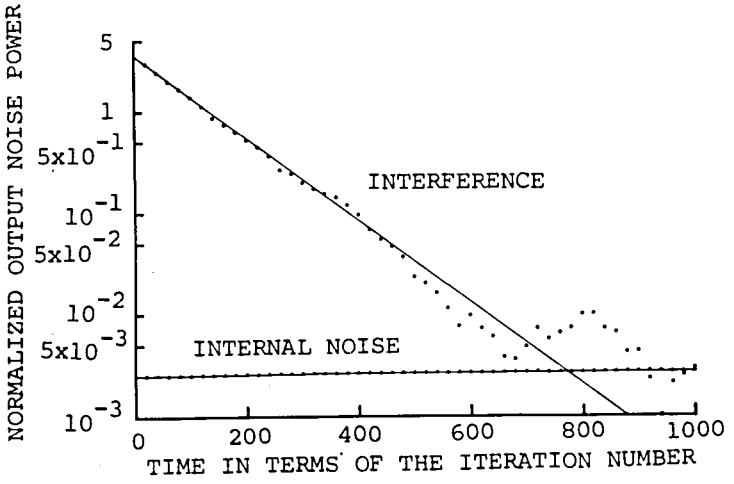

Fig.II.6.5 History of the output powers from each source. Solid lines are calculated theoretically and dots are the results of computer simulation experiments, respectively.

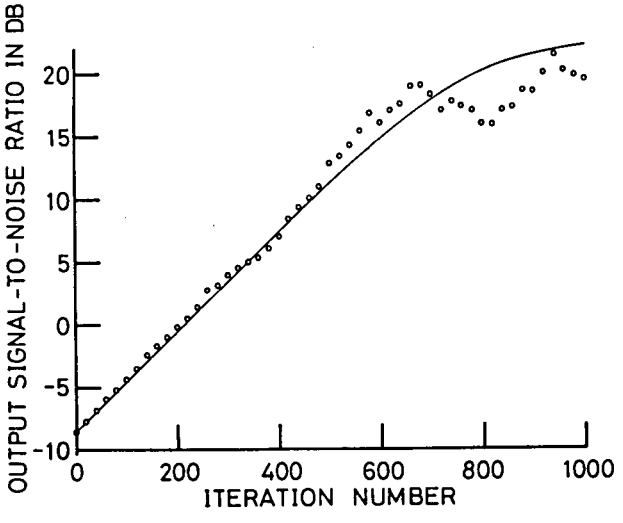

Fig.II.6.6 Transient behavior of the output signal-to-noise ratio. Solid line is calculated theoretically and circles are the results of computer simulation experiment, respectively.

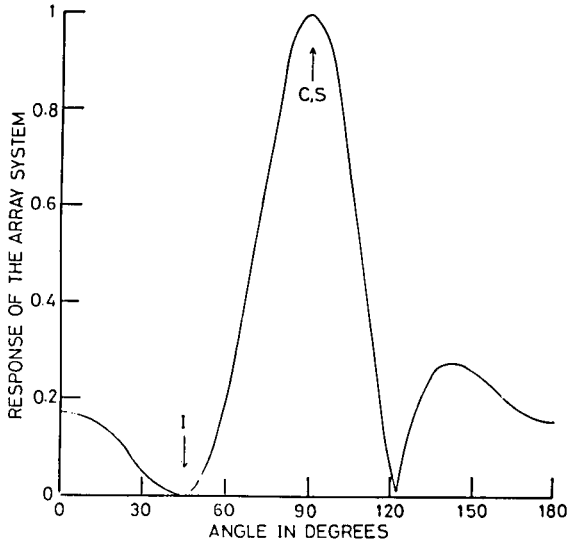

Fig.II.6.7 Radiation pattern of the adaptive array after 940 iterations.

C, S and I in the following figures denote the constraint, the desired signal and the interference direction, respectively.

step size μ as small as possible. However, step size μ is, as discussed in Chapters 4 and 5, directly proportional to the convergence rate of the system so that small choice of the step size requires a large amount of adaptation time for convergence. Additional computer experiments clearly indicate the effects of step size on a convergence rate and a deviation of data points from a result of the theory. Thus, in practice, selection of the step size must be performed in a compromised manner between a convergence rate and a deviation of data points. Fig.II.6.7 shows the radiation pattern which is calculated from the weights after 940 times of iterations. As expected from Figs.II.6.5 and II.6.6, deep null is steered toward the interference direction for reducing the interference power at the array output, while toward the constraint direction, which is the same with the desired signal direction, the array system response is maintained as unity.

To verify the effects of the incident direction of the interference with respect to the desired signal direction, some computer simulation experiments are also carried out. The list of parameters and the performances of the computer simulation experiments are summarized in Table II.6.1. Here, the processor gain is defined as the ratio of the output signal-to-noise ratio to input signal-to-noise ratio with the meaning of improvement by the system. The tendency of smaller processor gain with large θ_b is interpreted that the array tends to become more like a super gain antenna in order to produce a null at the interference direction in its radiation pattern as θ_b approaches to the

original mainbeam direction(90°), thus enhancing the internal noise power relatively. In Figs.II.6.8 to II.6.12, radiation patterns corresponding to the experiments described in Table II.6.1 are shown. It is apparent that deep null is steered toward the interference direction in each figure. In addition, as approaching the interference direction toward the constraint one, mainbeam is shifted toward the opposite side with respect to the constraint direction, while, at the constraint direction, the array system response is maintained as unity. Thus, the array system response at the mainbeam generally exceeds unity. But, it is to be noted that this situation maximizes the output signal-to-noise ratio under the given radio environment. This feature can be easily understood, if we will call to our minds the guiding principle of this system, i.e. minimization of the output power subject to the constraint condition. In other words, this system minimizes the noise power at the output of the array system on the balance of the internal noise and the interference. As shown in Table II.6.1, larger number of iterations is required for convergence as approaching the interference direction toward the constraint direction. This reason is, as discussed in detail in Chapter 4, on the fact that the eigenvalue which is inversely proportional to the time constant of convergence is reduced as the decrement of the angular separation between the interference and the constraint direction under the same step size. Though, it is not shown here, the behaviors of weights of the experiments agree well with the theory.

θ_c	θ_s	θ_b	P_s/P_r	P_b/P_r	μ	OUTPUT S/N	Iteration number	Remarks
90°	90°	65°	17dB	37dB	5×10^{-5}	22.8dB	240	Fig.II.6.8
90°	90°	70°	17dB	37dB	5×10^{-5}	22.2dB	410	Fig.II.6.9
90°	90°	75°	17dB	37dB	5×10^{-5}	20.7dB	710	Fig.II.6.10
90°	90°	80°	17dB	37dB	5×10^{-5}	18.1dB	1680	Fig.II.6.11
90°	90°	85°	17dB	37dB	5×10^{-5}	4.7dB	3820	Fig.II.6.12

Table II.6.1 Parameters and performances of computer experiments

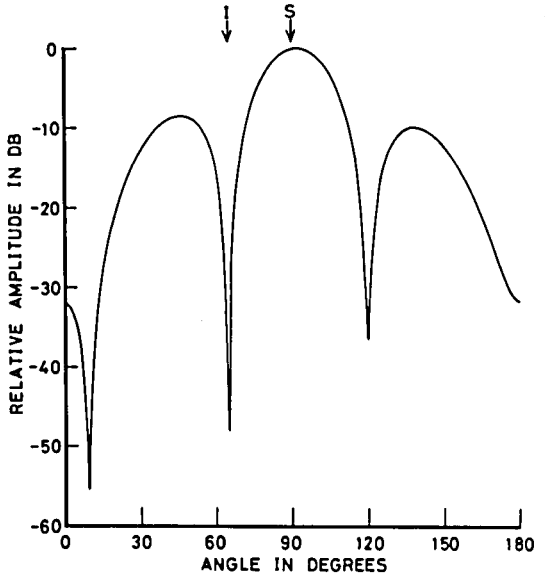

Fig.II.6.8 Radiation pattern of the adaptive array obtained by the computer experiment. (see Table II.6.1)

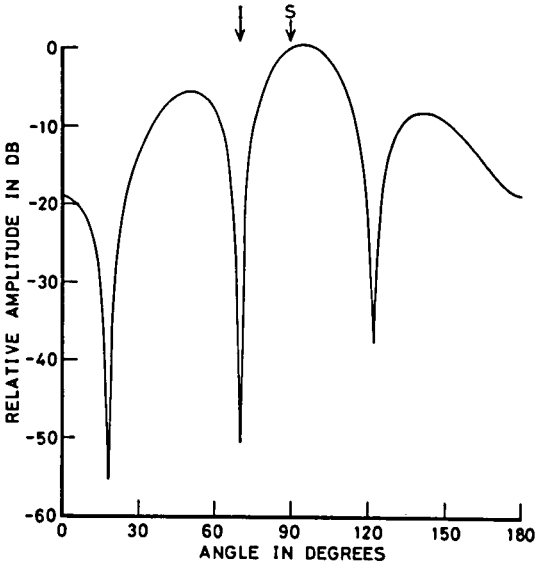

Fig.II.6.9 Radiation pattern of the adaptive array obtained by the computer experiment. (see Table II.6.1)

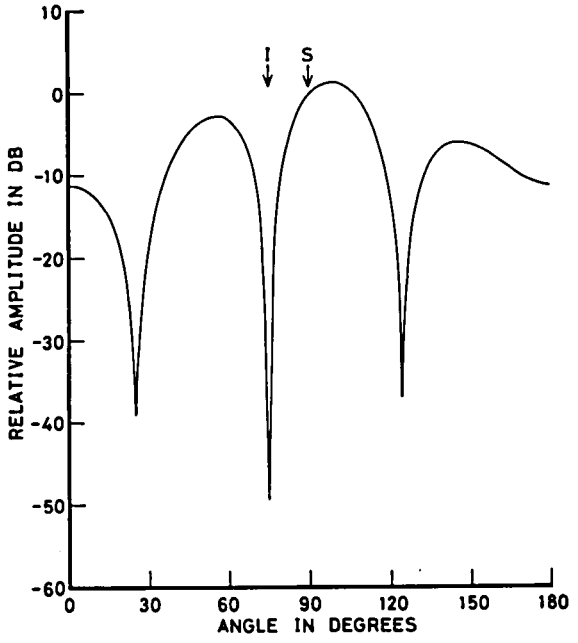

Fig.II.6.10 Radiation pattern of the adaptive array obtained by the computer experiment. (see Table II.6.1)

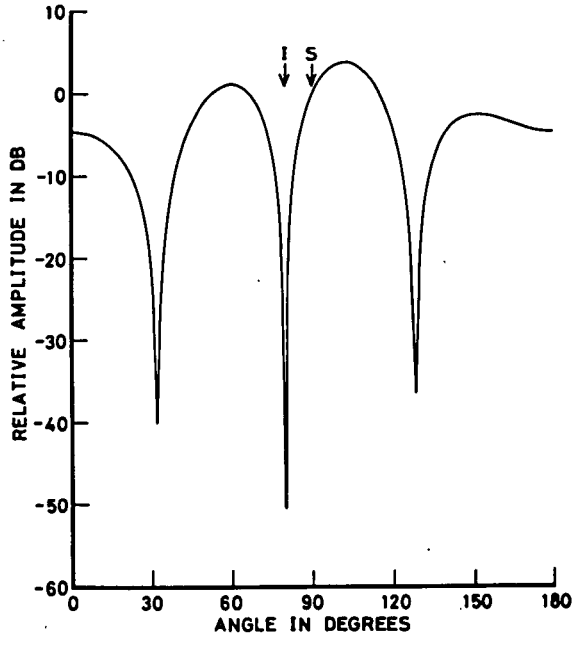

Fig.II.6.11 Radiation pattern of the adaptive array obtained by the computer experiment. (see Table II.6.1)

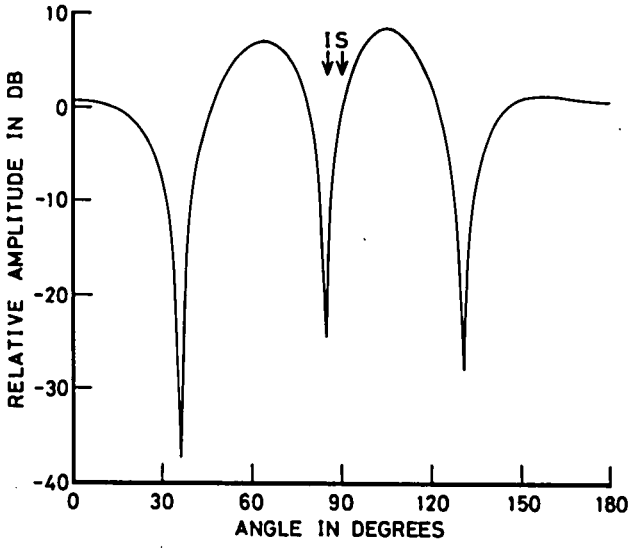

Fig.II.6.12 Radiation pattern of the adaptive array obtained by the computer experiment. (see Table II.6.1)

The case with two interferences is also experimented by means of computer simulation. The parameters used are summarized in Table II. 6.2. Again in these cases, the behaviors of weights obtained by computer simulation experiments agree well with the theoretical predictions. Radiation patterns calculated from the weights after 1300 times and 3800 times of iterations obtained by the experiments are shown in Figs.II.6. 13 and II.6.14, respectively. In both figures, deep nulls are directed toward the directions of each interference. Especially, it is interesting, as shown in Fig.II.6.14, both lobes outside of the interference directions with respect to the constraint direction exceed the lobe toward the constraint direction. This effect may be caused by the beamwidth limitation of the given array system. But, this condition is also introduced through the guiding principle of minimization of the output power under the constraint condition.

In the above, we treat the case in which the desired signal direction coincides with the constraint direction so that at the output of the array system, the desired signal power is perfectly guaranteed as a constant value. But, in practice, it is considered that the perfect a priori knowledge about the incident direction of the desired signal is not available. Only the approximated direction may be used for processing.

Thus, some computer simulation experiments are carried out to verify the analysis in Chapter 4 on this problem. First, we paid our attention to the case in which the interference power is large enough compared with the desired signal power and the internal noise

θ_c	θ_s	θ_{b_1}	θ_{b_2}	P_s/P_r	P_{b_1}/P_r	P_{b_2}/P_r	μ	Remarks
90°	90°	70°	130°	17dB	37dB	37dB	5×10^{-5}	Fig.II.6.13
90°	90°	70°	100°	17dB	37dB	37dB	5×10^{-5}	Fig.II.6.14

Table II.6.2 Parameters for computer experiments. (two interferences case)

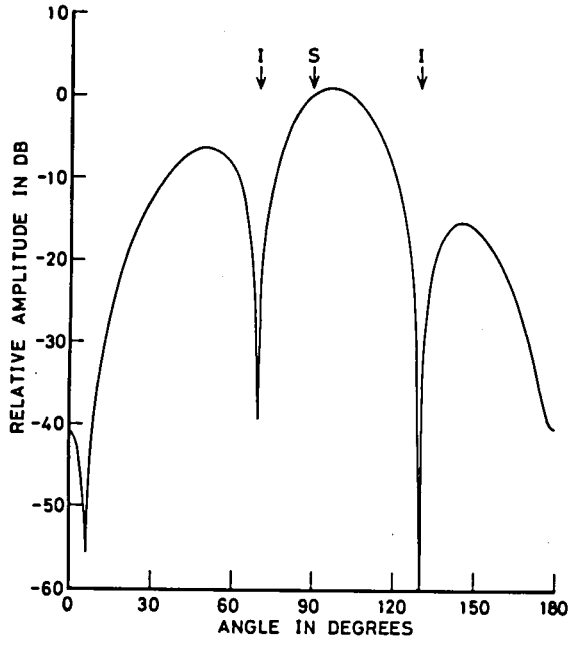

Fig.II.6.13 Radiation pattern of the adaptive array after 1300 iterations. (see Table II.6.2)

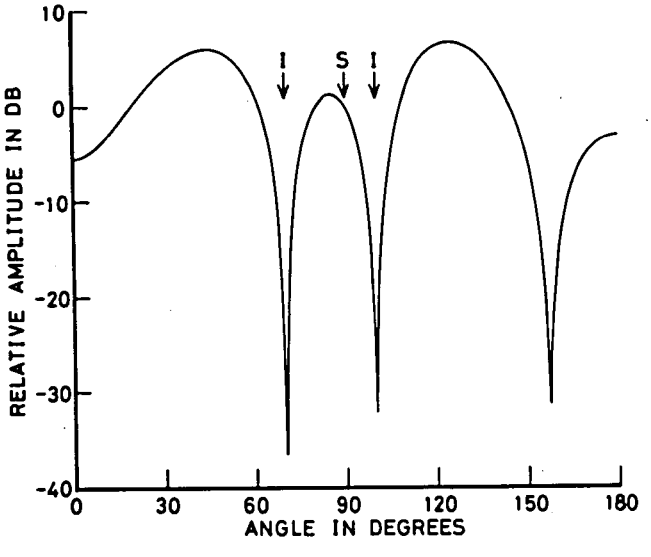

Fig.II.6.14 Radiation pattern of the adaptive array after 3800 iterations. (see Table II.6.2)

power and the difference between the incident direction of the desired signal and the constraint direction is small, i.e. one fifth of the beamwidth of the same antenna system with equal amplitude excitation. The parameters used in the experiments are summarized in Table II.6.3. Fig.II.6.15 shows the histories of the desired signal power, interference power and the internal noise power at the array system output during adaptation. Referring to this figure, the output interference power decreases steadily almost in an exponential manner, while the desired signal power is almost maintained at the initial value. This result verifies the discussion appeared in Chapter 4, 4.4, i.e. the array system response toward the interference direction decreases rapidly, because it is regarded as a main target which must be suppressed. Contribution of the desired signal component to the control signal for adaptive processing is so small compared with the interference component that the interference is rejected almost at the array output. This feature is introduced not only by the fact the interference power is large enough compared with that of the desired signal but also by the desired signal phase vector, Z_s, is almost perpendicular to the constraint plane so that its influence has been scarcely effective. Fig.II.6.16 shows the radiation pattern obtained by the simulation experiment described here. Deep null is placed toward the direction from which the interference is incident. The array system response toward the desired signal direction is slightly small compared to unity. This is due to the fact the desired signal di-

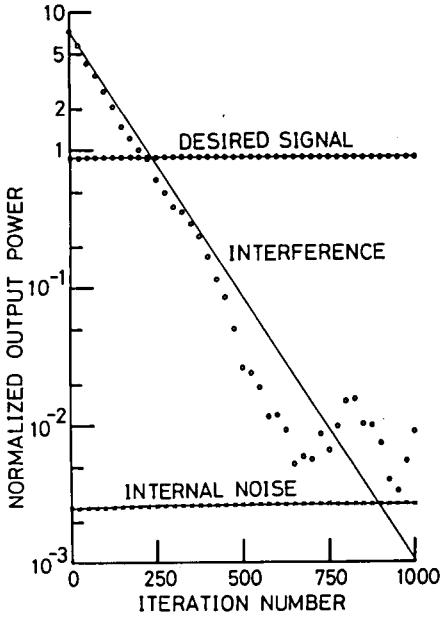

Fig.II.6.15 History of the output powers from each source. Solid lines show the theoretical results and symbolized dots are the results of computer simulation experiment, respectively. (see Table II.6.3)

θ_c	θ_s	θ_b	P_s/P_r	P_b/P_r	μ	Remarks
90°	84°	45°	17dB	37dB	2.5×10^{-5}	Fig.II.6.15 Fig.II.6.16 Fig.II.6.17
90°	87°	45°	17dB	11dB	10^{-2}	Fig.II.6.18 Fig.II.6.19

Table II.6.3 Parameters for computer experiments. (Case with prediction error of the incident direction of the desired signal)

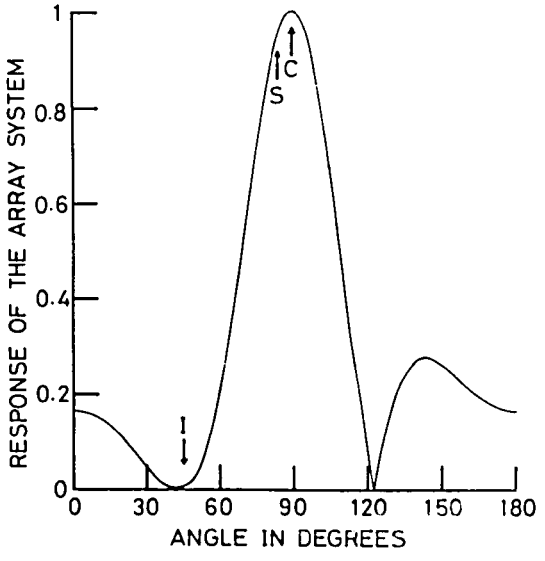

Fig.II.6.16 Radiation pattern of the adaptive array after 1000 iterations. (see Table II.6.3)

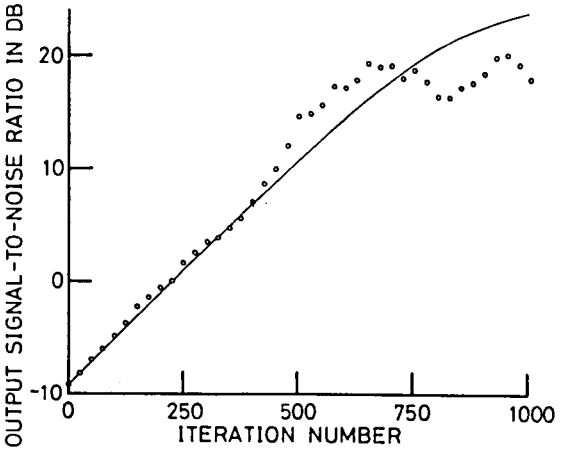

Fig.II.6.17 Transient behavior of the output signal-to-noise ratio. Solid line is calculated theoretically and circles show the results of computer simulation experiment. (see Table II.6.3)

rection is off from the constraint direction. However, this condition does not result in the major effect on the degradation of the output signal-to-noise ratio. It is apparent from Fig.II.6.15, the output signal-to-noise ratio is improved steadily as shown in Fig.II.6.17. Under the condition in which the interference power is large enough compared with the desired signal power, as discussed in Chapter 4, the small difference between the desired signal direction and the constraint direction does not affect the performance of the improvement of the output signal-to-noise ratio.

But, care must be taken to the radio environment in which signal-to-noise ratio of the field strength is relatively high. As analyzed in Chapter 4, difference between the constraint direction and the incident direction of the desired signal may result in the large amount of degradation of the output signal-to-noise ratio under the condition discussed here. To verify this effect, comparisons are made between the theory and the experimental results by computer simulation. Fig.II.6.18 shows the histories of the output powers related to the desired signal, the interference and the internal noise, respectively. Again, the experimental results agree well with the theoretical curves except for the small quantities which can be neglected. The directional error in this case is three degrees, which is one half of the previous case in which good adaptation is obtained. The learning curve of the output signal-to-noise ratio of this case is shown in Fig.II.6.19. At a first stage of adaptation, once the signal-to-noise ratio is improved,

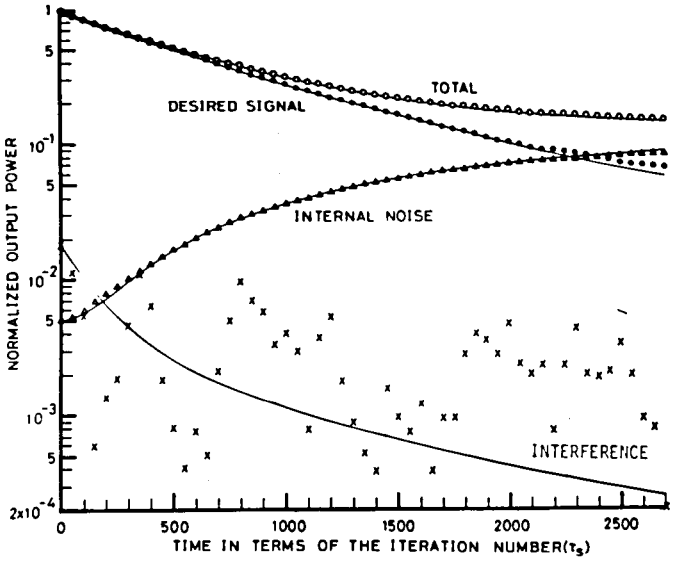

Fig.II.6.18 History of the output powers from each source. Solid lines are calculated theoretically and symbolized dots are the results of computer simulation experiment.

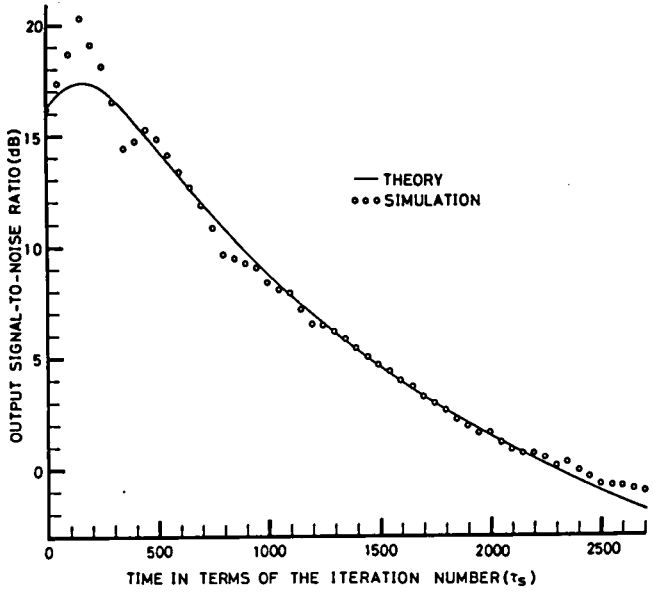

Fig.II.6.19 Transient behavior of the output signal-to-noise ratio. Solid line is calculated theoretically and circles are the results of computer simulation experiment. (see Table II.6.3)

but, after the time when the output signal-to-noise ratio is maximized, it decreases monotonously. This results from the existence of two time varying terms as shown in (II.4.85).

Through the two experiments described above, it is verified that the parameter which governs the catastrophe of the adaptive array discussed here is not only a difference between the constraint direction and the desired signal direction but also the signal-to-noise ratio of the radio environment.

To solve this problem, double directional constraints system has been proposed in Chapter 5. In the followings, results of computer simulation experiments of this system are shown comparing with the theory. First of all, the situation in which single directional constraint system falls into the unacceptable feature is treated. The difference lies only in the presence of double directional constraints. The parameters used in the computer simulation experiments are summarized in Table II.6.4. In Fig.II.6.20, behaviors of weights in terms of iteration number are shown for the real and the imaginary part. As the interference power is so small that null steering is not complete, but, as discussed latter, it is sufficient for improvement of the output signal-to-noise ratio. Therefore, the deviations of each weight from the initial value are small. Again, good agreements are exhibitted between the theoretical curves and experimental data points. According to this fact, histories of the output powers from the desired signal, the interference and the internal noise agree well with the theoretical

θ_{c_1}	θ_{c_2}	θ_s	θ_b	P_s/P_r	P_b/P_r	μ	Remarks
90°	84°	87°	45°	17dB	11dB	10^{-2}	Fig.II.6.20 Fig.II.6.21 Fig.II.6.22
90°	84°	87°	60°	17dB	37dB	5×10^{-5}	Fig.II.6.24 Fig.II.6.25 Fig.II.6.26 Fig.II.6.27

Table II.6.4 Parameters for computer experiments (double directional constraints system)

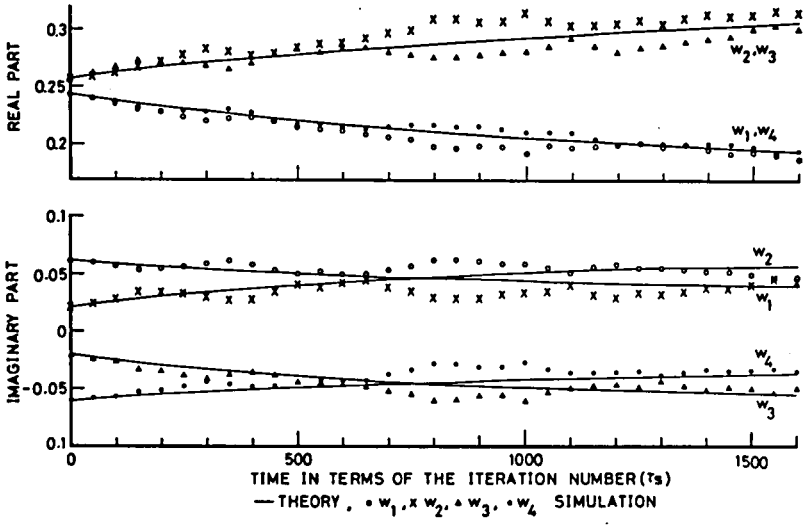

Fig.II.6.20 Transient behavior of the real and the imaginary parts of the weights. Solid lines show the theoretical results and symbolized dots show the results of computer simulation experiment. (see Table II.6.4)

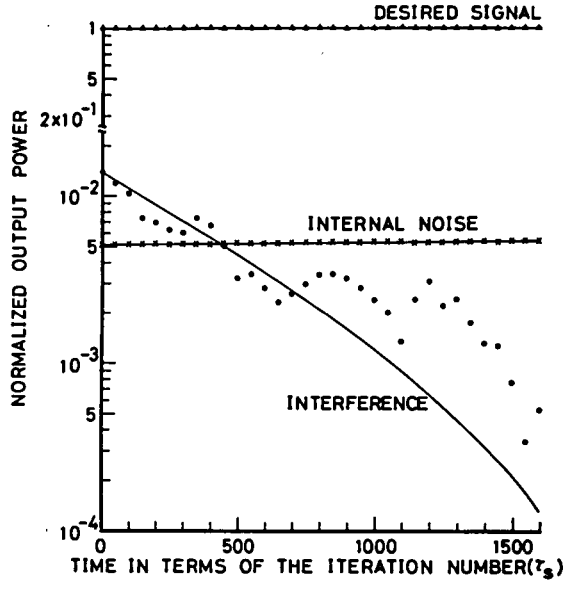

Fig.II.6.21 History of the output powers from each source. Solid lines are calculated theoretically and symbolized dots show the results of computer simulation experiment. (see Table II.6.4)

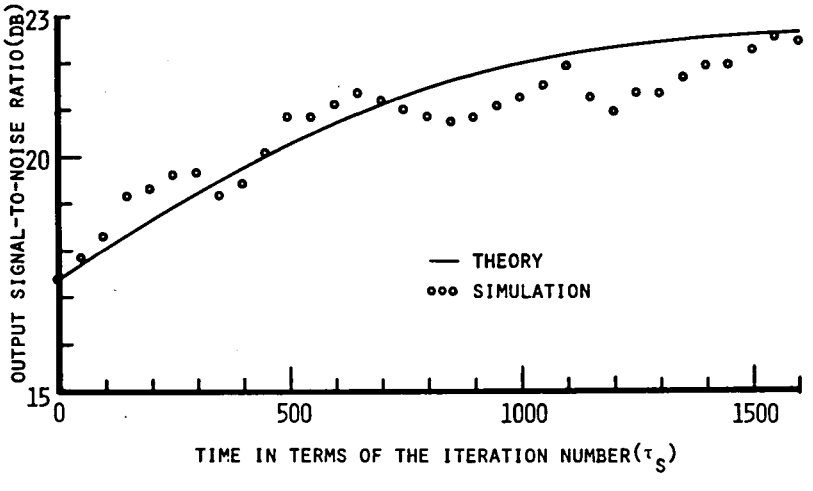

Fig.II.6.22 Transient behavior of the output signal-to-noise ratio. Solid line shows the theoretical result and circles are the results of computer simulation experiment. (see Table II.6.4)

curves, which are shown in Fig.II.6.21. As shown in this figure, the desired signal component is maintained while the interference component decreases steadily, and large enhancement of the internal noise power at the output disappears. This advantage is resulted from the introduction of the double directional constraints condition. The history of the output signal-to-noise ratio is shown in Fig.II.6.22.

In spite of the difference of the desired signal direction from each of both constraint directions, the array system response is maintained almost equal to the initial value. This is due to the fact that steering null toward the desired signal direction which is closely located to the constraint directions brings on the large enhancement of the internal noise at the system output. As the guiding principle of the system considered here is to minimize the output power subject to the constraints so that the system does not over running to such extreme condition. Conceptual sketch of this feature is shown in Fig.II.6.23. In addition to them, the time constant which governs the decrement of the array system response toward the desired signal direction is large compared with that toward the interference direction so that it does not affect the interference rejection property.

Under the radio environment of the sufficiently low signal-to-noise ratio of the field strength, the double directional constraints system acts also very well for rejecting the interference as the single directional constraint system. The data points obtained by the computer experiments fit well with the theory. The transient behavior of

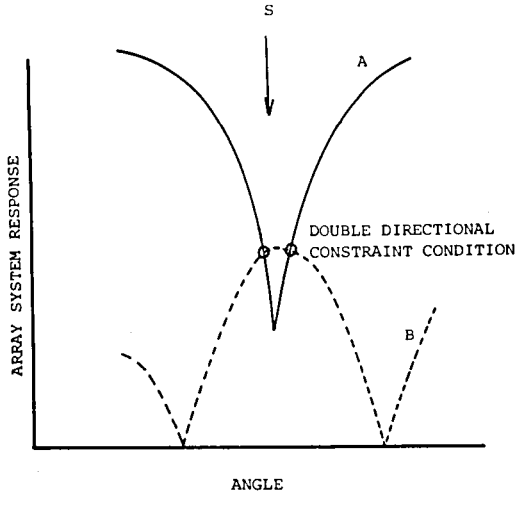

Fig.II.6.23 Conceptual sketch of the double directional constraint system.

A : large enhancement of the output internal noise power.

B : relatively low output internal noise power.

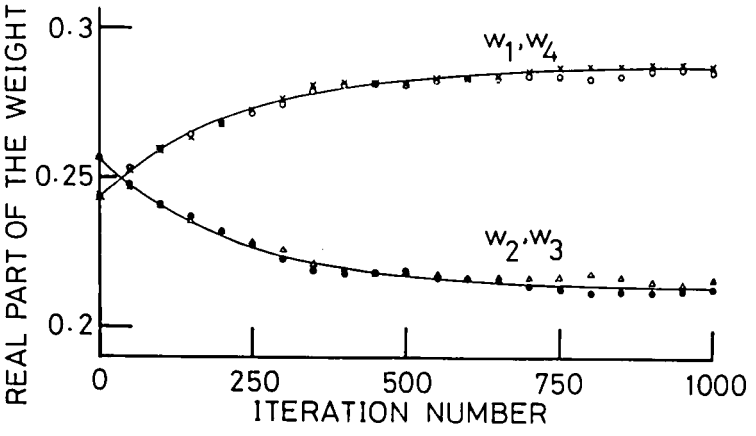

Fig.II.6.24 Transient behavior of the real parts of the weights. Solid lines show the theoretical results and symbolized dots are the results of computer simulation experiment. (see Table II.6.4)

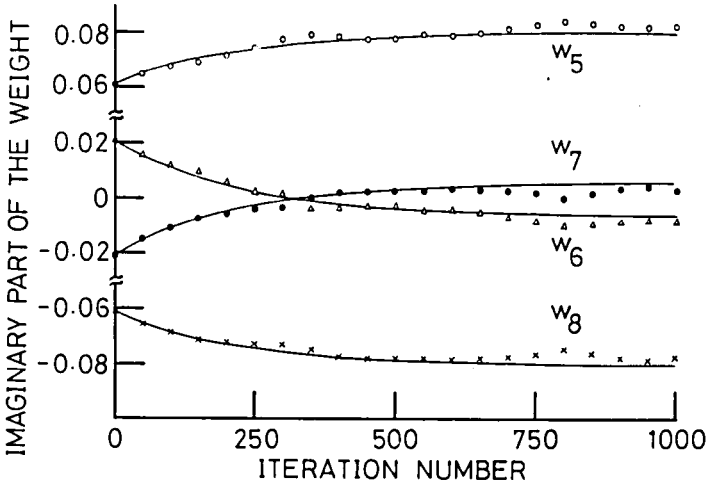

Fig.II.6.25 Transient behavior of the imaginary parts of the weights. Solid lines show the theoretical results and symbolized dots are the results of computer simulation experiment. (see Table II.6.4)

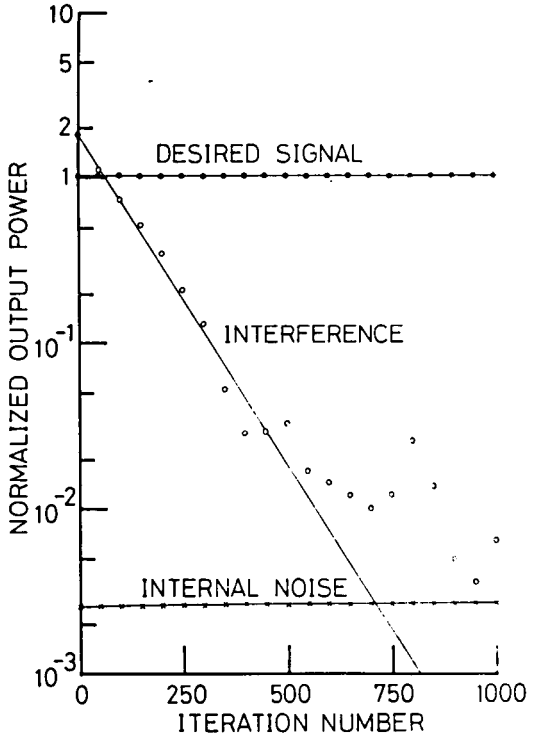

Fig.II.6.26 History of the output powers from each source. Solid lines show the theoretical results and symbolized dots are the results of computer simulation experiment. (see Table II.6.4)

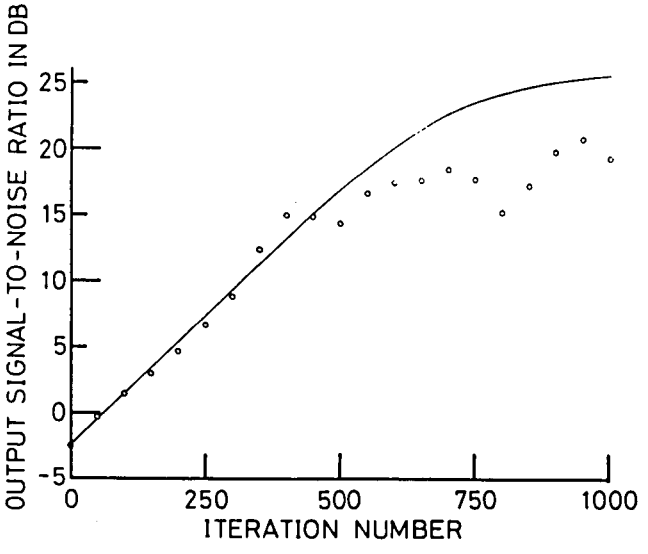

Fig.II.6.27 Transient behavior of the output signal-to-noise ratio. Solid line shows the theoretical result and circles are the results of computer simulation experiment. (see Table II.6.4)

the weights, the output powers from each source and the output signal-to-noise ratio during adaptation are shown in Figs.II.6.24, II.6.25, II.6.26 and II.6.27, respectively, with parameters listed in Table II. 6.4.

6.4 Concluding Remarks

As discussed in this chapter, the experimental results by means of computer simulation agree well with the theory. Some deviations of the experimental data points from the theoretical curves exist. This effect may be introduced through the difference between the feedback algorithms, i.e. the sampling feedback loops and the continuous feedback loops. Theory shows the mean behavior of the system, on the contrary, the experiments are carried out using the sampled data for the feedback signal so that the behavior of the system may be disturbed by the sampled value of the noise which is simulated to be randomly fluctuated. In spite of the effects discussed above, the theoretical and the experimental data points agree well except for the negligibly small quantities.

Some comparisons of the theory and the experimental results clearly indicate the usefulness of the theory described in Chapters 4 and 5 to predict the behavior of the system when exposed to a certain radio environment. Though, in the computer experiments, one interference is assumed to exist except for two cases, experiment can also be performed with multiple interferences condition.

Chapter 7. SUMMARY AND CONCLUSION

In this PART 2, the concept, analyses and experiments by means of computer simulation are discussed on the adaptive antenna array with directional constraint. The new constraint condition named "directional constraint" is introduced, in which the a priori knowledge about the incident direction and the center frequency of the desired signal is utilized for discriminating the desired signal from some interferences. The distinctive feature of this system discussed in this part lies in that the accurate a priori knowledge about the desired signal is not necessary for processing. To enlarge the margin for the desired signal direction, the concept of double directional constraints has also been introduced after analogy with the double peaked tuning circuit with wide bandwidth characteristics.

The adaptive algorithm developed by Frost is adopted to minimize the accumulation of the errors occured in the computing process such as the quantization error or round off error. This algorithm is excellent, but he did not show the behavior of the system in a closed form. Only the conditions which guarantee the convergence of the system can be deduced.

The present author applies the differential equation approach to clarify the transient behavior of the system. The adaptive algorithm is reformulated in the equivalent differential equation with coefficints which represent the expected radio environment. The weight vector is

defined in the hyperspace, which can be divided into some eigenspaces spanned by the eigenvectors of $P R_{XX} P$, the coefficient of the first order term of $W(t)$ of the differential equation. The solution of this differential equation can be calculated through the projection onto each eigenspace spanned by the eigenvectors. In addition to them, appropriate and practical choice of the initial weight vector eliminates the undetermined terms. The perfect prediction of the behavior of the system is now possible when exposed to a certain radio environment with known parameters. The same method is also applied to the double constraint system and again the solution is obtained in a closed form. The solution clearly indicates the feature of the system, i.e. the convergence is governed by the interference power, and the configuration of the constraint and the interference directions. The first property shows that the adaptive antenna array acts faster against the stronger interference. Steering nulls toward the interference directions causes the deviation of weights from the equal amplitude excitation, resulting in the enhancement of the internal noise power at the output. Although this enhancement becomes remarkable as the interference direction approaches to the constraint direction, it has a limit since the guiding principle of this system is to minimize the total output power subject to constraint so that the output signal-to-noise ratio is maximized even in such condition. The effect of the prediction error of the desired signal direction is also analyzed and it is proved that under the radio environment in which the signal-to-noise

ratio of a field strength is low enough, the system acts almost identical with the case without prediction error. It is to be recalled that the adaptive antenna array is often needed especially under such radio environment. However, under the radio environment in which the signal-to-noise ratio of a field strength is high, the prediction error of the desired signal direction causes the large enhancement of the internal noise at the output which results in the large amount of degradation of the output signal-to-noise ratio.

On the other hand, the double directional constraint system acts well under such radio environment in which single directional constraint system falls in the unacceptable feature. The double directional constraint condition guarantees the array system response toward the desired signal direction in spite of the difference between the desired signal direction and either constraint directions, for decrease of the array system response toward the desired signal direction which is closely located near the two constraint directions would bring about the large enhancement of the internal noise power which would be against minimization of the output power. The performance to the low signal-to-noise ratio environment is almost identical to the single constraint system. Thus, the double directional constraint system is more flexible over the single directional constraint system.

Some experiments by means of computer simulation are carried out to verify the feature predicted by the theory. The data points of experiment fit well with the theory in spite of the difference of the

feedback concept, i.e. the sampled feedback and continuous feedback. Deviation of the experimental results from the theory depends on the feedback signal which is deduced from the instantaneous sampled values. These deviations are closely related to product of the input power and the step size of the feedback loop. Choice of the smaller step size decreases such deviations, but requires large amount of convergence time. Automatic setting of a step size to follow the input power variation from the environment must be studied in future.

Throughout this part, array system is assumed to be linear with half wavelength spacing, but extention to the array system with two or three dimensional arrangement can be treated in a straightforward manner. In addition, the theory can treat the case with larger number of interferences. However, it is to be noted that the equation of higher than fifth degrees cannot be solved analytically in general. The aid of computer is indispensable to analyze for such conditions.

Summarizing the results discussed in this part, the sufficient performance of the present system have been verified through analyses and computer simulation experiments. To demonstrate the favorable feature of the present system, additional discussions are given as follows. The proportional relationship between some adaptive arrays have been proved[64], which shows this system attains the same results with other systems under the most friendly environment. On the other hand, under more adverse condition, the predominance of the present system becomes obvious, i.e. the flexibility on the a priori

knowledge about the desired signal, while the adaptive array with least-mean-square-error criterion, for example, requires perfect synchronization between the reference signal and the received desired signal. The present system is applicable to the case in which the incident direction of the desired signal is approximately known a priori. In addition, if the source of the desired signal moves with time, the constraint direction may be changed in a program-tracking manner to maintain the reception with high signal-to-noise ratio.

APPENDIX

A satellite position can be derived usually from so-called the six orbital-elements, which are semimajor axis (a), eccentricity (e), orbital inclination (i), right ascension of ascending node (Ω), argument of perigee (ω) and mean anomaly (M). But, we will treat the circular orbit of a satellite, so that two of them, eccentricity and argument of perigee which are inherent in the elliptical orbit, are not taken into consideration.

In the orbital plane, a satellite revolves around the geocenter with constant angular velocity ω_s. Spherical earth is assumed in the following derivation. X_ω axis of the orbit plane coordinate system is taken toward the direction in which a satellite passes across the equatorial plane northward. Therefore, at time t, the position of a satellite in the orbit plane coordinate system can be written as,

$$\begin{vmatrix} X_\omega \\ Y_\omega \\ Z_\omega \end{vmatrix} = R_o \begin{vmatrix} \cos\omega_s t \\ \sin\omega_s t \\ 0 \end{vmatrix} \qquad \text{(A.1)}$$

It is to be noted that reference of time is taken at the instance when the satellite passes across the equatorial plane northward for simplicity of the derivation. R_o is the radius of the orbit.

Following the assumptions above, the right ascension-declination coordinate system and the orbit plane coordinate system are related to each other as shown in Fig.A.1. Transformation between

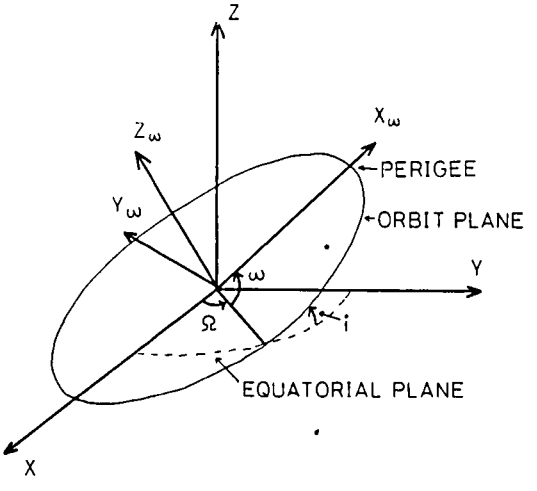

Fig.A.1 Right ascension-declination coordinate system and orbit plane coordinate system.

these coordinate systems is as follows.

$$\begin{pmatrix} X \\ Y \\ Z \end{pmatrix} = \begin{pmatrix} \cos\Omega & -\sin\Omega\ \cos i & \sin\Omega\ \sin i \\ \sin\Omega & \cos\Omega\ \cos i & -\cos\Omega\ \sin i \\ 0 & \sin i & \cos i \end{pmatrix} \begin{pmatrix} X_\omega \\ Y_\omega \\ Z_\omega \end{pmatrix} \qquad (A.2)$$

Substituting (A.1) into (A.2), the position of a satellite in the right ascension-declination coordinate system can be obtained as follows.

$$X = R_o(\cos\Omega\ \cos\omega_s t - \sin\Omega\ \cos i\ \sin\omega_s t) \qquad (A.3)$$

$$Y = R_o(\sin\Omega\ \cos\omega_s t + \cos\Omega\ \cos i\ \sin\omega_s t) \qquad (A.4)$$

$$Z = R_o\ \sin i\ \sin\omega_s t \qquad (A.5)$$

The position of the observer in the right ascension-declination coordinate system is written as,

$$X = R_e\ \cos\Theta\ \cos\Omega_0 \qquad (A.6)$$

$$Y = R_e\ \cos\Theta\ \sin\Omega_0 \qquad (A.7)$$

$$Z = R_e\ \sin\Theta \qquad (A.8)$$

where Θ is the latitude of the observer and Ω_0 is the local sidereal time of the observer. R_e is the radius of the earth. As the angular velocity of earth rotation is noted by ω_e, the local sidereal time can be expressed by the following equation.

$$\Omega_0 = \Omega_i + \omega_e t \qquad (A.9)$$

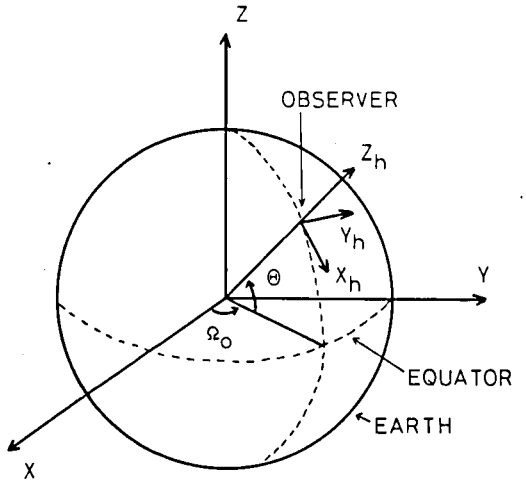

Fig.A.2 Right ascension-declination coordinate system and topocentric coordinate system.

where Ω_i is the local sidereal time at the reference time. Subtracting the position vector of the observer from that of a satellite, the position vector of a satellite seen from the observer is obtained as,

$$X = R_o(\cos\Omega \cos\omega_s t - \sin\Omega \cos i \sin\omega_s t) - R_e \cos\Theta \cos\Omega_0 \quad (A.10)$$

$$Y = R_o(\sin\Omega \cos\omega_s t + \cos\Omega \cos i \sin\omega_s t) - R_e \cos\Theta \sin\Omega_0 \quad (A.11)$$

$$Z = R_o \sin i \sin\omega_s t - R_e \sin\Theta \quad (A.12)$$

By the way, the right ascension-declination coordinate system and the topocentric coordinate system are related to each other as shown in Fig.A.2. And the relationship between them is written as follows.

$$\begin{pmatrix} X_h \\ Y_h \\ Z_h \end{pmatrix} = \begin{pmatrix} \sin\Theta \cos\Omega_0 & \sin\Theta \sin\Omega_0 & -\cos\Theta \\ -\sin\Omega_0 & \cos\Omega_0 & 0 \\ \cos\Theta \cos\Omega_0 & \cos\Theta \sin\Omega_0 & \sin\Theta \end{pmatrix} \begin{pmatrix} X \\ Y \\ Z \end{pmatrix} \quad (A.13)$$

Therefore, substituting (A.10), (A.11) and (A.12) into (A.13), (I.3.17), (I.3.18) and (I.3.19) of PART 1, Chapter 3 can be obtained as follows.

$$X_h = R_o\{\cos\omega_s t \sin\Theta \cos(\Phi+\omega_e t) + \sin\omega_s t \cos i \sin\Theta \sin(\Phi+\omega_e t) - \sin\omega_s t \sin i \cos\Theta)\} \quad (A.14)$$

$$Y_h = R_o\{\sin\omega_s t \cos i \cos(\Phi+\omega_e t) - \cos\omega_s t \sin(\Phi+\omega_e t)\} \quad (A.15)$$

$$Z_h = R_o\{\sin\omega_s t \cos\Theta \cos(\Phi+\omega_e t) + \sin\omega_s t \cos i \cos\Theta \sin(\Phi+\omega_e t)$$

$$+ \sin\omega_s t \sin i \sin\theta\} - R_e \qquad \text{(A.16)}$$

where Φ is the difference between the right ascension of observer's meridian at the reference time and the right ascension of ascending node, which can be written as,

$$\Phi = \Omega_0 - \Omega \qquad \text{(A.17)}$$

REFERENCES

(1) R. Toriumi, K. Matsumoto, K. Higuchi, H. Togawa and T. Kimura, "On the orbit determination procedures for the Doppler frequency measurement with the angular measurement tracking system (in Japanese)," Technical Report of National Aerospace Laboratory TR-168, December 1968.

(2) T. J. Grenchik and C. W. Murray, Jr., "Minitrack postdetection bandwidth considerations," NASA TM X-65311, Goddard Space Flight Center, June 1970.

(3) Y. Abe, "Study on satellite tracking (in Japanese)," Master Thesis (supervised by Prof. K. Maeda), Kyoto Univ., Kyoto, Japan, 1970.

(4) K. Takao and M. Fujita, "An interferometer receiver for tracking artificial satellites (in Japanese)," Trans. Inst. Electronics Comm. Engrs. Japan, vol.54-B, pp.90-91, February 1971.

(5) M. Fujita, "Determination of satellite orbits by means of an interferometer system," Master Thesis (supervised by Prof. K. Maeda), Kyoto Univ., Kyoto, Japan, 1971.

(6) F. M. Gardner, Phaselock Techniques, John Wiley & Sons, Inc., New York, 1966.

(7) K. Takao, Y. Nakadan and Y. Abe, "Experimental comparison between tracking systems for artificial satellites (in Japanese)," Trans. Inst. Electronics Comm. Engrs. Japan, vol.52-B, pp.541-546, September 1969.

(8) K. Takao and Y. Abe, "An approach to estimate the accuracy of the measurements of satellite orbits (in Japanese)," Trans. Inst. Electronics Comm. Engrs. Japan, vol.53-B, pp.770-776, December 1970.

(9) M. Fujita and K. Takao, "Baseline arrangement of radio interferometer array for tracking artificial satellites (in Japanese)," Trans. Inst. Electronics Comm. Engrs. Japan, vol.55-B, pp.241-248, May 1972.

(10) W. B. Kendall, "Unambiguous accuracy of an interferometer angle measuring system," IEEE Trans. SET-11, pp.62-70, June 1965.

(11) J. D. Kraus, Antennas, McGraw-Hill Co. Inc., New York, 1950.

(12) P. R. Escobal, Method of Orbit Determination, John Wiley & Sons, Inc., New York, 1965.

(13) K. Takao, "Study on a variable beam antenna array," Doctoral Thesis, Kyoto Univ., Kyoto, Japan, 1966.

(14) K. Takao, "Measurement of satellite orbits by means of a radio interferometer (in Japanese)," Technical Paper of the Professional Group on Antennas and Propagation, Inst. Electronics Comm. Engrs. Japan, A•P67-13, June 1967.

(15) K. Tao, "Refraction effect on space communications in the troposphere and the ionosphere," Technical Paper of the Professional Group on Radio Wave Propagation, Inst. Electrical Comm. Engrs. Japan, May 1962.

(16) H. Shibata, "Effects of atmospheric refraction on radio waves in

the earth-satellite communication link," J. Rad. Res. Labs., vol.10, no.52, pp.423-459, November 1963.

(17) R. H. Paul, "Refration error in measurement of angle of arrival with the radio interferometer," IEEE Trans. AES-4, pp.52-57, January 1968.

(18) R. H. Paul, "A comparison of radar and radio interferometer refraction errors," IEEE Trans. AES-5, pp.346-348, March 1969.

(19) J. W. Duncan, "The effect of ground reflection and scattering on an interferometer direction finder," IEEE Trans. AES-3, pp.922-932, December 1967.

(20) M. Fujita and K. Takao, "Phase error of an interferometer due to a reflected wave from inclined ground (in Japanese)," Record of the 1973 National Convention of Inst. Electronics Comm. Engrs. Japan, no.552.

(21) E. C. Jordan, Electromagnetic Wave and Radiating Systems, Prentice Hall, New Jersey, 1968.

(22) P. Beckmann and A. Spizzichino, The Scattering of Electromagnetic Waves from Rough Surface, Macmillan, New York, 1963.

(23) K. Maeda, Radio Engineering (Denpa Kogaku) (in Japanese)," Kyoritsu Shuppan Co., Tokyo, 1959.

(24) K. Takao, Y. Nakadan and Y. Abe, "Measurement of satellite orbits by means of a four-element interferometer (in Japanese)," Technical Paper of the Professional Group on Antennas and Propagation, Inst. Electronics Comm. Engrs. Japan, A·P68-47,

November 1968.

(25) M. Fujita and K. Takao, "Observation error of radio interferometer due to the secondary wave (in Japanese)," Technical Paper of the Professional Group on Antennas and Propagation, Inst. Electronics Comm. Engrs. Japan, A·P73-55, November 1973.

(26) A. Ksienski, "A survey of signal processing arrays," in AGARD Conference Proceedings No.16, Signal Processing Array, ed. W. T. Blackband.

(27) D. E. Svoboda, "A phase-locked receiving array for high-frequency communications use," IEEE Trans. AP-12, pp.207-215, March 1964.

(28) R. W. Bickmore, "Adaptive antenna arrays," IEEE Spectrum, August 1964.

(29) C. Drane, Jr. and J. McIlvenna, "Gain maximization and controlled null placement simultaneously achieved in aerial array pattern," Radio Elect. Eng., vol.39, pp.49-57, January 1970.

(30) O. L. Frost, III, "Adaptive least squares optimization subject to linear equally constraints," SEL-70-055, Tech. Rep. No.6796-2, Information System Laboratory, Stanford Univ., August 1970.

(31) L. J. Griffiths, "A simple adaptive algorithm for real-time processing in antenna arrays," Proc. IEEE, vol.57, pp.1696-1704, October 1969.

(32) J. P. Burg, "Three-dimensional filtering with an array of seismometers," Geophys., vol.29, pp.693-713, October 1964.

(33) M. J. Levin, "Maximum-likelihood array processing," Lincoln Laboratories, MIT, Lexington, Mass., Semiannual Tech. Summary Rept. on Seismic Discrimination, December 1964.

(34) D. G. Luenberger, Optimization by Vector Space Methods, translated into Japanese by M. Masubuchi and H. Kanoh, Corona Sha, Tokyo, 1973.

(35) R. A. Wiggins and E. A. Robinson, "Recursive solution to the multichannel filtering problem," J. geophys. Res., vol.70, pp.1885-1891, April 1965.

(36) S.W.W.Shor, "Adaptive technique to discriminate against coherent noise in a narrow band system," J. Acoust. Soc. Am., vol.39, pp.74-78, January 1966.

(37) S. P. Applebaum, "Adaptive arrays," IEEE Trans. AP-24, pp.585-598, September 1976; also Special Project Laboratory Report, SPL-TR66-1, Syracuse University Research Corporation, August 1966.

(38) B. Widrow, P. E. Mantey, L. J. Griffiths and B. B. Goode, "Adaptive antenna systems," Proc.IEEE, vol.55, pp.2143-2159, December 1967.

(39) C. L. Zahm, "Effects of errors in the direction of incidence on the performance of an adaptive array," Proc. IEEE, vol.60, pp.1008-1009, August 1972.

(40) L. J. Griffiths, "Signal extraction using real-time adaptation of a linear multichannel filter," SEL-68-017, Tech. Rep.

No.6788-1, System Theory Laboratory, Stanford Univ., February 1968.

(41) J. Capon, R. J. Greenfield and R. J. Kolker, "Multidimensional maximum-likelihood processing of a large aperture seismic array," Proc. IEEE, vol.55, pp.192-211, February 1967.

(42) R. T. Lacoss, "Adaptive combining of wideband array data for optimal reception," IEEE Trans. GE-6, pp.78-86, May 1968.

(43) J. F. Clearbout, "A summary, by illustrations, of least-square filter with constraints," IEEE Trans. IT-14, pp.269-272, March 1968.

(44) H. Kobayashi, "Iterative synthesis methods for a seismic array processor," IEEE Trans. GE-8, pp.169-178, July 1970.

(45) R. L. Riegler and R. T. Compton, Jr., "An adaptive array for interference rejection," Rep.2552-4, ElectroScience Laboratory, The Ohio State Univ., February 1970.

(46) R. L. Riegler, "Adaptive optimization of signal to noise ratio in receiving arrays," NASA CONTRACTOR REPORT, NASA CR-1778, ElectroScience Laboratory, The Ohio State Univ., August 1972.

(47) R. T. Compton, Jr., "Adaptive arrays for aircraft communication systems," Proceeding of Array Antenna Conference, no.25, February 1972.

(48) R. T. Compton, Jr., "An experimental four-element adaptive array," IEEE Trans. AP-24, pp.697-706, September 1976.

(49) J. H. Chang and F. B. Tuteur, "A new class of adaptive array

processor," J. Acoust. Soc. Am., vol.49, pp.639-649, March 1971.

(50) L. E. Brennan, E. L. Pugh and I. S. Reed, "Control loop noise in adaptive array antennas," IEEE Trans. AES-7, pp.254-262, March 1971.

(51) L. E. Brennan and I. S. Reed, "Effect of envelope limiting in adaptive array control loops," IEEE Trans. AES-7, pp.698-700, July 1971.

(52) A. Booker and C. Y. Ong, "Multiple-constraint adaptive filtering," Geophysics, vol.36, pp.498-509, June 1971.

(53) O. L. Frost, III, "An algorithm for linearly constrained adaptive array processing," Proc. IEEE, vol.60, pp.926-935, August 1972.

(54) W. E. Butcher and R. J. Sims, "Adaptive null steering for RF antenna arrays," Proceeding of Array Antenna Conference, no.28, February 1972.

(55) W. F. Gabriel, "Adaptive array antennas for AEW radar," Rep. of NRL Progress, pp.39-44, December 1972.

(56) C. L. Zahm, "Application of adaptive arrays to suppress strong jammers in the presence of weak signals," IEEE Trans. AES-9, pp.260-271, March 1973.

(57) L. E. Brennan and I. S. Reed, "Theory of adaptive radar," IEEE Trans. AES-9, pp.237-252, March 1973.

(58) C. A. Baird, "Recursive algorithm for adaptive array antennas,"

RADC-TR-74-46, Harris-Intertype Corporation, March 1974.

(59) K. Takao, M. Fujita and T. Nishi, "An adaptive antenna array under directional constraint," IEEE Trans. AP-24, pp.662-669, September 1976.

(60) L. P. Winkler and M. Schwartz, "Adaptive nonlinear optimization of the signal-to-noise ratio of an array subject to a constraint," J. Acoust. Soc. Am., vol.52, pp.39-51, August 1972.

(61) T. Nishi, "Study on signal processing antenna arrays (in Japanese)," Master Thesis (supervised by Prof. I. Kimura), Kyoto Univ., Kyoto, Japan, 1975.

(62) C. W. Helstrom, Statistical Theory of Signal Detection, Pergamon Press, New York, 1960.

(63) D. G. Brennan, "Linear diversity combining techniques," Proc. IRE, vol.47, pp.1075-1102, June 1959.

(64) M. Fujita and K. Takao, "Proportional relationship between adaptive arrays," Trans. Inst. Electronics Comm. Engrs. Japan, vol.E60, pp.349-350, July 1977.